# Characterization of cAMP-Specific Phosphodiesterase-4 (*R*)-[$^{11}$C]Rolipram Small Animal Positron Emission Tomography and Application in a Streptozotocin-Induced Model of Hyperglycemia

**Adam John Thomas**

*This thesis is submitted as a partial fulfillment*
*of the Master of Science program in*
*Cellular and Molecular Medicine*

*Submitted to the University of Ottawa, September 22, 2010*

# Characterization of cAMP-Specific Phosphodiesterase-4 (*R*)-[$^{11}$C]Rolipram Small Animal Positron Emission Tomography and Application in a Streptozotocin-Induced Rat Model of Hyperglycemia

*MSc Thesis 2011, Adam John Thomas,*
*Department of Cellular and Molecular Medicine, University of Ottawa*
*Ottawa, Ontario, Canada*

Elevated sympathetic nervous system (SNS) tone contributes to excess cardiac mortality associated with type 2 diabetes mellitus (T2DM). Chronic SNS stimulation has detrimental effects to the heart, in particular, with its cell signaling abilities. (*R*)-[$^{11}$C]Rolipram small animal positron emission tomography (PET), an noninvasive nuclear imaging modality, was used to assess phosphodiesterase-4 (PDE4) alterations in a high fat diet (HFD), streptozotocin (STZ) induced model of hyperglycemia in rats. Prior to investigation in the animal model, characterization of (*R*)-[$^{11}$C]rolipram small animal PET was completed. (*R*)-[$^{11}$C]Rolipram binds specifically to PDE4 in the rat heart demonstrated by competitive blockade with (*R*)-rolipram with the PDE4 enzyme susceptible to saturation with increasing injected masses of unlabeled rolipram. (*R*)-[$^{11}$C]Rolipram cardiac retention was elevated by acute norepinephrine stimulation via desipramine pharmacologic challenge. Quantitative (*R*)-[$^{11}$C]rolipram PET was highly reproducible in the heart and presents an ideal avenue to investigate PDE4 alterations. (*R*)-[$^{11}$C]rolipram small animal PET did not reveal changes in PDE4 expression and activity in STZ-treated hyperglycemic animals compared to STZ-treated euglycemic and control groups. *In vitro* measures of PDE4 enzyme expression and activity, with or without desipramine, were also not altered between treatment groups. Although (*R*)-[$^{11}$C]rolipram small animal PET does not reveal PDE4 alterations in this animal model of diabetes, its utility to assess PDE4 alterations in other over active SNS pathologies, such as heart failure and obesity, remains.

# LIST OF FIGURES

# LIST OF TABLES

# LIST OF ABBREVIATIONS

| | |
|---|---|
| $^{11}C$ | carbon-11 |
| $^{12}C$ | carbon-12 |
| $[Ca^{2+}]$ | calcium concentration |
| AC | adenylate cyclase |
| AKAP | A kinase anchoring protein |
| ANS | autonomic nervous system |
| AR | adrenergic receptor |
| $B_{max}$ | maximal binding density |
| BMI | body mass index |
| cAMP | 3', 5' cyclic adenosine monophosphate |
| cGMP | 3', 5' cyclic guanosine monophosphate |
| CHD | coronary heart disease |
| CHF | congestive heart failure |
| CREB | cAMP response element binding |
| CBP | CREB binding protein |
| CVD | cardiovascular disease |
| db-cAMP | dibutyryl 3', 5' cyclic adenosine monophosphate |
| DV | volume of distribution |
| FFA | free fatty acid |
| E | epinephrine |
| $ED_{50}$ | 50% effective dose |
| EDTA | ethylenediaminetetraacetic acid |
| Erk-2 | extracellular related kinase 2 |
| $G_{\alpha s}$ | stimulatory G-alpha subunit |

| | |
|---|---|
| $G_{\alpha i}$ | inhibitory G-alpha subunit |
| GPCR | G protein-coupled receptor |
| Glut-1/2/4 | glucose transporter 1/2/4 |
| GRK | G protein-coupled receptor kinase |
| HARBS | high affinity rolipram binding site |
| HF | heart failure |
| HFD | high fat diet |
| HPLC | high performance liquid chromatography |
| IBMX | 3-isobutyl-1-methylxanthine |
| $I_{Ca}$ | calcium current |
| $IC_{50}$ | 50% inhibitory concentration |
| %ID/g | percent of injected dose per gram of tissue |
| ISO | isoproterenol |
| $K_1$ | uptake constant (blood to tissue) |
| LV | left ventricle |
| $M_{1/2}$ | metal binding site 1/2 |
| MBF | myocardial blood flow |
| MBPC | myosin binding protein C |
| MBR | myocardium-to-blood ratio |
| NE | norepinephrine |
| NIMH | national institute of mental health |
| PDE | phosphodiesterase |
| PET | positron emission tomography |
| PKA | protein kinase A |
| PLB | phospholamban |

| | |
|---|---|
| pSNS | parasympathetic nervous system |
| PTX | pertussis toxin |
| Rp-cAMP | Rp-adenosine-30,50-cyclic monophosphorothioate |
| RV | right ventricle |
| RyR | ryanodine receptor |
| SA | specific activity |
| SNR | signal-to-noise ratio |
| SNS | sympathetic nervous system |
| SR | sarcoplasmic reticulum |
| STZ | streptozotocin |
| T2DM | type-2 diabetes mellitus |
| TAC | time activity curve |
| TG | triglyceride |
| %SUV | percent of standardized uptake value |
| UCR | upstream conserved region |
| $V_{max}$ | maximal velocity |

# ACKNOWLEDGEMENTS

The completion of this thesis represents two years of scientific research in the field of nuclear imaging, pharmacology and pathology. This body of literature could not have been made possible with the cooperative efforts of a wide team of individuals at the University of Ottawa Heart Institute, National Cardiac PET Centre.

To begin, I owe a debt of gratitude to my supervising project investigator, Dr. Jean N. DaSilva. His guidance and expertise has been invaluable, while demanding the most out of me academically and spurring my personal growth. In addition to his encouragement in the laboratory environment, he is also the source of my attendance at multiple conferences – events that provided outstanding learning opportunities and a truly complete Masters experience.

Secondly, to my co-supervisor, Dr. Robert S. Beanlands, whose rigorous approach to research, medicine and science imparted the traits of persistence and dedication throughout this body of work.

Thirdly, I'd like to acknowledge Dr. Robert A deKemp. Working very closely with me in preparation of my first manuscript submission, I owe a wealth of thanks for the guidance provided in this regard. Further, I thank Dr. deKemp for inviting me to enjoy the 'lighter' side of research world.

To my immediate colleagues – Miran Kenk, James Thackeray, Stephanie Thorn, Rawad Antoun, Kumiko Mackasey and Natasha Arksey – I wish you all the best in your continuing pursuits and thank each of you for helping to make me a better student, scientist and person.

Not to be forgotten are a wide group of individuals who assisted in various ways along the course of my studies – Myra Kordos, Samantha Mason, Jeffrey Collins, Julian Walcott, Elena Dobrota, Ana Valdivia, Jeniffer Renaud, Mireille Lortie, Ran Klein, and Tyler Dumochel.

An individual is not without the heavy influence of their family. Mom – thanks for your *truly* unconditional love. Dad – giving me my analytic mind and dedicated personality that got me here… and let me finish. Amanda – the best sister I could ask for; you've grown into a lovely young woman and I am so proud to have you as my sister.

Finally, I'd like to dedicate this thesis to Arden, whose love, emotional support and cooking (!!) gave me the strength to make it to the end of this journey. You make me a better person, inspire me to reach new heights and I love you more with each day we're together. Looking forward to the future!

# 1. Introduction

## *1.1 Cardiac Cell Signaling*

### 1.1.1 Sympathetic Nervous System

The autonomic nervous system (ANS) maintains homeostasis through a balance of its parasympathetic (pSNS) and sympathetic nervous system (SNS) branches (figure 1.1). SNS function is mediated through release of the neurotransmitters epinephrine (E) and norepinephrine (NE) which exert their effects at the molecular level through signaling cascades that evoke specific responses dependent on the target tissue. In the heart, the SNS regulates the rate and intensity of cardiac contractions to modulate cardiac output in normal and stressed conditions.[1,2] Alterations in the SNS signaling pathway have been implicated in several pathologies, such as diabetes,[3] obesity[4] and heart failure.[5]

### 1.1.2 Adrenergic Receptors

The adrenergic receptors (ARs) are the target effectors of the SNS and are activated by NE and E. Several subtypes of the ARs have been characterized in the cardiovascular system – $\alpha_1$, $\alpha_2$, $\beta_1$, $\beta_2$, $\beta_3$.[6-10] $\alpha_1$ and $\alpha_2$ subtypes are responsible for vasoconstriction[7,10] assisting in blood pressure regulation. $\beta_3$-AR function remains controversial – there is evidence in favour[11] and against[12,13] a cardiopressant effect, though it may arise as a secondary outcome mediated by the $\beta_1/\beta_2$-AR.[8] $\beta_1$- and $\beta_2$-ARs play highly prominent roles in control of cardiac pacing and contractility[6,9] and will be focused on herein.

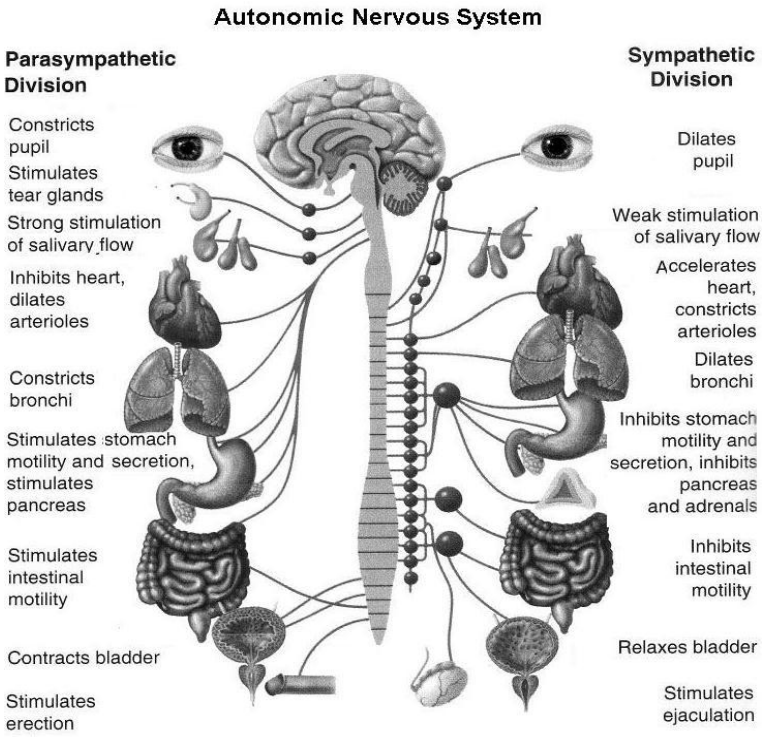


**FIGURE 1.1.** Functional divisions of the autonomic nervous system, effector organs and major physiologic outcomes. Reproduced from http://www.yesselman.com/ans.jpg.

#### *1.1.2.1 $\beta_1$ and $\beta_2$ Adrenergic Receptors*

$\beta_1$- and $\beta_2$-ARs comprise a well studied subclass of G protein-coupled receptors (GPCRs). As members of the GPCR superfamily, they are plasma membrane proteins characterized by their unique seven transmembrane-spanning motif and are coupled to intracellular G proteins.[1] $\beta_1$-AR and $\beta_2$-AR have a 48.9% conserved sequence identity between one another,[14] indicating a considerable amount of variation between the two, leading to their individual functional outcomes (section 1.1.3.1 and 1.1.3.2). The right atrium has a $\beta_1$:$\beta_2$ receptor density ratio ranging from 2:1[15,16] to as high as 4:1[17,18] in humans. The left ventricle has a ratio of ~3:1 in canine[19] and human left ventricle;[18,20,21] this ratio may be closer to 1:1 in the rat ventricle.[22,23]

### 1.1.3 cAMP/PKA-Dependent Intracellular Signaling

Activation of β−ARs to increase cardiac output via agonist binding results in a conformational change within the GPCR itself.[24,25] This change allows the stimulatory G protein ($G_{\alpha s}$) subunit of the heterotrimeric G protein to exchange a GDP molecule for a GTP molecule resulting in the separation of the $G_{\alpha s}$ subunit from the β/γ subunits. The GTP-bound $G_{\alpha s}$ subunit is then free to stimulate adenylyl cyclase (AC).[20,24,25] Activation of AC results in the production of second messenger 3', 5' cyclic adenosine monophosphate (cAMP) and can occur as quickly as 5 seconds after β−AR stimulation in adult rat ventricular myocytes.[26] Rapid oscillations in intracellular cAMP concentration occurs with a faster peak (35%) and decay rate (55%) at the plasma membrane compared to the cytosol,[26] consistent with membrane-bound AC creating the diffusible secondary messenger. Importantly, cAMP transient oscillations are known to precede and

coordinate cardiac function[27] by binding to the regulatory subunits of protein kinase A (PKA), alleviating the inhibition of the catalytic site of this kinase. This event allows PKA phosphorylation of a variety of downstream target proteins related to calcium handling and contraction in the heart which allows alteration of cardiac contractile force and rate.[2] Accordingly, genetic deletion of AC-6, one of two predominant AC isoforms in the heart, caused a 50% reduction in β-AR stimulated cAMP production, reduced PKA activity and phosphorylation of downstream targets.[28]

### *1.1.3.1 $G_{\alpha s}$ Coupling of $\beta_1$-AR and $\beta_2$-AR*

Both $\beta_1$-AR and $\beta_2$-AR couple $G_{\alpha s}$ (figure 1.2),[2] consistent with PKA activation in the presence of cAMP. Activation of this pathway allows ventricular $\beta_1$- and $\beta_2$-ARs to increase the inotropic and chronotropic responses of the left ventricle[13,19,20,29] with similar results obtained in the atrium.[30] Genetic mutation which overexpressed human $\beta_1$-AR 5-15-fold in mice led to enhanced cardiac function in the short-term, but eventually yielded to detrimental outcomes including hypertrophy, reduced contractility and ejection fraction at 30-35 weeks.[31] With functioning $\beta_1$-AR present, $\beta_2$-AR knockout mice responded normally to β-AR agonist isoproteronol (ISO) stimulation suggesting that the role of $\beta_2$-AR cardiac output regulation is limited in the healthy heart.[32] Similar effects are noted with whole-cell patch clamp techniques, where rat ventricle cells increase calcium current ($I_{Ca}$) 98% by $\beta_1$-AR-dependent stimulation.[33] The limited role of $\beta_2$-AR in cardiac function is likely due to $\beta_2$-AR coupling to the inhibitory G protein ($G_{\alpha i}$)[29] in addition to its coupling to $G_{\alpha s}$. Due to this, $\beta_2$-AR may only take on a more prominent role regulating cardiac function in disease states, such as diabetes.[34,35]

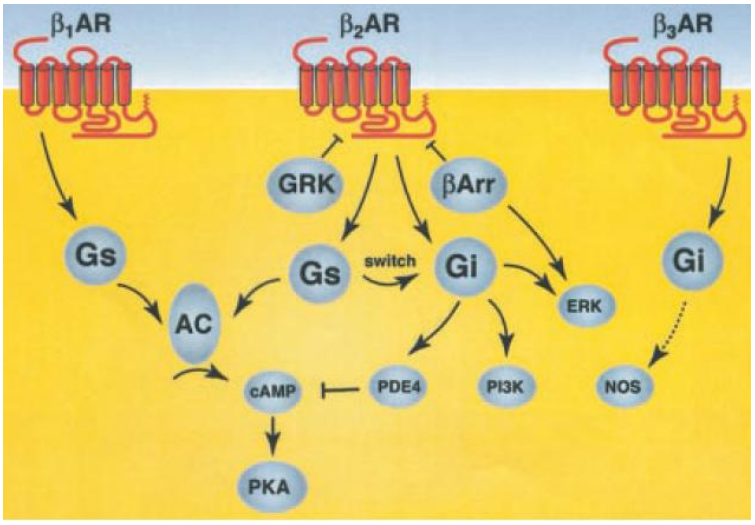


**FIGURE 1.2.** β-AR/$G_{\alpha s}$ subunit coupling and the effect on intracellular cAMP accumulation. GRK = G protein-coupled receptor kinase, βArr = β-arrestin, $G_s$ = stimulatory G protein, $G_i$ = inhibitory G protein, ERK = extracellular-signal regulated kinase, PI3K = phosphatidylinositol 3-kinase, NOS = nitric oxide synthase. Adapted from Lohse et al., 2003.

### *1.1.3.2 $G_{\alpha i}$ Coupling of the $\beta_2$-AR*

As noted above (section 1.1.3.1), $\beta_2$-AR couples to the inhibitory G protein, $G_{\alpha i}$,[36] in a PKA mediated event.[37] $\beta_1$-AR, however, does not couple to $G_{\alpha i}$ as its functional outcomes are unaffected by inhibition of the G protein with pertussis toxin (PTX).[38] Activation of $G_{\alpha i}$ by $\beta_2$-AR has the effect of inhibiting AC and reducing cAMP production.[38] In fact, inhibition of $G_{\alpha i}$ in transgenic mice overexpressing $\beta_2$-AR by PTX increased $I_{Ca}$ and $[Ca^{2+}]$ in a cAMP-dependent fashion.[29]

## 1.1.4 cAMP/PKA-Dependent Activation of Cardiac Machinery

As discussed (section 1.1.3.1), cAMP allows for the activation of PKA, enabling PKA to phosphorylate a variety of downstream effector proteins involved in calcium handling and cardiac contraction. Indeed, $\beta_1$-AR stimulation results in PKA activation leading to marked contractile increases demonstrated in a series of experiments using $\beta_1$-, $\beta_2$- and $\beta_1/\beta_2$-AR knockout mice.[13] $\beta_2$-AR stimulation has been reported to result in PKA activation,[39] with PKA independent pathways also implicated.[13]

### *1.1.4.1 Role of PKA in Cardiac $Ca^{2+}$ Cycling*

The calcium current in- and efflux triggered following $G_{\alpha s}$ activation fundamentally regulates cardiac contraction and heart rate.[40] Following PKA activation by cAMP, PKA has been shown to phosphorylate target proteins known to be related to cardiac contraction (figure 1.3). At the initial stages of contraction, calcium-induced calcium release is triggered by the $I_{Ca}$ generated from PKA-mediated phosphorylation of

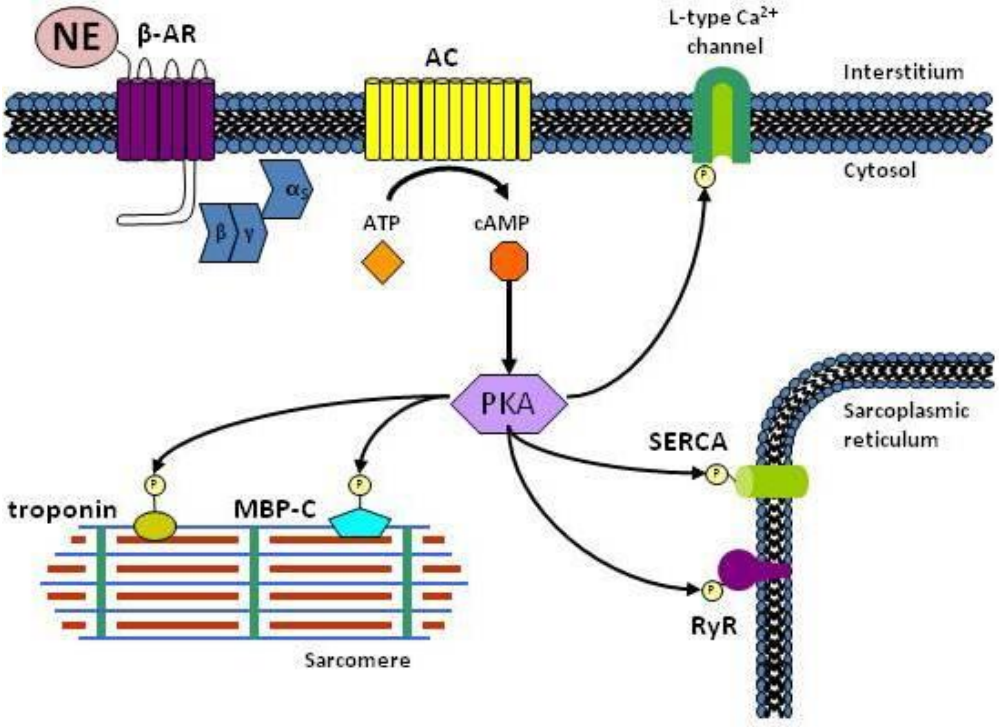


**FIGURE 1.3.** Representative schematic illustrating key intracellular target proteins activated by cAMP-dependent PKA phosphorylation in the heart. NE = norepinephrine, AC = adenylate cyclase, $\alpha_s/\beta/\gamma$ = G protein subunits, ATP = adenosine triphosphate, cAMP = cyclic adenosine monophosphate, PKA = protein kinase A, RyR = ryanodine receptor and MBP-C = myosin binding protein C.

$Ca_v1.2a$ membrane channels.[33] Importantly, activation of PKA by ISO stimulation in rat ventricular myocytes preceeds the increase in $I_{Ca}$.[26] This inward $I_{Ca}$ begins depolarizing the myocyte triggering $Ca^{2+}$ release from the sarcoplasmic reticulum (SR) ryanodine receptor (RyR) – and phosphorylation of RyR enhances this $Ca^{2+}$ release.[41,42] These events ultimately cause complete depolarization of the myocyte, allowing for contraction to occur. Phospholamban (PLB) – an inhibitor of the SR $Ca^{2+}$-ATPase, which is responsible for $Ca^{2+}$ removal from the intracellular environment leading to relaxation – is also phosphorylated by PKA which enhances contractile relaxation[43,44] and occurs in response to $G_{\alpha s}$ pathways.[45,46] Hastened relaxation by this mechanism allows for increases in heart rate as the ventricle is prepared for subsequent contractions in a shorter time frame.

#### *1.1.4.2 Role of PKA Phosphorylation of Cardiac Contractile Proteins*

PKA-mediated phosphorylation of myofibrallar proteins, including myosin binding protein C (MBPC) of myosin filaments[47,48] and troponin I of actin filaments,[44,49] assist in cross-bridging of the contractile fibers and increase contraction force and rate. Contraction of ventricular rat myocytes was depressed by PKA delocalization resulting in reduced myocyte shortening with *in vitro* preparations and decreased heart rate and left ventricle (LV) pressure in perfused hearts.[44]

### 1.1.5 Regulation of cAMP levels via Beta-Adrenergic Receptor Control

β-AR cell surface expression can be modified by the processes of internalization or down-regulation[50] impacting cAMP levels by providing greater or fewer receptors to activate in the presence of agonists. The combination of these two mechanisms dampen cell signalling through reduced cAMP production. Internalization occurs rapidly following acute receptor stimulation,[51] whereas downregulation occurs in response to chronic NE stimulation.[52,53]

#### *1.1.5.1 Beta-Adrenergic Internalization*

Internalization (figure 1.4) is mediated through phosphorylation of sites on the β-AR believed to be exposed during agonist-induced conformational change.[54] Phosphorylation of these sites is mediated by G protein-coupled receptor kinases (GRKs)[51] that act on agonist-activated ARs.[55] This activity facilitates interaction between intracellular β-arrestin proteins[55] and the receptor at multiple sites.[56] β-Arrestins interact with clathrin molecules allowing internalization of the receptor via clathrin coated vesicles.[57,58] These vesicles are either directed to early endosomes for degradation by lysosomes,[59] or recycled back to the cell surface.[60]

#### *1.1.5.2 Beta-Adrenergic Downregulation of Protein Expression*

Downregulation, through reduced protein expression or increased degradation, of cardiac β-ARs occurs in response to chronic overstimulation by catecholamines.[61] Kudej et al.[53]show that chronic ISO treatment (13 days) results in a 54% reduction in total

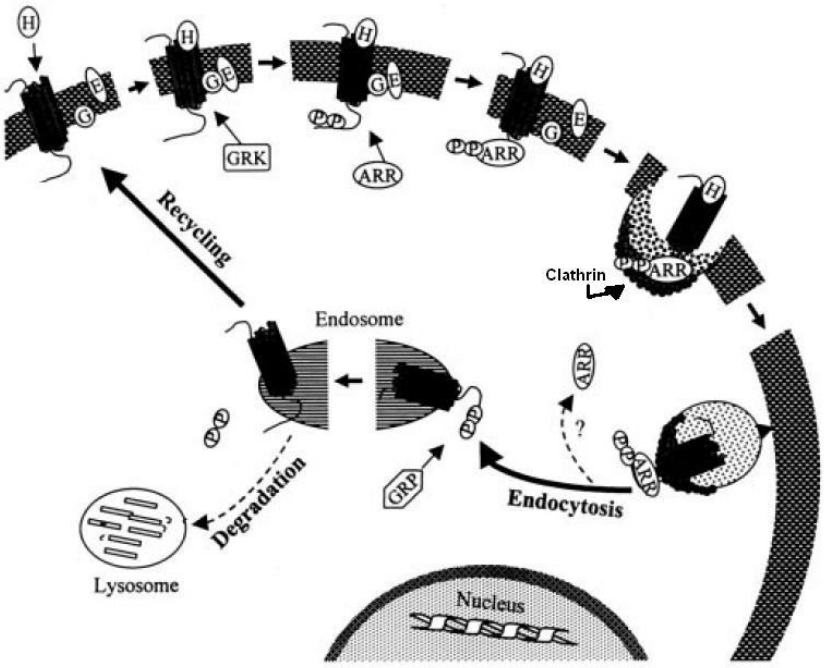


**FIGURE 1.4.** Schematic diagram of GPCR internalization highlighting the roles of GRK, β-arrestin and clathrin molecules. GRK = G protein-coupled receptor kinase, Arr = β-Arrestin. Adapted from Dzimiri, 1999.

β-AR density in the murine left ventricle. Further, following chronic exposure, acute stimulation with ISO resulted in a 60% reduction in AC activity and the inability of the heart to augment its heart rate, fractional shortening and ejection fraction compared to controls. These observations are echoed in rats where chronic ISO treatment (14 days) ameliorated the positive inotropic responses to acute ISO stimulation in left ventricle and shifted the response to db-cAMP rightward 3.2-fold.[62] This outcome is also seen with 5-day chronic NE treatment (12-fold increase in NE vs. controls) in the left ventricle reducing β-AR density by 31% and leading to a 33% drop in basal AC activity.[63]

This principle extends beyond *in vitro* studies to pathological states that suffer from enhanced SNS signalling where β−AR densities are known to change. In heart failure (HF) for example, the $\beta_1$:$\beta_2$ ratio of 72:28 (healthy state) altered to 45:55 (disease state) in canine isolated cardiomyocytes.[19] In human HF, where cardiac NE spill over can be elevated 4-fold over healthy controls,[65] a greater downregulation of $\beta_1$-AR over $\beta_2$-AR occurs; the ratio between the receptors alters from 3:1 in the baseline state to approximately 1:1.[66,67] In congestive heart failure (CHF), a rabbit model of cardiac pacing showed a 50% reduction in total β−AR of the left ventricle at 8 weeks when NE plasma content was 10-fold greater than controls.[64]

### 1.1.6 Regulation of cAMP levels via Phosphodiesterases

#### *1.1.6.1 PDE Superfamily*

The phosphodiesterase (PDE) superfamily provides a second mechanism to decrease cAMP intracellular accumulation based on enzymatic degradation; PDEs

hydrolyze the secondary messengers cAMP and cyclic guanine monophosphate (cGMP) to their inactive, 5'-linear forms.[68] Derived from 21 genes, the PDE superfamily consists of 11 primary families (figure 1.5) that share large, conserved catalytic sequences towards the C-terminal.[68] These main PDE families are subdivided further on the basis of their numerous isoforms and splice variants.[69] In addition to classification by differential protein structure, PDE isoforms are grouped together for their sensitivities and preferences for cAMP or cGMP substrate; PDE1, 2, 3, 10 and 11 families hydrolyze both cAMP and cGMP, while PDE4, 7 and 8 are cAMP-specific and PDE5, 6 and 9 are cGMP-specific.[68]

### *1.1.6.2 PDE Dependent cAMP Intracellular Gradients*

Tight and appropriate control over cAMP-dependent outcomes is reliant on compartmentation of the secondary messenger by PDEs leading to transient gradients and isolated pockets of accumulation.[70,71] This was demonstrated using 3-isobutyl-1-methylxanthine (IBMX), a pan-PDE inhibitor, to decrease $I_{Ca}$ compartmentation in frog ventricular myocytes by 9-fold.[72] However, in addition to containment of cAMP in an absolute sense, the relative spatial organization of the messenger is also critical to proper cell function and is dependent on specific PDE localization. For example, immunocytochemistry and confocal microscopy of rat ventricular myocytes identified PDE3A localizing to the interior plasma membrane and PDE4B and PDE4D showing strong signals in the cytosol, with additional pockets localized to sarcomeric m-line and z-lines, respectively.[73] Importantly, adult rat myocytes have enhanced PKA activity at the sarcomeric z-line in IBMX treated cells.[74] These findings support the hypothesis of PDEs

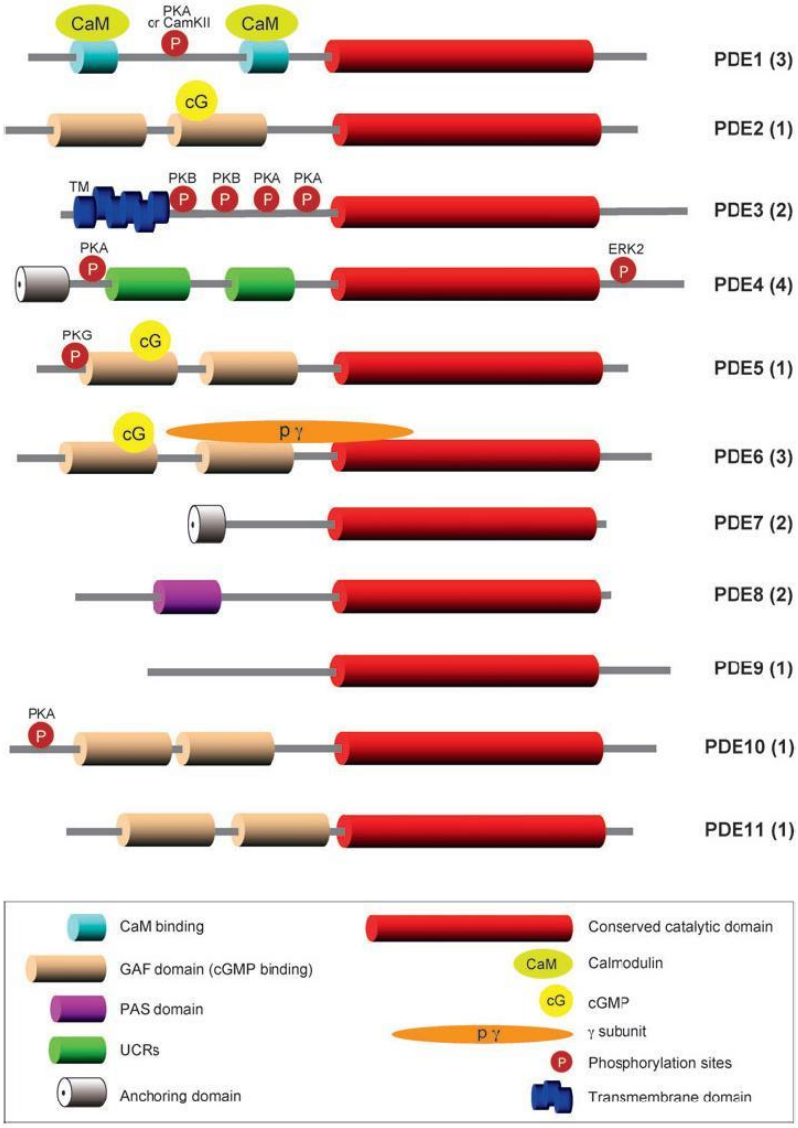


**FIGURE 1.5.** Identification of PDE isoforms by family. Reproduced from Conti and Beavo, 2007.

congregating in locations of cAMP production and/or locations of PKA phosphorylation – two areas that would allow for optimal regulation of cAMP-dependent activities. This spatial relationship is known to also occur in other cells, such as sertoli cells, where PDE4D3 was shown to co-localize with PKA in the centromere by staining and maintained a functional scaffold as the two proteins coimmunoprecipitated together.[75] In further support, muscle-selective A-kinase anchoring protein (AKAP), with isoforms known to localize at the z-line and t-tubule SR,[76] were found to provide a molecular framework between PKA and PDE binding, as it coimmunoprecipitated with PDE4 in the rat heart.[77] The functional role was confirmed by the precipitate's reduced ability to stimulate PDE4 activity in the presence of rolipram (a PDE4 selective inhibitor) and, moreover, it caused PDE4D3 relocation following increased expression.[77]

### *1.1.6.3 Cardiac PDE3 and PDE4*

The PDE3 and 4 enzymes predominate cardiac cAMP hydrolysis in several species. In the ovine heart the primary isoforms are PDE3 and PDE4,[69] representing 44% and 56% of cAMP hydrolyzing activity.[78] In frog ventricles, large disruptions of $I_{Ca}$ compartmentation were seen following treatment with pan-PDE inhibitor IBMX – an effect that was replicated with the combination treatment of PDE3 and PDE4 inhibitors.[72] The importance of PDE4 in rodent cardiac cAMP breakdown was confirmed using isolated mice cardiomyocytes where ~70% of $\beta_1$-derived cAMP is hydrolyzed by PDE4[79] and in isolated rat myocytes where $\beta_1$-related cAMP is handled by PDE4 hydrolysis alone, but β2 stimulated cAMP requires hydrolysis by PDE3 and PDE4 together.[80] Further, nearly 90% of rat cardiac cAMP degradation is provided by PDE3 and PDE4,

with PDE4 being approximately double that of PDE3.[73] In addition, rats pre-treated with PDE4 selective inhibitor rolipram resulted in a 56% increase in contractile force in the presence of $\beta_1$-AR stimulation in rats.[81] Given the above findings, PDE4 is highly relevant to rat cAMP regulation and will be focused on for the remainder of this thesis.

### 1.1.7 PDE4

The PDE4 family has 4 genes (PDE4A, B, C, D) transcribed to produce more than 20 splice variants[68,69] and has had its three dimensional structure characterized (figure 1.6).[82] In addition to its abundance in the heart, PDE4 is expressed throughout the body in varying degrees, with particularly high levels in the brain, skeletal muscle, and pancreas.[83-86] In the heart, functional emphasis is placed on isoforms PDE4A/B/D as immunoprecipitation revealed the largest quantities of these 3 variants in rats.[80] Similarly, PDE4B and PDE4D were found to contribute approximately 90% of PDE4 activity in rat neonatal myocytes, with PDE4A and PDE4C providing the remainder.[72]

#### *1.1.7.1 PDE4 Regulation*

#### *1.1.7.2 PDE4 Regulation by Apoenzyme vs Holenzyme Complex*

Catalytic PDE4 enzyme activity is dependent on the apoenzyme and holoenzyme conformations, where high and low affinity states of the PDE enzyme for cAMP are regulated by physiologic metal ions.[82] PDE4 enzymes bind two metal ions ($M_1$ and $M_2$) to form the enzyme-cofactor holoenzyme which increases affinity and hydrolytic activity for cAMP as well as the affinity for rolipram inhibition *in vitro*.[87] The association of PDE with $M_1$ and $M_2$ ions is believed to stabilize the high affinity PDE4 conformation, and

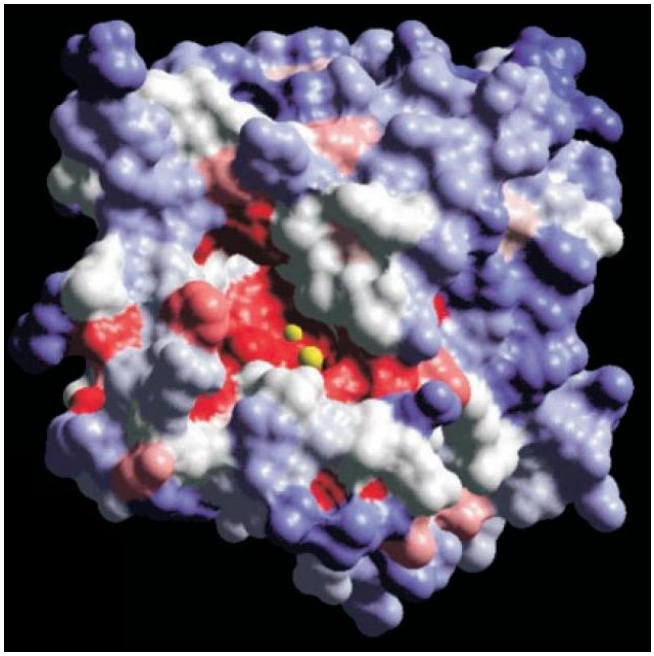

**FIGURE 1.6.** 3-Dimensional representation of the PDE4 molecule (red = completely conserved residues, white = partially conserved residues, blue = highly variable residues, yellow = metal binding sites). Reproduced from Xu et al., 2000.

may also enhance catalysis by positioning a water molecule in the catalytic site that could act as a nucleophile in the cAMP hydrolysis reaction.[82]

#### 1.1.7.2.1 Ionic Regulation of PDE4 Holoenzyme

Several metal ions are known to bind PDE4 – copper, manganese and zinc activate PDE4A at low concentrations (1-5 μM), while zinc, nickel and copper have biphasic effects with increasing concentrations that ultimately reduce PDE4A activity a higher concentrations (> 5 μM, > 100 μM and > 100 μM, respectively).[88] Magnesium and manganese do not demonstrate biphasic responses over the same concentration range (0.5-10000 μM) and may provide the optimal ion sources for PDE4 activation.[88] Deciphering the exact roles of ion contribution to PDE4 activity becomes increasingly difficult with the consideration of enzyme phosphorylation by PKA. PDE4A activity was stimulated in a dose-dependent linear fashion by increasing concentrations of $Mg^{2+}$ (0.1-10 μM), while this was enhanced to an exponential relationship in the presence of PKA treatment.[89]

The di-metal-PDE4 holoenzyme union is known as the high affinity rolipram binding site (HARBS) conformation due to its enhanced affinity for the selective and specific inhibitor (*R*)-rolipram in the presence of co-factor metals magnesium,[88,90] manganese, and copper.[87] This enhanced affinity for (*R*)-rolipram is quite dramatic, as treatment with metal cofactors resulted in a $K_d$ of 3-8 nM vs. 150 nM – a difference of nearly 20-fold – in the low-affinity state lacking metal co-factors magnesium, manganese, and copper.[87] These collective observations highlight the difficulty in replicating the true *in vivo* processes occurring in living animals in an *in vitro* setting, where the precise nature of $M_1$ and $M_2$ binding is not fully elucidated.

### *1.1.7.3 Acute PDE4 Regulation*

Acute cAMP elevations increase phosphorylation of PDE4 by PKA and extracellular related kinase 2 (Erk-2; section 1.1.7.3.1). Addition of the PKA catalytic subunit and [$^{32}$P]ATP in the presence of human PDE4A4 expressed in baculovirus/Sf9 expression system increased cAMP hydrolysis 4-fold compared to untreated controls (0.2 vs. 0.8 μmol/mg/min) within 2 hours.[89] Thyroid cells stimulated with thyroid releasing hormone caused activation of PDE4D3, increasing to peak activity by 5 minutes and remaining elevated for 30 minutes; this enhanced activity was susceptible to blockade by PKA inhibitors and could be recovered with incubation of cells in PKA-activating 8-(4-chlorophenylthio)adenosine-cAMP.[91] In aortic vascular smooth muscle cells, forskolin activation of AC resulted in increased PDE4 activity and phosphorylation of the PDE4D isoforms which again could be abolished by blockade with a PKA inhibitor, H89.[92] Similar observations are made in U937 undifferentiated macrophage cells,[93] hepatocytes,[94] and adipocytes.[95]

#### 1.1.7.3.1 PDE4 Regulation by Site-Specific Phosphorylation

In their 1998 report Hoffman et al.[96] demonstrate that PKA-mediated phosphorylation of PDE4D3 occurred at Ser-54 of the RRES motif increasing catalytic ability 2.3 fold compared to control values which is in agreement with Sette and Conti, 1996.[97] Further, the $IC_{50}$ for rolipram inhibition shifted leftwards in the phosphorylated state (0.11 μM vs. 0.68 μM) suggesting enhanced affinity for the inhibitor to the phosphorylated state of the enzyme. This was confirmed using a mutant model of the enzyme where the Ser54 residue was substituted with a negatively charged aspartate or

glutamate residue mimicking the phosphorylated PDE4D3 state causing 2.9 and 2.0 fold increases in activity compared to controls and decreasing rolipram $IC_{50}$ to levels similar to the PKA phosphorylated state. Following this study, Hoffman et al.[98] reported that Erk-2 mediated phosphorylation also occurs on PDE4D3 isoform, but at the Ser579 residue, which can be ablated by Ser579→Ala mutation. Additionally, catalytic maximal velocity ($V_{max}$) of the enzyme reduced to 25% of control values after maximal phosphorylation by Erk-2 at 30 minutes, which can be recovered to control levels by treatment with phosphatase 1 or by incubation of cells in the absence of Erk-2.[98] Evidently, phosphorylation by Erk-2 provides an inhibitory effect on PDE4D3 activity.

The interplay of PKA and Erk-2 phosphorylation of PDE4D3 causing increasing and decreasing catalytic activity, respectively, provides an interesting mechanism by which cAMP levels are regulated. Hoffman et al.[98] pursued this dual-phosphorylation mechanism by demonstrating that Ser13→Asp and Ser54→Asp mutations, mimicking constitutively phosphorylated PKA residues, were still available for Erk-2 dependent phosphorylation at Ser579. Similarly, the Ser579→Asp mutation, mimicking Erk-2 mediated phosphorylation, remained accessible to PKA-mediated phosphorylation at Ser13 and Ser54. Functionally, phosphorylation by PKA was shown to override Erk-2 phosphorylation by returning PDE4D3 to control levels in wild-type cells.[98] This dual-phosphorylation of PDE4D3 may provide a possible mechanism to allow cAMP to build up following Erk-2 phosphorylation and then decrease due to PKA phosphorylation. Some controversy does surround this idea as Baillie et al. showed that PDE4B1 and C2 isoforms were available for Erk-2 phosphorylation at analogous residues to PDE4D3's Ser579 (residues Ser659 and Ser535, respectively) causing suppressed activity, while

PDE4A isoforms were not phosphorylated at all.[99] To complicate matters further, transfected and endogenous PDE4B2, a 'short' PDE4 isoform, responded with increased activity in a series of studies consistent with Erk-2 mediated phosphorylation at analogous Ser579 residue Ser487. The importance of 'short' and 'long' isoform length to differential regulation by phosphorylation may owe to the interaction of available upstream conserved regions (UCRs),[100] unique to the PDE4 isoform,[68] as the PKA-mediated phosphorylation of Ser54 of the UCR1 domain in PDE4D3 caused a reduced interaction with the UCR2 domains.[101]

### *1.1.7.4 Chronic PDE Regulation*

Sustained cAMP elevations increase PDE4 content through increased *de novo* protein synthesis that is mediated by PKA. In response to cAMP binding PKA, the PKA catalytic subunit is able to passively diffuse into the cell nucleus, gaining access to cellular DNA.[102] While in the cell nucleus, catalytic PKA subunits are capable of phosphorylating the cAMP response element binding (CREB) protein at Ser133.[103] Phosphorylation of CREB recruits CREB binding protein (CBP)[104] allowing transcription through its association with RNA polymerase II.[102] This is supported by increased cAMP concentrations leading to elevated reporter gene expression of PDE4D5 in hamster ovary, with mutation at site -201 of CREB disrupting the effect.[105] Cultured vascular smooth muscle cells treated with forskolin increased PDE3A, PDE3B and PDE4D mRNA levels in aortic and femoral preparations, while a similar effect was noted with db-cAMP increasing protein levels of the same PDE isoforms.[106] PDE4D1 and D2 isoforms are also known to be regulated in a similar fashion.[107]

## *1.2 Imaging PDE4 with (R)-[$^{11}$C]Rolipram Positron Emission Tomography*

### 1.2.1 Positron Emission Tomography

Positron emission tomography (PET) is a non-invasive, *in vivo* nuclear imaging modality used to assess a variety of physiological processes in living organisms.[108,109] Compounds of known biologic function can be labeled with a positron emitting isotope, such as carbon-11, oxygen-15, fluorine-18 or ammonia-13[108,109] that can be detected by the camera apparatus (figure 1.7, panel C) and used to quantify the tissue distribution of the labeled compound after image reconstruction (figure 1.7, panel B) and analysis. Quantifying the radiotracer distribution in the body gives a measure of the physiologic process being evaluated in the tissue of interest.

#### *1.2.1.1 Small Animal PET Imaging*

Small Animal PET technology (figure 1.7, panel D) has been developed for application of PET imaging in smaller animals, such as mice and rats, for the purpose of preclinical and research-related imaging. Given the difference in size of small animals compared to humans, dedicated small animal PET scanners are designed for optimal resolution and sensitivity with smaller subjects.[110] Imaging of small animals allows *in vivo* experimentation on a number of genetic, pharmacological and surgical models of disease,[108] facilitating the transition from basic research to clinical phases. Further, PET imaging offers the added benefit of using fewer animals to complete studies as tissue tracer distribution and retention can be assessed in a non-invasive and non-terminal

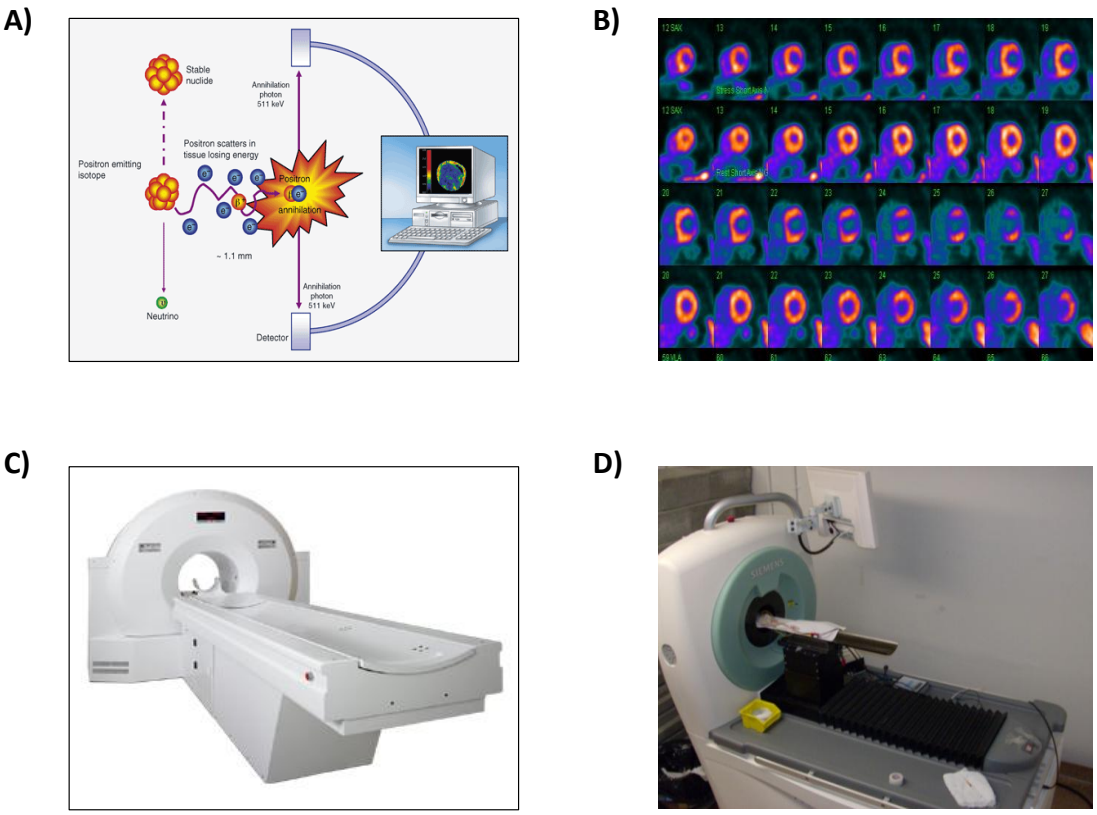


**FIGURE 1.7. A)** Schematic overview of the principle behind PET imaging. **B)** Reconstructed cardiac PET 18-flurodeoxyglucose images at stress (row 1 and 3) and at rest (row 2 and 4) demonstrating a defect of the left ventricle wall that is only visualized during increased cardiac output. **C)** Siemen's human PET camera. **D)** Siemen's small animal PET camera at the University of Ottawa Heart Institute.

approach, leaving the animal intact and to be used again in retest studies as its own control.[111]

### 1.2.2 Principle of PET Imaging

The principle of PET imaging relies on the ability to label compounds with a positron emitting isotope whose predictable nature of decay is exploited to delineate the localization of the injected compound in the body.

Positron emitting isotopes are defined by the property of radioactive decay by positron emission.[112] Following a decay event, the emitted positron is capable of travelling a short distance (figure 1.7, panel A) dependent on its kinetic energy which is related to the isotope from which it was emitted.[109,112] While the positron travels, its kinetic energy diminishes and its momentum slows to a point at which it can interact with an electron particle. This interaction is known as an 'annihilation event' and results in the destruction of both particles, converting their energies into a pair of gamma photons that travel in nearly opposite directions to one another with precisely 511 KeV of energy.[112] The camera (detector) component to the system is a scintillation crystal which is capable of registering the arrival of the photon and converting it into an electrical signal that can be interpreted by the reconstruction software. Importantly, the arrival of each photon at two detectors, directly opposite of one another, allows for a line of response to be determined – that is, an imaginary line connecting two detectors oppositely positioned on which the annihilation event *must* have occurred.[112] The reconstruction software estimates where the positron originated from based on its terminal location (site of the annihilation event along the line of response) and kinetic energy (ability of the positron to

travel). From this deduction, the signal can be localized to a specific region in the camera's field of view.

### 1.2.3 Quantification in PET

#### *1.2.3.1 Arterial Input Function*

The arterial input function is critical to accurate quantitative analysis of PET imaging.[113] The input function represents the time-course of radioactivity present in the blood plasma and available for targeted tissue uptake. While PET measurements and blood sampling techniques can measure radioactivity present in the blood, not all activity circulating in whole blood can be extracted for tissue-specific uptake.[113,114] Thus, the input function represents the proportion of total circulating radioactivity available for specific binding.

Radioactivity in circulating blood is comprised of four components: 1) activity associated with unchanged parent tracer in plasma, 2) activity associated with carbon-11 labeled metabolites in plasma, 3) activity associated with labeled tracer and metabolites in blood cells and, 4) activity bound to plasma proteins.[113,114] Optimally, only the first component – radioactivity of unchanged parent tracer in plasma – is quantified for the arterial input function as it is the only component available for extraction to tissue and specific binding. Conversely, activity associated with the hematocrit is considered unavailable for extraction as red blood cells and other pellet constituents sequester the activity and prevent specific uptake.[113,114] The same applies to the fraction of activity that is plasma protein bound.[113,114] Further still, circulating carbon-11 labeled metabolites of

the parent tracer need to be accounted for, even if they are not expected to bind in the same fashion as authentic parent compound.[113,114]

In sum, three components – activity sequestered in blood cells, plasma protein bound tracer and carbon-11 labeled plasma metabolites – act to dilute the activity available for targeted uptake. Ideally, to achieve meaningful quantification, these pools of activity should be differentiated from the unchanged parent radiotracer in plasma to avoid underestimating the true tissue uptake and retention of the radiotracer.

#### *1.2.3.2 Specific Activity and Injected Mass*

Prior to addressing the implications of receptor occupancy – a critical consideration for quantification in small animal PET (section 1.2.3.3) – it is important to discuss the concepts of specific activity (SA) and injected mass. SA refers to the amount of radiolabeled compound relative to the total amount of compound (expressed as activity/concentration – MBq/μmol, for example) in a formulation. Thus, radiotracer formulations with 'high SA' have a greater proportion of labeled compound to total compound compared to lower SA formulations as a consequence of radiosynthesis production.[112] Alternately, the term injected mass refers to the quantity of unlabeled compound coadministered to the subject within the radiotracer formulation and describes the relationship between the injected activity, SA and body mass (i.e. a dose – mg/kg, for example). Indeed, these related concepts arise from the inability to label a compound with a 100% success rate. In the case of carbon-11 labeled radiotracers, this is owed to the fact that carbon-12 is exponentially more prevalent in nature than is carbon-11 and even the 'tightest, cleanest' systems are subject to carbon-12 contamination.

Ultimately, SA is an indication of radioactivity concentration, while injected mass is a measure of the quantity of unlabeled compound injected per subject weight.

### *1.2.3.3 Receptor Occupancy and Tracer Doses*

Quantitative PET assessment requires that the target site not be significantly occupied by the injected mass coadministered with the radiotracer formulation. In human studies, this concept is relatively negligible due to the large size of humans diminishing the relative amount of injected mass.[115] However, with small animals, such as mice and rats, this consideration becomes decidedly influential,[116,117] as the ratio between rat and human body weight is ~ 1:280.[117]

Receptor[a] occupancy issues with small animals arise because of the difficulty in producing an image with similar quality to that of human cameras. To maintain image quality, small animal cameras require the same number of total detection events as in human scans; this implies that greater camera sensitivity is needed with small animals, or else the amount of tracer administered needs to be similar to that which is given to humans.[117] Thus, administering a similar amount of injected activity to a rat compared to a human would result in an injected mass of ~280 times greater, possibly (and very likely) saturating vulnerable receptor systems. Dedicated small animal cameras are better suited in terms of sensitivity and resolution, however, not sufficiently so as to reduce the amount of injected activity to the proportionate level (injected activity : body weight) seen in humans.[109] This excess of injected mass can only be limited by marked increases

[a] *In section 1.2.3.3, the term 'receptor' does not refer the classical concept of a plasma membrane receptor, rather, it describes the saturable target protein of the radiolabeled compound, which may include enzymes, plasma membrane receptors, or biological substrates, for example.*

in SA of the radiotracer formulation, or else the injected activity must be reduced at the sacrifice of image quality.[117]

Receptor occupancy, then, refers to the percentage of total receptors occupied by the injected mass.[116] Accurate quantification of the binding potential of the radioligand requires that the occupied receptor sites scale in a linear, 1:1 ratio with the injected activity, representing a set of first order kinetics. To ensure that this condition is met, radioligand studies are restricted to 'tracer doses' of the injected compound. A tracer dose is defined as the amount of injected mass which occupies 1-5% of the total receptor population, indicating that 1) its effect on the native biological system is negligible, and 2) that the receptor population available for specific binding is proportionate to the injected radiotracer. Indeed, a tracer dose is contrasted by the larger 'clinical dose', which would describe the dose to achieve a clinically significant outcome for a given compound.

The above theory is put into practice quite regularly in tracer characterization studies, but is highlighted methodically in the following reports.[117-119] Alexoff et al. report a distribution volume ratio (relationship between specifically bound to non-specifically bound ligand) of 2.43 in high SA studies (< 1.5 nmol/kg injected mass) of [$^{11}$C]-raclopride in rat brain, with the finding that lower SA, correlating to injected masses > 1.6 nmol/kg had a statistically significant reduction in distribution volume ratio.[118] Jagoda et al. report a similar finding with the saturable serotonin receptor and [$^{18}$F]-FCWAY, demonstrating that addition of 50 nmol injected mass reduces the differential uptake ratio by ~75% compared to baseline, while addition of 200 nmol injected mass reduced the differential uptake ratio even further to 10% of baseline.[117]

Finally, Fujita et al. describe (*R*)-[$^{11}$C]rolipram produced with high SA (71 GBq/μmol) demonstrating specific binding in the rat brain, while low SA (0.19-0.38 GBq/μmol) formulations mimicked characteristics of non-specific binding,[119] such as diffuse and uniform distribution.

### 1.2.4 (*R*)-Rolipram

(*R*)-Rolipram (*(R)*-4-(3-cyclopentyloxy-4-methoxyphenyl-2-pyrrolidone), a PDE4 selective inhibitor,[120] has previously been labeled with carbon-11[121] with the aim of using it as an *in vivo* PET imaging agent. As a therapeutic agent, it was shown efficacious as an anti-depressant with comparable outcomes to imipramine at 14-28 days,[122] but has since being discontinued from clinical practice due to associated side-effects (emesis and nausea)[123,124] at high, clinically effective doses (0.75 mg, 3 times daily).[122] *(R)*-Rolipram has a 10- to 30-fold higher affinity to PDE4 than does the S-enantiomer and[125] binds stereospecifically to the active $Mg^{2+}$-PDE4 HARBS complex.[90,126] This binding inhibits its hydrolytic ability without being a substrate for the catalytic domain.[125,127]

#### *1.2.4.1 (R)-[$^{11}$C]Rolipram Characterization of Selectivity and Specificity*

Previous work performed in our lab supports the use of *(R)*-[$^{11}$C]rolipram (figure 1.8) for *in vivo* small animal PET imaging of rats. *Ex vivo* biodistribution characterization studies of the radioligand in male Sprague Dawley rats demonstrated *(R)*-[$^{11}$C]rolipram to be selective for PDE4 by pharmacologic delineation using PDE1-5 inhibitors.[128] (*R*)-[$^{11}$C]Rolipram was also shown to bind specifically in a variety of organs including the heart, brain, skeletal muscle, lung and pancreas by method of competitive blockade using 1 mg/kg (*R*)-rolipram. This approach reduced (*R*)-[$^{11}$C]rolipram tissue retention by 80%

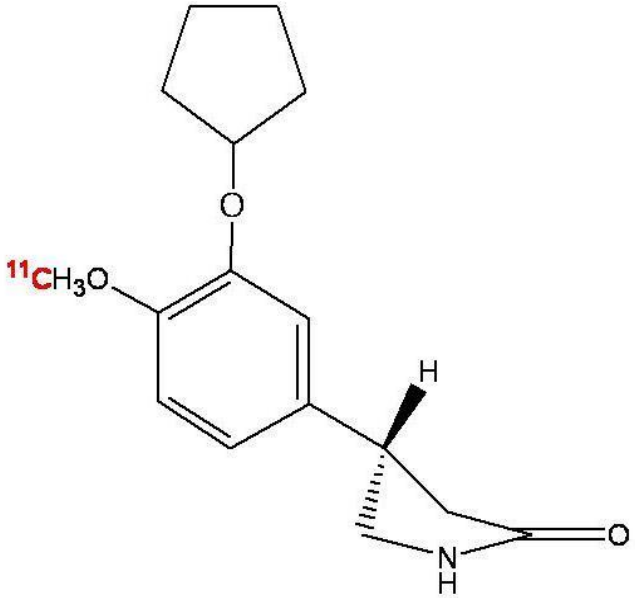


**FIGURE 1.8.** *(R)*-[$^{11}$C]Rolipram chemical structure; [$^{11}$C] label is highlighted in red.

in the brain and ~30% in the left ventricle, with an $ED_{50}$ of 0.03 reported in both tissues.[128] Finally, (*R*)-[$^{11}$C]rolipram was shown sensitive to desipramine (a NE reuptake transport inhibitor) challenged rats (20 mg/kg, 3 hours prior to tracer injection), revealing a 21.6% increase in PDE4-specific binding of *(R)*-[$^{11}$C]rolipram in the left ventricle.[129]

#### *1.2.4.2 (R)-[$^{11}$C]Rolipram Metabolism*

High performance liquid chromatography (HPLC) was used to evaluate the radioligand metabolism in blood plasma and the heart.[130] Unchanged tracer in plasma at 30 and 45 minutes represents 28% and 25% of the radioactivity signal respectively. In the heart at 45 minutes post-injection, 44% of radioactivity signal detected is accounted for by labeled metabolites that do not specifically bind to PDE4, 15% by nonspecific binding and the remaining 41% by PDE4-specific binding. Lastly, no labeled metabolites were detected in brain tissue, indicating that (*R*)-[$^{11}$C]rolipram metabolites do not cross the blood-brain barrier. These findings indicate that (*R*)-[$^{11}$C]rolipram undergoes significant metabolism within a relatively short time period and needs to be accounted for in PET image quantification (section 1.2.3.1).

### 1.2.5 (*R*)-[$^{11}$C]Rolipram PET: General Imaging

In addition to the *ex vivo* and *in vitro* characterization studies performed by our laboratory, a collection of studies explores the potential of *in vivo* (*R*)-[$^{11}$C]rolipram PET imaging.

The first of these *in vivo* studies documenting (*R*)-[$^{11}$C]rolipram PET occurred in the *rhesus* monkey with promising results.[131] (*R*)-[$^{11}$C]Rolipram was specifically bound in the cortical regions, striatum, hippocampus and thalamus of the monkey brain. This

tissue retention was reduced by SCH23390 (a dopamine receptor antagonist) pre-treatment and potentiated by methamphetamines, indicating (*R*)-[$^{11}$C]rolipram sensitivity to dopaminergic stimulation.[131]

A year later, DaSilva et al.[132] applied (*R*)-[$^{11}$C]rolipram PET to humans, finding the human brain displayed high radioactivity accumulation in the cerebellum, striatum, thalamus and prefrontal cortex (figure 1.9) that peaked after 10 minutes and was subject to a prolonged, slow washout over the remaining 80 minutes of the scan,[132] which was in good agreement with Tsukada et al.[131] Since tracer retention was visualized throughout the entire brain, a reference region could not be defined, resulting in the need for compartmental modelling. To this end, the time activity curves (TACs) in this study were well-fit to a two compartment model. Finally, metabolism of parent tracer in plasma was relatively stable from 15-60 minutes, as ~60% of unchanged parent compound persisted over this period with significant plasma protein binding (96%) determined.[132]

Three years following this study in humans, a series of studies at the National Institute of Mental Health (NIMH) were published between 2005 and 2010, investigating (*R*)-[$^{11}$C]rolipram small animal PET in rat.[119,133-135] Fujita et al. 2005,[119] was the first of these, using (*R*)-[$^{11}$C]rolipram to quantify PDE4 in the brain. They report that (*R*)-[$^{11}$C]rolipram produced with high SA (71 GBq/μmol) displayed tissue uptake consistent with specific binding, while low SA (0.19-0.38 GBq/μmol) (*R*)-[$^{11}$C]rolipram and high SA (55-71 GBq) (*S*)-[$^{11}$C]rolipram images had diffuse, non-specific binding profiles (figure 1.10), with percent of standardized uptake value (%SUV) in high SA (*R*)-[$^{11}$C]rolipram images greater at all time points.[119] The high SA (*R*)-[$^{11}$C]rolipram experiments showed peak uptake times of 5-10 minutes in the caudate putamen,

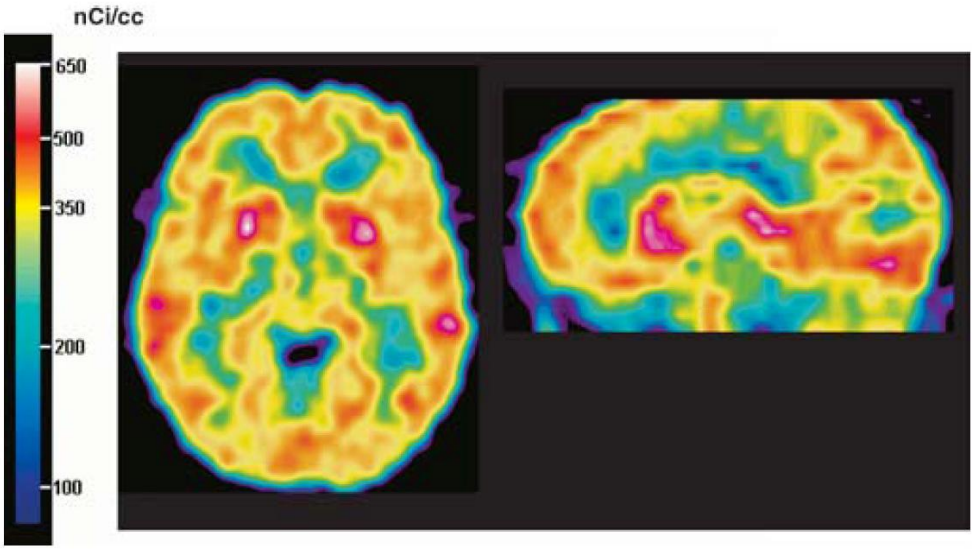


**FIGURE 1.9.** *(R)*-[$^{11}$C]Rolipram reconstructed PET image of the human brain from a 90 minute scan; transverse (left) and sagittal (right) orientations are shown. Reproduced from DaSilva et al., 2002.

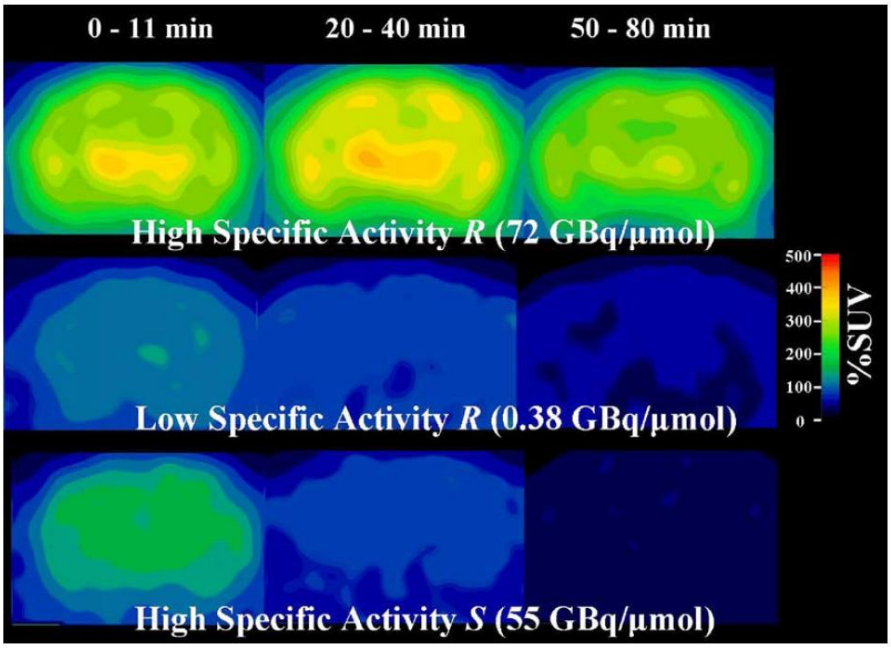


**FIGURE 1.10.** Reconstructed PET images of rat brain with high SA (*R*)-[$^{11}$C]rolipram (top), low SA (*R*)-[$^{11}$C]rolipram (middle) and high SA (*S*)-[$^{11}$C]rolipram (bottom). Reproduced from Fujita et al., 2005.

thalamus, hypothalamus, hippocampus, parietal cortex and midbrain, with activity at the end of the scan still at 38-52% the peak radioactivity in these regions.[119] These findings highlight the importance of SA and enantiomer choice, as the higher specific studies were representative of specific binding in the rat brain, while the S-enantiomer was consistent with non-specific binding, even at high SA.

The above study was expanded on in 2007 with the effect of antidepressant imipramine studied on (*R*)-[$^{11}$C]rolipram rat brain uptake.[133] They found that chronic imipramine treatment via osmotic mini-pump did not alter (*R*)-[$^{11}$C]rolipram brain uptake, nor did treatment alter PDE4A/B/D isoform expression by *in vitro* measure using immunoblotting. This result was unexpected given that antidepressant treatment is believed to be effective on the basis of stimulating cAMP production, which in turn elevates PDE4 presence.[136]

The series of studies from NIMH concludes at present with a pair of studies by Itoh et al.[134,135] where the influence of conscious vs. unconscious state is explored in rats using (*R*)-[$^{11}$C]rolipram small animal PET imaging. They determined that $B_{max}$ in conscious rats is ~30% greater than anaesthetized controls, accompanied by a ~60% increase in disassociation constant ($K_d$) value.[134] This anaesthetic-dependent effect is well noted in PET animal studies,[109-111] as anaesthesia is known to have a significant impact on the respiratory and cardiovascular systems. Continuing with their work in conscious rat brain, they found unilateral administration of PKA activator or inhibitor (db-cAMP or Rp-cAMP, respectively) caused increased and reduced (*R*)-[$^{11}$C]rolipram brain radioactivity, elegantly demonstrating the tight relationship between PKA and PDE4 using an *in vivo* approach.[135]

In addition to the NIMH rat brain studies, experimentation was also completed in pigs[137] and canines.[138] Parker et al. demonstrate the higher affinity for the (*R*)-enantiomer using *in vivo* PET and *in vitro* autoradiography in pig brain, with a finding that the affinity ratio between the two was ~8 *in vitro* and 12.5 *in vivo*, allowing for reasonable extension of *in vitro* findings to the *in vivo* setting.[137] Alternately, Lortie et al. studied the kinetic modelling of (*R/S*)-[$^{11}$C]rolipram in canine hearts, with a finding that a two-compartment model, with or without a parallel compartment to account for labeled metabolites, provided a very good fit to the data and describe the tracer kinetics well.[138]

### 1.2.6 (*R*)-[$^{11}$C]Rolipram: Application in Disease States

(*R*)-[$^{11}$C]Rolipram has been used by our laboratory group to investigate PDE4 in disease states where over active SNS stimulation is suspected to cause altered cell signalling.[139,140] Greene at al. evaluated PDE4 tissue biodistribution in diet-induced obese rats with the finding that basal levels of (*R*)-[$^{11}$C]rolipram are unchanged compared to diet-resistant controls, however, the normal response to desipramine challenge was absent in diet-induced obese animals in the heart and brain.[139] This study was followed by a 2010 report investigating adriamycin-induced cardiotoxicity in rat, with a similar finding that (*R*)-[$^{11}$C]rolipram basal levels in the heart were unaltered compared to controls, but the response to acute NE stimulation by desipramine challenge was ablated in the adriamycin treatment group.[140] These findings suggest that chronic SNS signalling as a result of obesity or cardiotoxicity affect the heart's capacity to respond to increased SNS output. This lack of response would be particularly detrimental in stress response situations where enhanced cardiac output is required and may be involved in poor cardiac outcomes in these conditions.

Indeed the above reports (sections 1.2.5 and 1.2.6) support quantification of PDE4 with (*R*)-[$^{11}$C]rolipram in a variety of species and disease states, with applicability in the brain and heart showing particular promise. Thus, we sought to apply this imaging technology to study the effect of type-2 diabetes mellitus on cardiac PDE4.

## *1.3 Application of (R)-[$^{11}$C]Rolipram Cardiac Small Animal PET in a Rat Model of Hyperglycemia*

### 1.3.1 Type 2 Diabetes

Type-2 diabetes mellitus (T2DM), defined by fasting plasma glucose levels greater than 7 mM, is caused by insulin resistance – the reduced ability of cells to respond to insulin signaling – and hypoinsulinemia. Under normal conditions, insulin acts to increase the glucose uptake rate into muscle and adipose tissue through the insulin receptor.[141,142] Stimulation of the insulin receptor recruits glucose 4 transporters (Glut-4) to the plasma membrane mediating the removal of glucose from the blood,[141-143] and dysregulation of this signaling pathway leads to altered glucose handling and the development of T2DM.

β-cells of the pancreas are responsible for endocrine release of insulin in response to elevated blood-glucose levels in the fasting and post-prandial state.[144] In the case of developing T2DM where hyperglycemia prevails, β-cells overproduce insulin to overcome the elevated glucose levels in the blood. This excess of circulating insulin leads to a hyperinsulinemic state and causes overactivation of the insulin receptor.[145,146] Over time, chronic receptor activation results in desensitization and downregulation of the insulin receptor,[145,146] negatively impacting the already hyperglycemic environment. Further, as the β-cells continue to overproduce insulin they begin to exhaust and endocrine function deteriorates; T2DM in obese and lean humans is associated with 40-60% decreased β-cell mass, and 3-10-fold increases in β-cell apoptosis.[147] Ultimately, these events lead to the transition from a hyperinsulinemic to a hypoinsulinemic state. In

this final stage of disease progression, hypoinsulinemia and receptor insensitivity combine to hinder glucose clearance further leading to full onset of the pathologic state.

### 1.3.2 T2DM and Cardiovascular Disease

A distinct and negative relationship exists between the heart and diabetes, whereby diabetes confers a 2-4 fold increase in coronary heart disease (CHD)[148] and diabetes increases heart failure mortality by 1.5-2 times that of non-diabetics.[149] Approximately 70% of T2DM volunteers showed LV hypertrophy as measured by echocardiography,[150] suggesting strong ties between pathology and cardiac function. To this end, a wealth of knowledge implicates vasculature[151] and metabolic[152] changes as part of the source of excess cardiovascular disease (CVD) in T2DM, while altered cardiac signaling,[3] such as seen in diabetic cardiomyopathy – a form of cardiac hypertrophy independent of atherosclerosis or hypertension – implicates the heart directly and will be focused on herein.

#### *1.3.2.1 Role of T2DM Altered Cell Signaling in CVD*

Downregulation of the β-AR population in the diabetic heart is consistently observed and is at the root of altered cell signaling in the myocyte. In the case of moderate-dose (45-50 mg/kg) streptozotocin (STZ)-dependent diabetic animal models, it appears that a total β-AR reduction may be observed,[153] with the $\beta_1$-ARs subtype reduced in number, [154] while $\beta_2$-AR expression is increased.[155] Similar observations are made with high dose (≥ 65 mg/kg) STZ[22,23,156-158] and Alloxan[159] animal models.

The reduction in β-AR population has a detrimental effect on downstream targets of the SNS signaling cascade demonstrated by reduced β-AR-dependent cAMP activity in the diabetic state.[160,161] This is best evidenced on the basis of impaired calcium handling[3] by reduced output at the sarcoplasmic reticulum,[162] ryanodine receptor,[163] SERCA2a $Ca^{2+}$ ATPase[164] and L-type $Ca^{2+}$ channels.[165] The importance of these proteins was discussed above (sections 1.1.4.1 and 1.1.4.2), with each of these targets playing important roles in normal cardiac contraction. Thus, it is not surprising to find that functional cardiac deficiencies follow these biochemical changes, such as impaired fractional shortening (45% reduction compared to controls) pairing with a reduction in $Ca^{2+}$ current by 38% shown in diabetic mouse cardiomyocytes.[165]

### 1.3.3 SNS Pressor Effect and Increased NE in T2DM

The basis for SNS-dependent alteration in cardiac myocyte signaling may arise from several factors that are typically present in T2DM. For example, obesity was found to be an independent predictor of increased myocardial oxygen consumption[166] and the development of T2DM.[167] High body mass index (BMI) and caloric intake, often present in a T2DM population, were independently associated with increased 24-hour urinary NE excretion, an indicator of SNS activity.[168] Similarly, in T2DM patients plasma NE was elevated 6-fold over controls, while E was elevated 10-fold.[169] In STZ diabetic rats at 11-13 weeks, a 3-fold increase in cardiac-specific NE and 1.5-fold increase in E is reported,[170] which is echoed by Paulson and Light at 12 days, though they did not observe a significant difference in E.[171] Further, though no significant differences were noted at 2 and 4 weeks post-STZ treatment, significant elevations in NE were observed at 8 weeks.[172] This may in part be owed to the fact that the presence of insulin stimulates

sympathetic activity and that this occurs in the normal physiologic range.[173-175] Indeed, insulin resistance independently predicted increased myocardial fatty acid uptake, utilization and oxidation, indicating reduced cardiac efficiency.[166] Added to this is the evidence indicating that glucose is a promoter of NE release[176, 177] further implicating the unhealthy diet and insulin resistance in enhanced SNS activity.

#### *1.3.3.1 Expected Changes in PDE4 due to SNS Pressor Effect in T2DM*

Given the above findings of increased NE exposure to the heart, decreased $\beta_1$-AR presence and reduced cAMP signaling, it can be postulated that PDE4 may be reduced in reciprocal given the intimate regulation of PDE4 expression and activity by cAMP. Though this field of research is quite limited, a pair of studies lend support to the idea of hyperglycemia-induced PDE4 cardiac deficiencies.[178,179] A 25-35% reduction in cAMP breakdown was seen in a STZ rat model of diabetes in Langendorff perfused hearts.[178] In agreement, hydrolysis of cAMP in rat hearts of Alloxan-induced diabetics was reduced by 33%.[179] Unfortunately, neither study investigated the role of PDE4 expression, leaving their findings to hydrolytic activity alone. Beyond this, studies of T2DM-dependent alterations in cAMP hydrolysis are limited to non-cardiac tissues, including reductions in adipose tissue,[180] liver,[181] and lung.[182]

#### *1.3.3.2 Role of Other Intracellular Signalling Pathways*

It is possible that a variety of intracellular signaling pathways or players may be altered in parallel to the hypothesized changes in the cAMP-PKA-PDE4 signaling axis. cGMP, protein kinase C and/or Erk-2, for example, may also accompany the changes in

the cAMP-PKA-PDE4 axis given their often overlapping roles. Activation of Erk-2 by β-arrestin (figure 1.2) following β-AR overactivation demonstrates the type of feedback interactions that can take place to recruit additional signaling pathways upon β-AR stimulation. Possible changes in these parallel pathways could act to either blunt or enhance the changes at the PDE4 level, but the exact affect is unknown and is beyond the scope of this thesis discussion.

### 1.3.4 Streptozotocin-Induced Model of Hyperglycemia

The high fat diet-fed (HFD), moderate-dose STZ induced rat model provides a platform for studying the chronic response of PDE4 to increased NE, reduced β-AR population, overt hyperglycemia and insulin resistance[154] – all defining characteristics of late stage progression of untreated T2DM.

STZ (2-deoxy-2-([(methylnitrosoamino)carbonyl]amino)-D-glucopyranose) is a pancreatic β-cell glucose analog that acts as a DNA alkylating agent used for the selective necrosis of β-pancreatic cells and is used as a pharmacologic diabetogenic agent.[183] Upon STZ treatment, selective uptake of STZ by the β-cell occurs via glucose transporter 2 (Glut-2) leading to a triphasic response to plasma glucose (figure 1.11).[183] In phase one (1-5h following injection), blood glucose rises in response to the inability of pancreatic β-cell to secrete insulin. Phase two (5-10h) is characterized by a marked reduction in plasma glucose due to β-cell lysis which releases large stores of insulin into the bloodstream.[183] In the final phase (48-72h), chronic hyperglycaemia is induced as the high insulin levels experienced in phase two diminish and the lack of functional β-cells becomes truly apparent.[183]

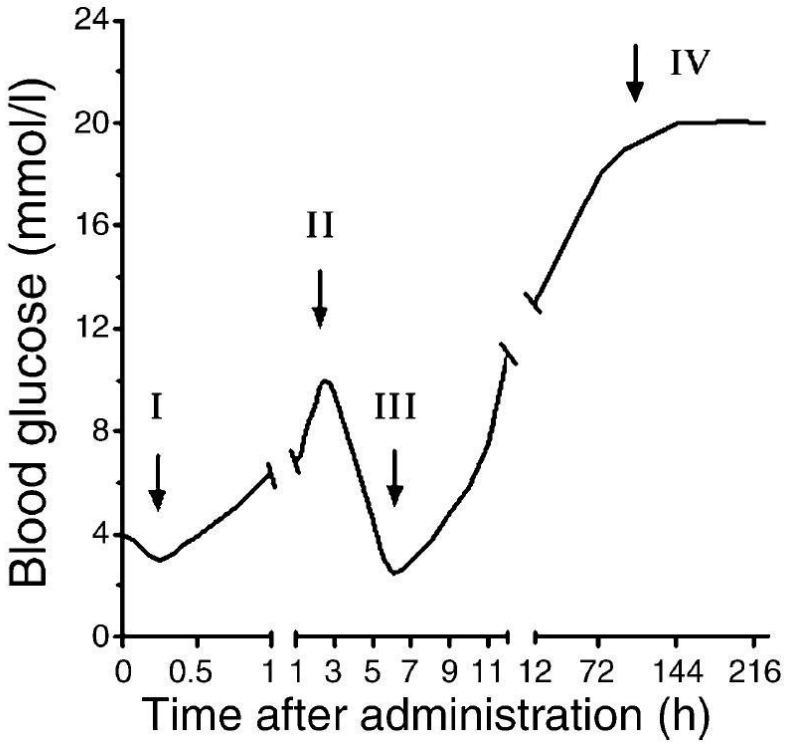


**FIGURE 1.11.** Phasic blood glucose response to a diabetogenic dose of alloxan (tetraphasic, I–IV) or streptozotocin (triphasic, II–IV; the first phase does not develop in the case of streptozotocin;). Reproduced from Lenzen, 2008.

Although STZ is sufficient for causing overt hyperglycaemia, a second, and critical, aspect to T2DM is insulin resistance which is not conferred by STZ administration alone. To achieve the combined effect of hyperglycemia and insulin resistance, STZ treated rats are maintained on a HFD as elevated circulating fats lead to insulin resistance,[184-186] through interactions involving the Randle-cycle.[187,188] Indeed, rats receiving 45 mg/kg STZ and fed a HFD are a model for late-stage T2DM[189-191] and the model is well characterized by our own group.[154]

## *1.4 Project Aim*

The above observations collectively point to the role of hyperglycemia and insulin resistance in T2DM impacting cardiac cell signalling at the molecular level, providing the basis for the current scientific investigation. It is hypothesized that there will be a reduction in the cAMP-specific hydrolyzing PDE4 population paralleling the decrease in β-AR expression and cAMP activity seen in T2DM. Further, consistent with the ablation of desipramine response in diet-induced obesity and adriamycin cardiotoxicity, it is anticipated that the heart will be non-responsive to acute NE challenge, demonstrating the SNS's inability to modulate cardiac output in this disease state. This hypothesis will be tested in the moderate-dose STZ/HFD rat model of hyperglycemia and insulin resistance using the PDE4-specific radioligand (*R*)-[$^{11}$C]rolipram and PET imaging.

Thus, it is the overall aim of this thesis to 1) characterize the radioligand (*R*)-[$^{11}$C]rolipram cardiac binding profile *in vivo* using small animal PET and 2) to apply (*R*)-[$^{11}$C]rolipram small animal PET to study intracellular signalling at the PDE4 level in the moderate-dose STZ/HFD rat model of hyperglycemia and insulin resistance.

# 2. Hypotheses & Objectives

## *2.1 Hypotheses*

(i) The *in vivo* characterization of the radioligand (*R*)-[$^{11}$C]rolipram will display positive imaging characteristics in the heart as measured by small animal PET including clear cardiac-to-background signal, specific binding to the PDE4 enzyme, susceptibility to enzyme occupancy by unlabeled (*R*)-rolipram and responsiveness to increases of the PDE4 enzyme by NE.

(ii) The T2DM state, as tested using the moderate-dose STZ/HFD rat model of hyperglycemia and insulin resistance, will result in decreased (*R*)-[$^{11}$C]rolipram cardiac binding due to elevated sympathetic tone causing a downregulation in the β-AR population, dampening cAMP-dependent accumulation and reducing the PDE4 presence and, further, resulting in (*R*)-[$^{11}$C]rolipram being unresponsive to increases in NE.

*NB: The scientific reports found under the heading 'In Vivo Tracer Characterization' (sections 3.2, 4.1 and 5.1) have been accepted for peer-reviewed publication to the Journal of Nuclear Medicine (2011), with myself as first author.*

## *2.2 Objectives*

### 2.2.1 *In Vivo* Tracer Characterization

(i) To correct the arterial input function for (*R*)-[$^{11}$C]rolipram small animal PET by quantifying the proportion of radioactivity accounted for by the carbon-11 labeled metabolites in blood plasma and determining the ratio of total radioactivity in plasma : whole blood.

(ii) To demonstrate reproducible (*R*)-[$^{11}$C]rolipram binding in the rat myocardium using small animal PET imaging.

(iii) To demonstrate that (*R*)-[$^{11}$C]rolipram myocardial retention is PDE4-specific and saturable with increasing doses of unlabeled (*R*)-rolipram using small animal PET.

(iv) To demonstrate that (*R*)-[$^{11}$C]rolipram retention increases in the myocardium of rats pre-treated with desipramine compared to controls using small animal PET.

## *2.3 Investigation of PDE4 Alterations in STZ/HFD-Induced Hyperglycemia*

(v) To demonstrate in hyperglycaemic, insulin resistant rats of the moderate-dose STZ/HFD protocol that there is reduced *in vivo* (*R*)-[$^{11}$C]rolipram PDE4 binding in the myocardium compared to controls that is not sensitive to elevations in NE.

(vi) To correlate *in vivo* (*R*)-[$^{11}$C]rolipram cardiac retention in moderate-dose STZ/HFD rats with *in vivo* measures of PDE4 expression and activity using immunoblotting (Western assay) and PDE4 enzymatic activity assay.

# 3. Methods

## *3.1 Materials*

Unlabeled (*R*)-rolipram was purchased from Ascent Scientific (New Jersey, USA) and was dissolved in ethanol : propylene glycol : 0.9% saline (5:20:75, v/v/v). Desipramine hydrochloride was purchased from Sigma-Aldrich (Toronto, ON) and dissolved in 0.9% saline. Streptozotocin was purchased from Sigma-Aldrich (Toronto, ON) and dissolved in 0.1 M citrate buffer (pH 4.5).

### 3.1.1 Radioligand Production

(*R*)-[$^{11}$C]rolipram was synthesized with the precursor (*R*)-desmethyl-rolipram (either produced in-house or purchased from ABX, Radeberg Germany) and *O*-methylated with [$^{11}$C]methyliodide produced from either lithium aluminum hydride and HI as described previously (figure 3.1),[121] or with [$^{11}$C]methane and iodine[192] to produce (*R*)-[$^{11}$C]rolipram in high radiochemical purity (> 95%), with low-to-high SA (7.4 to 315 GBq/μmol). The radiosynthesis procedure using lithium aluminum hydride results in lower SA (~11-55 GBq/μmol) of carbon-11 labeled radiotracer, as the production of $^{11}CO_2$ is prone to greater contamination by 'normal' $^{12}CO_2$ than is the alternate method using [$^{11}$C]methane and iodine (SA production of ~55-300 GBq/μmol). Semi-preparative HPLC (figure 3.2, panel A; Luna C-18 SCX column with flow of rate of 8 mL/min using 40/60 v/v acetonitrile/0.1M ammonium formate, retention time of ~6 mins) and analytical HPLC (figure 3.2, panel B; Luna C-18 SCX column with flow of 2 mL/min using 50/50 v/v acetonitrile/0.1M ammonium formate, retention time of ~3.5 mins) are used to purify

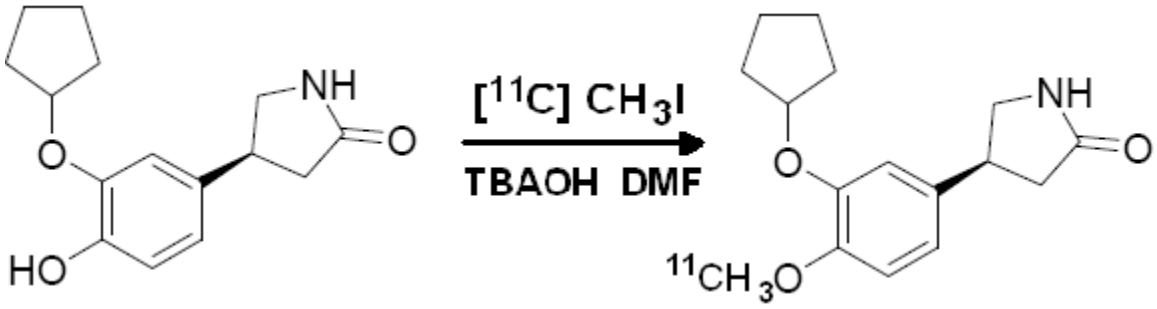


**FIGURE 3.1.** Synthesis of *(R)*-[$^{11}$C]rolipram from *(R)*-desmethylrolipram via O-[$^{11}$C]methylation.

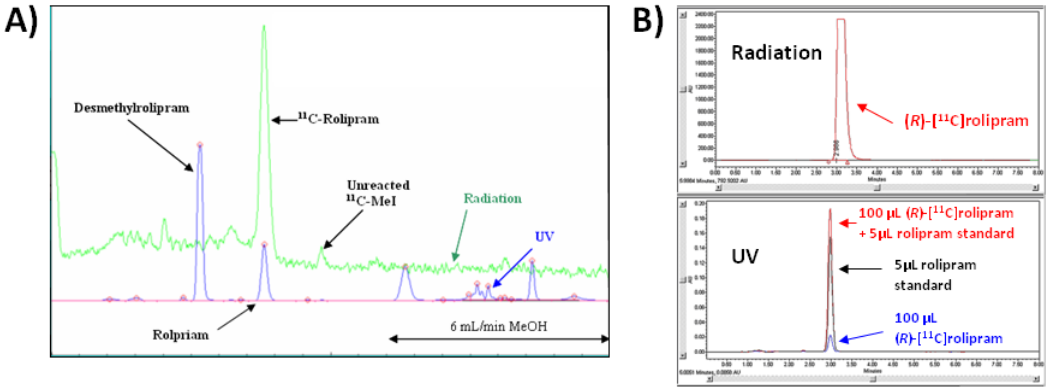


**FIGURE 3.2. A)** Representative chromatogram from semi-preparative HPLC purification of (*R*)-[$^{11}$C]rolipram. **B)** Representative chromatograms from analytical HPLC displaying pure (*R*)-[$^{11}$C]rolipram using UV detector (λ=280 nm; bottom panel) and inline radiation detector (top panel).

(*R*)-[$^{11}$C]-rolipram from unreacted methyl iodide, the precursor compound and associated by-products. SA is calculated by comparing the area under the curve of the analytical HPLC in a sample aliquot with that of a standard:

$$SA = (Act_{sample} \times AUC_{standard})/AUC_{sample} \times V_{sample} \times C_{standard})$$

Where AUC = area under the curve, V = volume and C = concentration.

[$^{13}$N]Ammonia is routinely produced in our radiochemistry facility for clinical and research applications using published protocols.[193,194]

#### *3.1.1.1 Quality Control*

Various quality control tests are in place to assure the purity and safety of the radioligand formulation. The physical quality of the produced solution is verified by testing the following: chemical and radiochemical purity (> 90%), pH (4.5 – 8.5), osmolality (290 ±30 mOs/kg), negative pyrogenicity, and solution sterility. These tests ensure the highest quality formulations are administered in the experimental protocols, enhancing animal safety and the reproducibility of the studies.

## *3.2 In Vivo Tracer Characterization*

### 3.2.1 Arterial Input Function

#### *3.2.1.1 Proportion of Activity in Whole Blood and Plasma*

Activity in whole-blood and plasma was measured in n=9 rats at serial time points (30 seconds, 1, 5, 20, 30, 45 and 60 minutes) to determine the proportion of radioactivity in plasma to whole-blood for the arterial input function correction. In preparation for blood collection, rats were treated with buprenorphine analgesic (0.04 mg/kg, i.p, 1 hour

prior to surgery) and anesthetised with 1-2% isofluorane. A cannula was inserted into the carotid artery and tied in place to allow for serial blood collection. (*R*)-[$^{11}$C]rolipram (1.1 – 66.6 MBq) was injected via the tail vein and arterial blood (150-300 μL) was collected in pre-weighed ethylenediaminetetraacetic acid (EDTA) Microvette tubes via a 4 way stop-cock connected to the cannulation line. Blood sample tubes were weighed and counted for activity in a gamma counter (Packard Cobra II Gamma Counter, MA, USA), back-corrected to the time of injection. Sample tubes were then centrifuged for 5 minutes at 4,000 x g, the supernatant collected, weighed and counted to determine the activity associated with blood plasma. Activity counts for both whole-blood and blood plasma were standardized by weight.

#### *3.2.1.2 Carbon-11 Labeled Metabolites in Plasma*

HPLC studies were performed to determine the proportion of radioactivity in plasma represented by unchanged *(R)*-[$^{11}$C]rolipram using methods previously described.[130] Previously published data from our lab by Kenk et al. 2008[130] was used to complete the plasma metabolite time course analysis by providing metabolite information at 30 and 45 minutes post-injection.

Rats received a high dose of *(R)*-[$^{11}$C]rolipram (300-370 MBq) and were sacrificed by decapitation at 5, 15, and 60 minutes (n=3 at each time point) for collection of trunk blood to assess carbon-11 labeled metabolites in blood plasma. Blood samples were centrifuged for 5 minutes at 4,000 x g, plasma fraction collected and double filtered through 0.22 um syringe filters to remove excess plasma components to ensure free-flow through the columns. Plasma was then loaded on the HPLC apparatus. Briefly, step 1 (0-

4 mins) (figure 3.3): solvent 1 (1/99 acetonitrile/water (v/v)) delivers the sample to the capture column packed with hydrophilic-lipophyllic balanced (Waters Oasis) solid phase sorbent. The eluent is analyzed serially by UV absorbence detection (Waters 486 Absorbance Detector, Waters Corporation, MA, USA) at 280 nm and dual bismuth germanium oxide (BGO) coincidence radiation detector (Bioscan, D.C., USA). After complete elution of non-retained sample, as indicated by UV recession to baseline, step 2 (4-6 mins) is initiated by switching both the six- and four- port valves to redirect the flow of solvent 1 to the waste and solvent 2 (45/55 acetonitrile/0.1M aqueous ammonium formate (v/v)) to the capture column to elute the trapped contents from the capture column onto the analytical column (Reversed Phase C18, Aqua 5 μm Phenomenex) and analyzed by the serial detectors. In step 3 (6-20 mins), after passage of the solvent front, the capture column is re-equilibrated under solvent 1 to prepare for the next injection. The retention time of authentic *(R)*-[$^{11}$C]rolipram is ~11.6 minutes (figure 3.4).[130]

### 3.2.2 PET Imaging Protocol

Rats were imaged using a Siemens Inveon DPET small animal PET camera (Knoxville, TN). This system has < 1.4 mm isotropic spatial resolution and > 10% absolute sensitivity). Animals were anaesthetized with 1-2% isofluorane, positioned supine and centered on the PET scanner bed with the heart in the center of the field of view. Heart rate, respiratory rate and body temperature were monitored throughout the experiment. [$^{13}$N]ammonia imaging was performed to quantify myocardial blood flow (MBF) and to assist with region-of-interest placement in co-registered (*R*)-[$^{11}$C]rolipram images. [$^{13}$N]ammonia is a PET tracer routinely used for the quantification of MBF in humans and animals[195] and has been validated at our facility.[196]

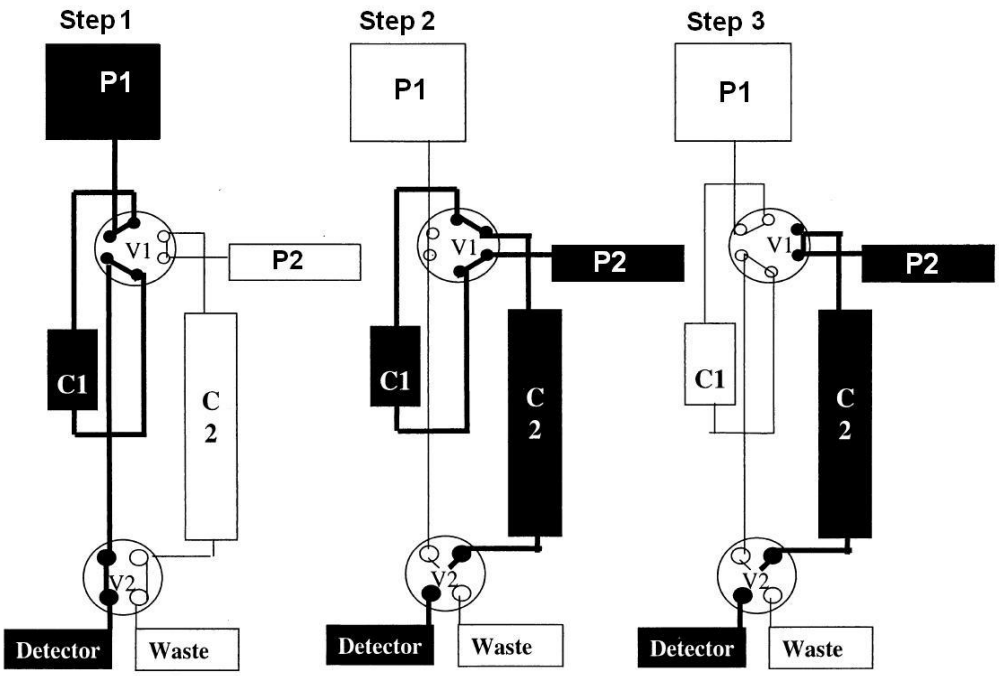


**FIGURE 3.3.** Schematic outlining the HPLC column-switch protocol. C1 = capture column, C2 = analytical column, P1 = pump 1 and P2 = pump 2. Adapted from Hilton et al, 2000.

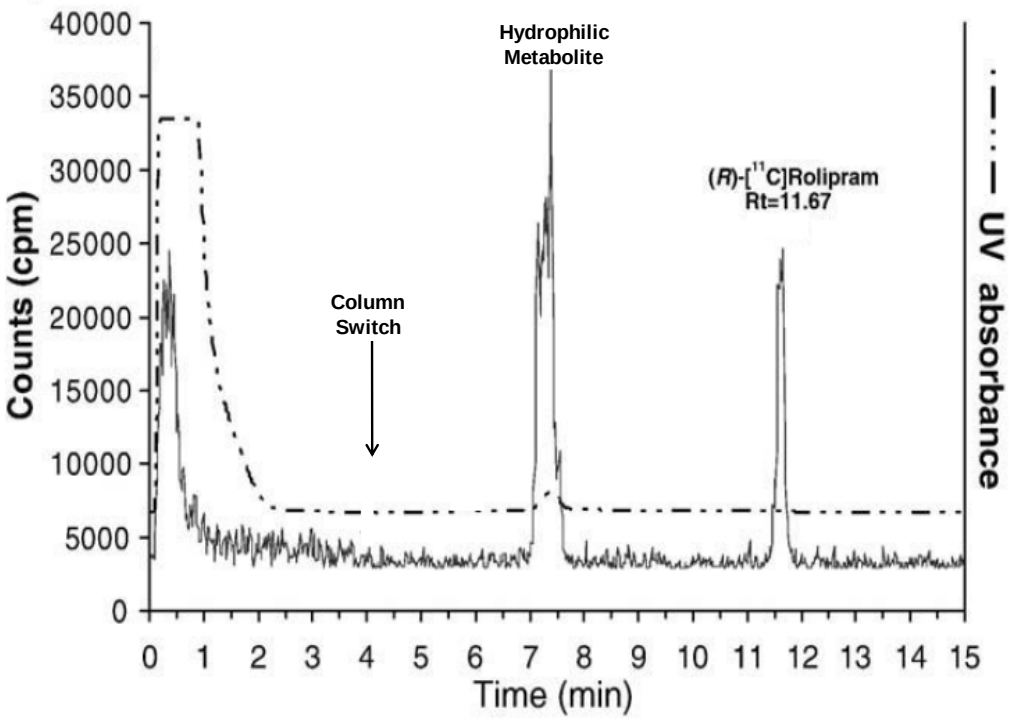


**FIGURE 3.4.** HPLC chromatogram of UV and radioactivity analysis revealing authentic *(R)*-[$^{11}$C]rolipram in rat plasma eluting at 11.67 minutes. Adapted from Kenk et al., 2008.

Dynamic [$^{13}$N]ammonia imaging was conducted over 30 minutes with 51.8 to 125.8 MBq (92.5 ± 24.8 MBq) injected activity, followed by a 30-minute washout period prior to *(R)*-[$^{11}$C]rolipram imaging. (*R*)-[$^{11}$C]rolipram (7.4 – 92.5 MBq) was administered as a single, slow bolus (~5 seconds) via tail vein. A 60 minute dynamic scan (9x10s, 3x30s, 2x60s, 5x300s) was started prior (1-5 seconds) to tracer injection to capture the rapid uptake kinetics of the tracer. To derive an attenuation correction, a $^{57}$Co transmission scan of 10 minutes was also conducted, either before or after rolipram imaging. Images of isotope concentration (Bq/cc) were reconstructed on a 128x128 matrix within a 10 cm transverse and 12.7 cm axial field-of-view using the vendor OSEM3D/MAP (β=1) algorithm with all corrections enabled.

### 3.2.3 Image Analysis

Image analysis was performed using FlowQuant© (University of Ottawa Heart Institute, Cardiac PET Center, ON, Canada) to generate time-activity curves of tracer concentration in arterial blood and polar maps representing left ventricle myocardial tracer uptake and clearance kinetics. (*R*)-[$^{11}$C]rolipram images were quantified with Logan slopes (mL/cm$^3$), derived graphically over the interval of 20-60 minutes post-injection using a constant partial-volume recovery coefficient of 0.6. The Logan slope is a function of free receptor or enzyme concentration, and provides an index of *in vivo* binding potential used in the study of reversibly bound tracers.[197,198]

Quantitative MBF values derived from [$^{13}$N]-ammonia scans were generated using a 1-tissue-compartment model and expressed as mL/min/g.[199]

Miran Kenk, PhD, is experienced in image analysis and contributed by confirming quantitative accuracy throughout this study by acting as a second image analysis operator.

#### *3.2.3.1 Logan Slope*

There are several PET quantification approaches currently practiced, each with their own applications, including: compartmental/kinetic modeling, reference tissue or graphical analysis methods.[114,200] Compartmental/kinetic modeling is based on mathematical estimates of rate constants (movement of radioactivity between hypothesized compartments) dependent on corrected input functions. Reference tissue approaches avoid the complication of correcting the arterial input function, but require a reference region where a background reading (non-specific binding) can be taken from. Finally, graphical analysis approaches, such as Patlak and Logan, compare the radioactivity of the input function against the radioactivity in the ROI until an equilibrium point is reached and then use the slope of the curve to estimate the receptor density.[198]

The Logan slope approach was used for quantitative analysis in these studies. Briefly, the Logan slope estimates the volume of distribution (DV) of reversibly bound radioligands. In the analysis process, the input function and data acquired from the ROI are transformed to express a linear relationship between arterial signal (input) and tissue (eventual output). This linear slope is dependent on the time point at which the intercept approaches a constant (t*), which occurs when equilibrium is reached between the exchange of activity between blood and the target tissue (figure 3.5, panel C).

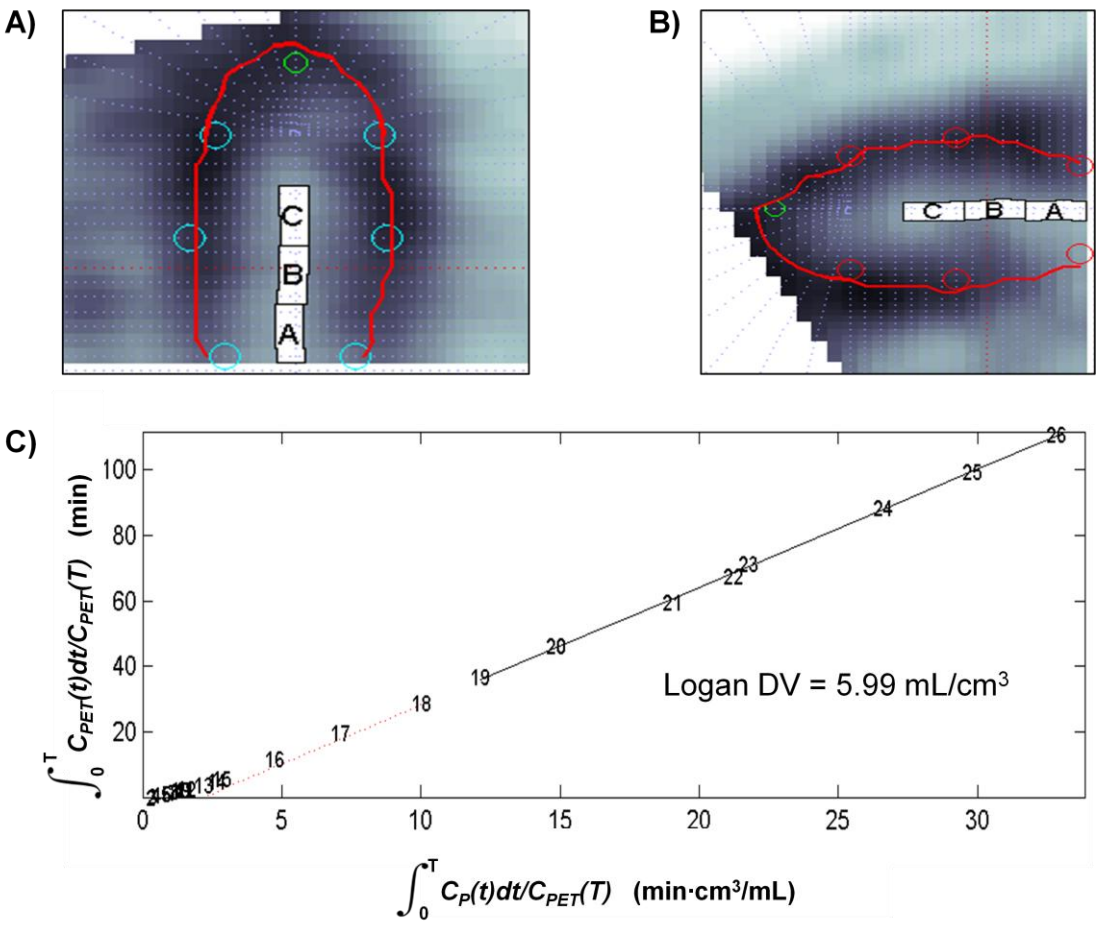


**FIGURE 3.5.** Reconstructed (*R*)-[$^{11}$C]rolipram images showing high tracer uptake in the rat heart (frame 15, 4-5 minutes post-tracer; 17 MBq injected activity, 0.04 ug injected mass, 0.00016 mg/kg injected mass). Myocardial (red) regions of interest (ROI) placed using **A)** horizontal long-axis and **B)** vertical long-axis orientations with whole-blood regions taken at locations A, B and C, representing the left atrium, base and cavity of the heart respectively. **C)** Representative Logan slope plot showing the linear relationship from 20-60 minutes (frames 19-26). In axis, $C_P(t)$ = concentration of parent (*R*)-[$^{11}$C]rolipram in plasma and $C_{PET}(t)$ = concentration of (*R*)-[$^{11}$C]rolipram in tissue after correction for blood volume and partial volume loss.

Importantly, at all times > t* complete saturation of non-specific binding is assumed and the tracer kinetics can be described by a one compartment tissue model, reflective of the available receptor population ($B_{max}$).[198,200]

The DV estimated by the Logan slope approach does not purely reflect the DV of (*R*)-[$^{11}$C]rolipram; previous studies have revealed that labeled metabolites are present in rat cardiac tissue. However, these intracardial metabolites of (*R*)-[$^{11}$C]rolipram do not bind specifically to PDE4.[130] Therefore, a component of the Logan slope can be attributed to the labeled metabolites present in the tissue, but despite this bias, the method still provides a useful index of the tracer binding potential in lieu of full compartmental modeling.

### 3.2.4 PDE4 Enzyme Saturation Studies

Studies (n=30) investigating the *in vivo* relationship between injected mass of unlabeled cold compound compared to the quantitative Logan slope, were conducted with the goal of estimating an $ED_{50}$[115,116] for (*R*)-rolipram in the rat heart. This relationship was evaluated over the range of 0.0001-1.09 mg/kg of injected mass.

Full blockade studies were conducted in a subset of n=3 rats pre-injected (2-5 minutes prior to injection of *(R)*-[$^{11}$C]rolipram) with a saturating dose of *(R)*-rolipram (1 mg/kg, i.v.)[128,201] to establish the proportion of activity contributed in the heart by the non-displaceable signal. Complete saturation of the PDE4 enzyme allows assessment of the *in vivo* specific binding of *(R)*-[$^{11}$C]rolipram to PDE4 by comparing Logan slopes against unsaturated, low-occupancy images.

To investigate the dose range of 0.003-0.35 mg/kg, a subset of n=5 rats received (*R*)-[$^{11}$C]rolipram co-administered with added unlabeled (*R*)-rolipram to add additional

injected mass to the tracer formulation. To image the effect of doses < 0.03 mg/kg in the remaining rats (n=22), the unlabeled component of the tracer formulation was exploited to contribute to the injected mass dose by tailoring the injected activity. Radiochemistry limitations of tracer specific activity permitted 0.00016 mg/kg as the lowest injected mass dose. PET camera sensitivity also limited exploration of lower injected masses, as the camera requires a minimum injected activity above 7.4 MBq to produce an acceptable image with rats.

Upon conclusion of these studies and determination of an $ED_{50}$ for (*R*)-rolipram in the rat heart, we established a baseline target of low receptor occupancy (< 10%) using the following equation proposed by Hume[116]:

$$Occ = (Act)/(Wt\ ED_{50}\ SpAct + Act),$$

where Occ = receptor occupancy, Act = injected activity, Wt = animal weight and SpAct = specific activity of the tracer. The injected mass correlating to < 10% occupancy was then used as a cut-off to guide the following studies.

### 3.2.5 (*R*)-[$^{11}$C]Rolipram Reproducibility Studies

Inter-rat variability was assessed at baseline, low-occupancy conditions (< 10%; 0.00018 ± 0.00002 mg/kg) in n=13 animals. The intra-rat variability was assessed using test-retest imaging (n=5 animals) separated by at least 9 days (mean 16.4 ± 6.7 days) to yield repeated measures.

### 3.2.6 Response to Acute NE Elevation

To evaluate binding of (*R*)-[$^{11}$C]rolipram in response to acutely elevated cardiac NE levels, n=5 rats were imaged first at baseline and then at a second time, 2-7 days later

(4.8 ± 1.8 days) following acute desipramine challenge (20 mg/kg, i.p., 3 hours pre-tracer). [$^{13}$N]-ammonia was used to assess whether MBF was modified by desipramine administration, potentially influencing tracer delivery of *(R)*-[$^{11}$C]rolipram, as desipramine can cause depressed hemodynamics at high doses.[202]

## *3.3 Investigation of PDE4 Alterations in STZ/HFD-Induced Hyperglycemia*

### 3.3.1 Animals

All experiments were conducted in accordance with the recommendations of the Canadian Council on Animal Care and with approval from the Animal Care Committee at the University of Ottawa.

Male Sprague Dawley rats (n=65) were obtained from Charles River (Montreal, QC) and were maintained in a temperature controlled environment with water and food *ad libitum*. Body weight and diet consumption were monitored throughout. Rats were fed HFD (Research Diets D12266B; 32/51/17 % fat/carbohydrates/protein, NJ, USA).

This experimental design is similar to that used previously in our lab.[154] Briefly, after 14 days of high fat feeding, rats were administered STZ (45 mg/kg, ip; n=43) or vehicle alone (n=22). Two weeks after STZ injection, animals were stratified by blood glucose to STZ-treated hyperglycemics (blood glucose $\geq$ 11 mM, n=26) or STZ-treated euglycemics (blood glucose < 11 mM, n=17). Fed-state blood glucose levels were measured weekly by glucose meter (Roche, QC, Canada) from the saphenous vein via 25g needle pinprick to pierce the vein and allow beads of blood to be sampled. Plasma insulin (Alpco Diagnostics, New Hampshire, USA), triglyceride (BioVision #K622-100, California, USA) and free fatty acid (BioVision #K612-100) were assessed using commercially available kits at the 8 week time point.

### 3.3.2 PET Imaging

PET scans were conducted as described above (section 3.2.2) at 8 (n=7 vehicle-treated control, n=5 STZ-treated euglycemics, n=7 STZ-treated hyperglycemics) and at 10 weeks with desipramine (20 mg/kg, ip) pre-treatment (n=7 vehicle-treated control, n=6 STZ-treated euglycemics, n=6 STZ-treated hyperglycemics). Anaesthetized rats (1-2% isofluorane) underwent a 30 minute [$^{13}$N]-ammonia scan (100 ± 17 MBq) prior to *(R)*-[$^{11}$C]rolipram imaging with a 30-minute washout period. Following this, (*R*)-[$^{11}$C]rolipram was administered (mean 55.5 ± 25.5 MBq). A transmission scan of 10 minutes was also performed (57-cobalt source, 122 keV emission), either before or after (*R*)-[$^{11}$C]rolipram imaging to provide a correction for signal attenuation.

### 3.3.3 Image Analysis

Image analysis was conducted as described above (section 3.2.3).

### 3.3.4 *Ex Vivo* Biodistribution

To validate the dynamic PET measurements with (*R*)-[$^{11}$C] rolipram, *ex vivo* biodistribution was conducted on a separate group of animals (n=11 vehicle-treated controls, n=8 STZ-treated euglycemics, n=8 STZ-treated hyperglycemics) at 8 weeks following STZ or vehicle administration as described previously.[128,129,139] Briefly, (*R*)-[$^{11}$C]rolirpam (33.3-70.3 MBq) was administered to conscious, restrained rats via a lateral tail vein. After 45 minutes, rats were sacrificed by decapitation with trunk blood collected. Atria, and ventricles were rapidly dissected, blotted, and counted (decay-corrected) in a gamma counter (Packard Cobra II) with 1 mL blood samples and 1% standard dilutions of the (*R*)-[$^{11}$C]rolipram injection volume. Radioactivity

biodistribution is expressed as percentage of injected dose per gram of tissue (%ID/g) normalized as a ratio to blood activity.[129] The PDE4 response to acute elevation of norepinephrine (n=5 vehicle-treated controls, n=6 STZ-treated euglycemics, n=6 STZ-treated hyperglycemics) was assessed by 3 hour pretreatment with the NE reuptake inhibitor desipramine (20 mg/kg, ip). Specific binding with (n=4 vehicle-treated controls, n=4 STZ-treated euglycemics, n=3 STZ-treated hyperglycemics) and without desipramine pre-treatment (n=10 vehicle-treated controls, n=4 STZ-treated euglycemics, n=4 STZ-treated hyperglycemics) was assessed by coinjection of a saturating dose of (*R*)-rolipram (1 mg/kg iv) with the radiotracer. Specific binding was defined as the portion of total binding susceptible to displacement by coinjection of (*R*)-rolipram (total binding minus non-specific binding).

### 3.3.5 *In Vitro* Measurements

#### *3.3.5.1 Tissue Collection*

Tissue was collected from a subset of animals (n=3 vehicle-treated controls, n=3 STZ-treated euglycemics, n=4 hyperglycemics) for *in vitro* assessment of PDE4 expression and activity. Rats were sacrificed at 8 or 10 weeks by decapitation and the heart dissected out, rapidly sectioned into the LV, right ventricle (RV), atria and septum, flash frozen in liquid nitrogen and stored in -80°C until use. Upon use, tissues were hand powdered using a pestle and mortar under liquid nitrogen. Aliquots were prepared for excess tissue and stored in -80 C for future use.

### *3.3.5.2 Immunoblotting*

Western blotting was used to correlate the *in vivo* imaging results with expression of PDE4. PDE4 protein levels were quantified in rats of the STZ/HFD protocol at 8 weeks post-treatment and 10 weeks post-treatment with desipramine challenge in each of the treatment groups. Antibodies used for Western blotting were anti-PDE4A polyclonal rabbit antibody (FabGennix Inc., Texas, USA; PDE4-112AP); anti-PDE4B polyclonal rabbit antibody (Santa Cruz Biotechnology, Inc., California, USA; sc-25812); anti-PDE4D polyclonal rabbit antibody (Santa Cruz Biotechnology, Inc.; sc-25814); mouse monoclonal antibody against GAPDH (Santa Cruz Biotechnology, Inc.; sc-32233). The protocol used has been previously described by our laboratory group.[140]

In brief, the prepared LV tissue powder was homogenized in 25 mM Tris-Cl and 20% triton, pH 7.6 with Complete Protease inhibitor cocktail (Roche) using a Polytron homogenizer (PT 1200, Kinematica AG, Lutzen). Membrane lysis followed for 15 minutes on ice. Homogenate was centrifuged for 3 minutes at 12,000 × g and the supernatant collected. Protein concentration was determined by a quantification kit (BCA protein assay). Western blot analysis was completed using the manufacture's guidelines (BioRad, ON, Canada). 8-10% agarose resolving gel was used for PDE4 protein separation based on protein size using gel electrophoresis (Mini-Protean Tetra Cell, BioRad). The proteins were transferred from the gel to a PVDF membrane over 2 hours (Mini Trans-Blot Transfer Cell, BioRad). 10% skim milk was used to block the membrane overnight. Incubation in primary antibody (PD4-112AP- anti-PDE4A, FabGennix Inc., TX, USA) and 5% milk followed for 3 hours. Secondary antibody incubation (goat anti-rabbit horse radish peroxidase) occured for 1 hour. A

chemiluminescence kit (Perkin Elmer, MA, USA) was used to stain the membrane. The image was obtained by using a CCD camera (FluorChem HD, Alpha Innotech, CA, USA) connected to AlphaEase FC IS-9900 image analysis software (Apha Innotech).

### *3.3.5.3 Enzyme Activity Assay*

Enzyme activity assays were used to correlate changes *in vivo (R)*-[$^{11}$C]rolipram distribution with changes in PDE4 activity levels. Enzyme activity was measured with a commercial kit (FabGennix Inc.) at 8 weeks post-treatment and 10 weeks post-treatment with desipramine challenge in each of the treatment groups. The underlying principle of the kit is a two-step conversion of [$^{3}$H]cAMP to [$^{3}$H]AMP, followed by dephosphorylation to [$^{3}$H]adenosine and has been described previously by our lab.[140]

Briefly, LV tissue powder was homogenized with manufacturer-provided buffer used for tissue lysis and homogenization (SolO buffer, Fabgennix). Membrane lysis followed for 15 minutes on ice. Homogenate was centrifuged for 3 minutes at 12,000 × g and supernatant collected. For the first enzymatic step, tissue samples were added to incubation mixtures containing manufacturer-provided buffers, cAMP, and (*R*)-rolipram (500 µM in blocked samples). Following addition of the [$^{3}$H]cAMP substrate, tubes were incubated for 10 minutes with shaking and the reaction terminated by boiling the samples for 3 minutes. For the second enzymatic step, Crotalus Atrox venom-derived secondary enzyme was added to the reaction and incubated for 15 minutes. To separate the resulting [$^{3}$H]adenosine from [$^{3}$H]AMP and [$^{3}$H]cAMP, pre-activated ion exchange resin was added to each tube. Tubes were centrifuged at 13,000 × g for 2 minutes, the supernatant mixed with scintillation fluid (BCS-NA scintillation cocktail, Amersham) and counted

using a β-scintillation counter (1219 RackBeta liquid scintillation counter, LKB Wallac, Perkin-Elmer). PDE4 activity (fmol/min·mg protein) was quantified by comparing the $^{3}H$ signal with the blocked samples, and using a sample of [$^{3}H$]cAMP to correlate radioactivity measurements (cpm to Ci).

## *3.4 Statistical Analysis*

Statistical analysis with the Student's t-test, paired t-test and ANOVA was completed using SPSS (version 18, SPSS Inc., IL, USA), with comparisons of $p < 0.05$ considered statistically significant. In cases of ANOVA analysis, the Tukey's post-hoc test was used to determine significance between individual groups.

# 4. Results

## *4.1 In Vivo Tracer Characterization*

### 4.1.1 Arterial Input Function

#### *4.1.1.1 Proportion of Activity in Whole Blood and Plasma*

Plasma to whole blood ratios varied between 0.8-1.2 from 0-60 minutes (figure 4.1), with more activity present in whole-blood at early time-points (0-20 mins), while at later time-points (35-60 mins) greater activity was present in plasma.

The following equation was fit to the ratio of the data:

$$F(t) = 1.15 - 0.24\, e^{-0.02t},$$

providing a whole-blood correction for radioactivity associated with plasma over time.

#### *4.1.1.2 Carbon-11 Labeled Metabolites in Plasma*

(*R*)-[$^{11}$C]rolipram was rapidly metabolized, whereby only 27% of radioactivity in plasma at 15 minutes was associated with the unaltered parent compound, while the remaining > 70% of activity derived from labeled metabolites (figure 4.2).

The following equation was fit to the metabolite data:

$$F(t) = 0.7\, e^{-0.23t} + 0.3\, e^{-0.007t},$$

providing a metabolite correction for unchanged parent tracer in plasma over time.

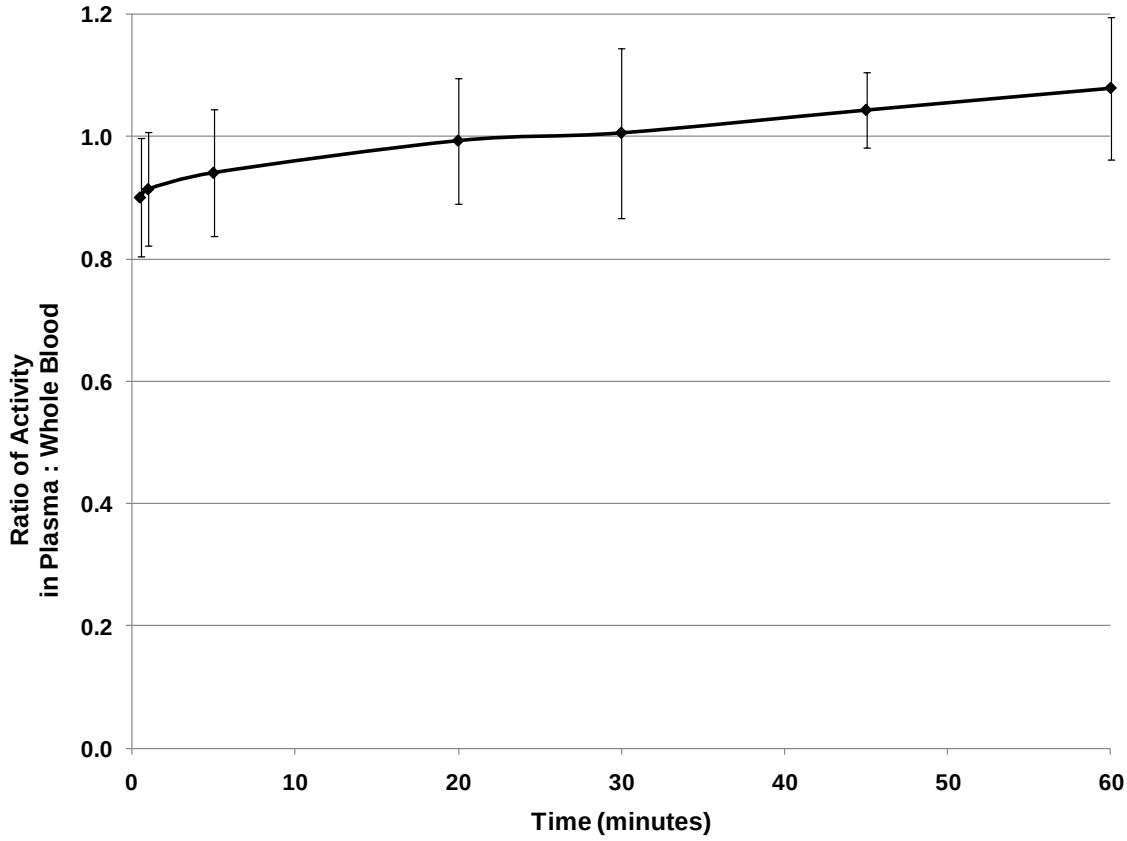


**FIGURE 4.1.** Ratio of plasma : whole blood activity over time (minutes) in rat for (*R*)-[$^{11}$C]rolipram as measured by carotid artery blood sampling (150-300 mL). Data are presented as mean ± std. dev. (n=3 at each data point). The fitted whole-blood to plasma correction function is $F(t) = 1.15 - 0.24e^{-0.02t}$.

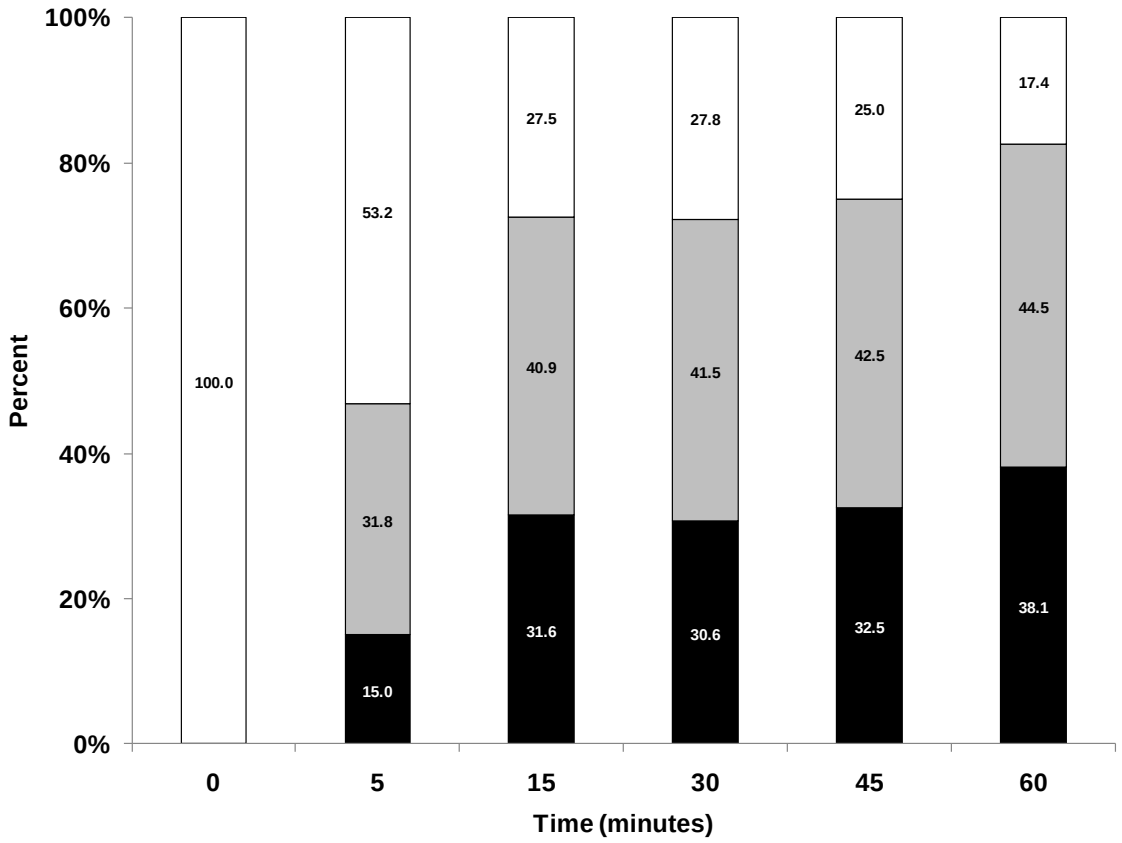


**FIGURE 4.2.** Proportion of plasma activity associated with hydrophilic metabolites eluted from the capture column (▒), hydrophilic metabolites eluted with the solvent front (■) and unchanged parent tracer (□) at various time points (minutes). The derived plasma metabolite correction function is $F(t) = 0.7\ e^{-0.23t} + 0.3\ e^{-0.007t}$.

### 4.1.2 (*R*)-[$^{11}$C]rolipram Imaging - General

The images generated by *(R)*-[$^{11}$C]rolipram small animal PET (n=30) consistently show the highest areas of uptake to be the heart, brain, and liver (figure 4.3). The myocardial signal-to-noise ratio (SNR) at 4-5 min post-tracer injection was 11 ± 3.2, and the myocardial-to-blood ratio (MBR) was 1.4 ± 0.23 across all imaging conditions.

### 4.1.3 PDE4 Enzyme Saturation Studies

An estimate of the $ED_{50}$ for myocardial (*R*)-rolipram binding was obtained by fitting a sigmoid curve, as is typical of competition binding assays, to the Logan slope (LS) values versus the corresponding injected masses (IM) for n=30 (*R*)-[$^{11}$C]rolipram images:

$$LS = [V_S / (1 + IM/ED_{50})] + V_{ND}$$

where $V_S$ represents the specific binding distribution volume, and $V_{ND}$ is the non-displaceable distribution volume of the tracer. From this relationship (figure 4.4), the $ED_{50}$ was estimated to be 0.0019 mg/kg (95% confidence interval 0.0014 to 0.0052; $r^2$ = 0.63), and the specific binding $V_s$ was estimated at 2 mL/cm$^3$.

Assuming this $ED_{50}$ value and using the equation presented by Hume (section 3.2.4),[116] 10% receptor occupancy of the PDE4 enzyme in the rat heart corresponds to an injected mass of 0.0002 mg/kg. In the subset of images at this baseline, low-occupancy condition (n=13; 0.00018 ± 0.00002 mg/kg), the Logan slope value was 5.5± 0.85 mL/cm$^3$ (table 1).

Images with complete PDE4 saturation (> 1 mg/kg, (*R*)-rolipram) were characterized by a lack of contrast between myocardium and blood signals (MBR of 1.1

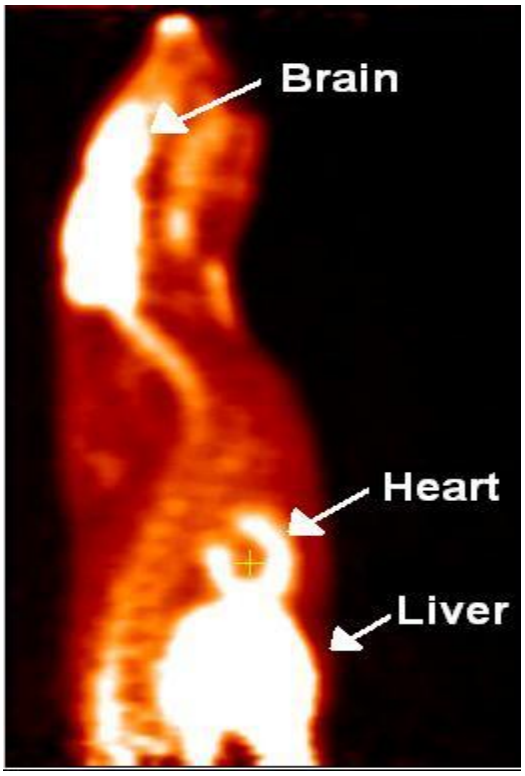


**FIGURE 4.3.** Reconstructed *(R)*-[$^{11}$C]rolipram PET image showing high tracer uptake and tissue contrast in the heart, brain and liver (74 MBq, SA = 157 GBq/μmol).

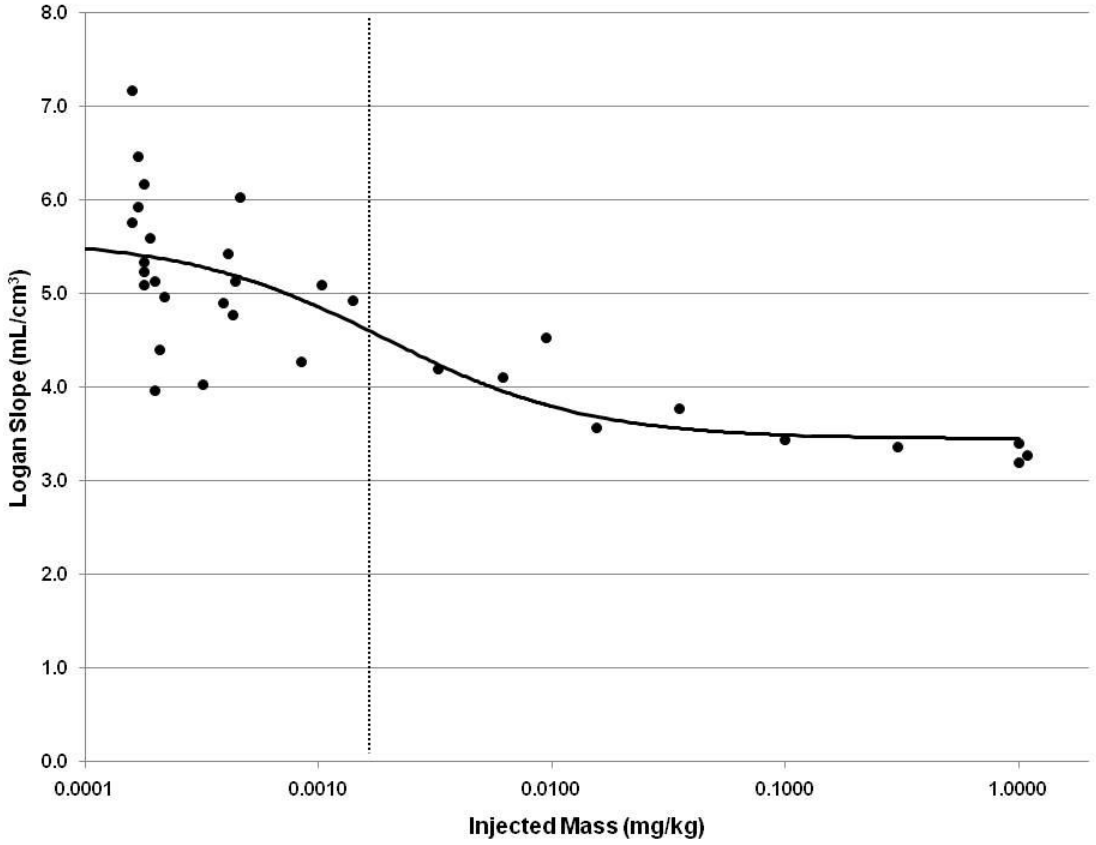


**FIGURE 4.4.** Dose-response curve in rat LV for the injected mass of (*R*)-[$^{11}$C]rolipram vs. Logan slope over the range of 0.00016-1.09 mg/kg. An $ED_{50}$ of 0.0019 mg/kg (95% confidence interval of 0.0013 to 0.0052, dashed vertical line) was estimated by fitting the following equation to the data: $LS = [V_S / (1 + IM/ED_{50})] + V_{ND}$; LS = Logan slope, $V_S$ = specific binding distribution volume, IM = injected mass, and $V_{ND}$ = non-displaceable distribution volume.

± 0.06) as compared to baseline (MBR of 1.6 ± 0.22, $p < 0.05$; figure 4.5). Quantitative assessment reveals a mean Logan slope of 3.3 ± 0.1 mL/cm$^3$ (table 1) in these animals representing a significant 40% reduction compared to baseline ($p < 0.01$).

### 4.1.4 (*R*)-[$^{11}$C]Rolipram Reproducibility Studies

Logan slope values for (*R*)-[$^{11}$C]rolipram scans at baseline (< 10% occupancy) ranged from 4.0 to 7.2, with a mean of 5.5± 0.85 mL/cm$^3$ in 13 studies (table 1), representing 15% coefficient of variation between independent animal studies. Test-retest studies revealed small variability within rats; the difference between repeated measures ranged from 1.9-8.6% with a mean difference of 4.6 ± 2.8%. Bland-Altman analysis showed a small 5% bias towards higher values in the second study relative to the first ($p < 0.05$, figure 4.6, panel A).

From the variability observed in the inter-rat evaluation, a sample size calculation was performed to determine the number of rats needed to observe a specified change for future studies. A sample size of 26, 8 and 6 would be needed to observe a change in cardiac PDE4 binding of 10, 20 and 30%, respectively (figure 4.6, panel B).

### 4.1.5 Response to Acute NE Elevation

Three-hour pre-treatment with desipramine resulted in Logan slopes with a mean of 6.8± 0.70 mL/cm$^3$. These same rats had baseline Logan slopes of 5.2 ± 0.77 mL/cm$^3$ representing a significant 30% increase in these rats ($p < 0.01$, figure 4.7) and a significant 24% increase compared to the baseline, low-occupancy group ($p < 0.01$).

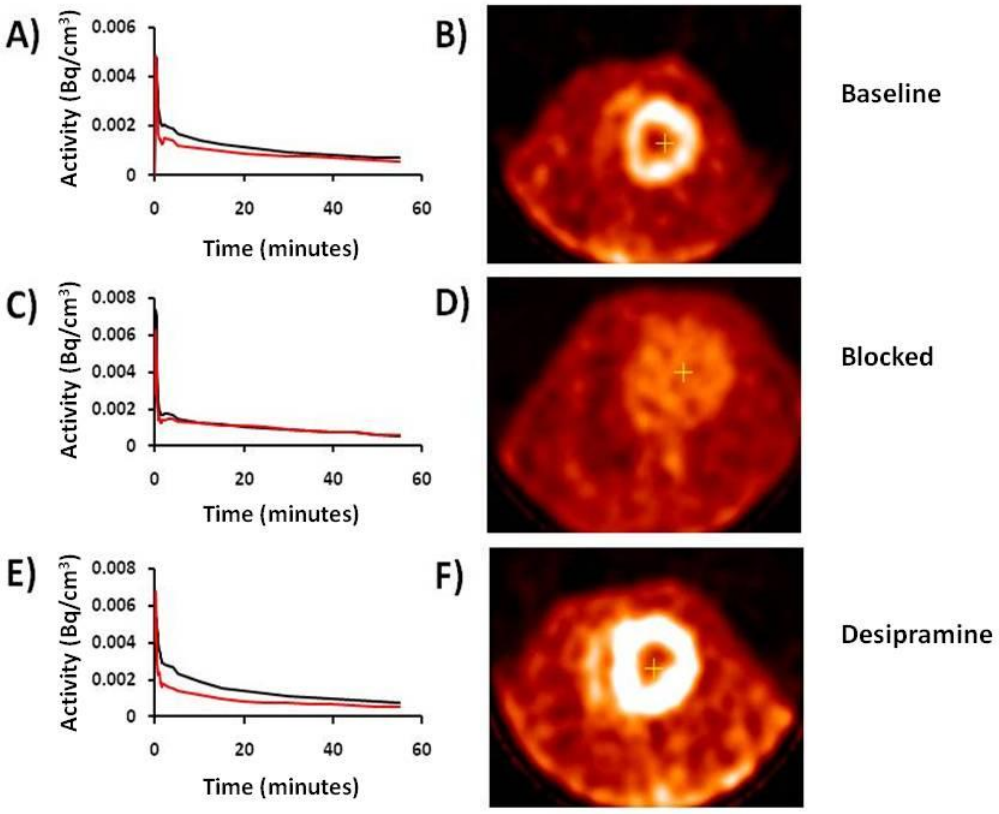


**FIGURE 4.5.** Representative time activity curves (panel **A, C and E**) for (*R*)-[$^{11}$C]rolipram in the rat LV (black trace) in baseline, blocking and desipramine challenge studies compared to blood (red trace; blood input function). Representative reconstructed (*R*)-[$^{11}$C]rolipram transaxial images (panel **B, D, and F**) in baseline, blocking and desipramine challenge studies.

**TABLE 1.** Quantitative (*R*)-[$^{11}$C]rolipram Logan slope and [$^{13}$N]ammonia MBF values for baseline, blocked and desipramine challenge groups.

| Group (*(R)*-Rolipram injected mass/body weight) | Logan Slope (± SD) | MBF (± SD) |
|---|---|---|
| Baseline, low occupancy (0.00018 mg/kg) | 5.5 (± 0.85) | 3.5 (± 0.60) |
| Blocked, total PDE4 saturation (> 1.0 mg/kg) | 3.3* (± 0.10) | 3.9 (± 0.61) |
| Desipramine challenge (0.00018 mg/kg) | 6.8†‡ (± 0.70) | 3.0 (± 0.55) |

* $p < 0.01$ Blocked vs Baseline

† $p < 0.001$ Desipramine vs Baseline

‡ $p < 0.001$ Desipramine vs. Blocked

A)

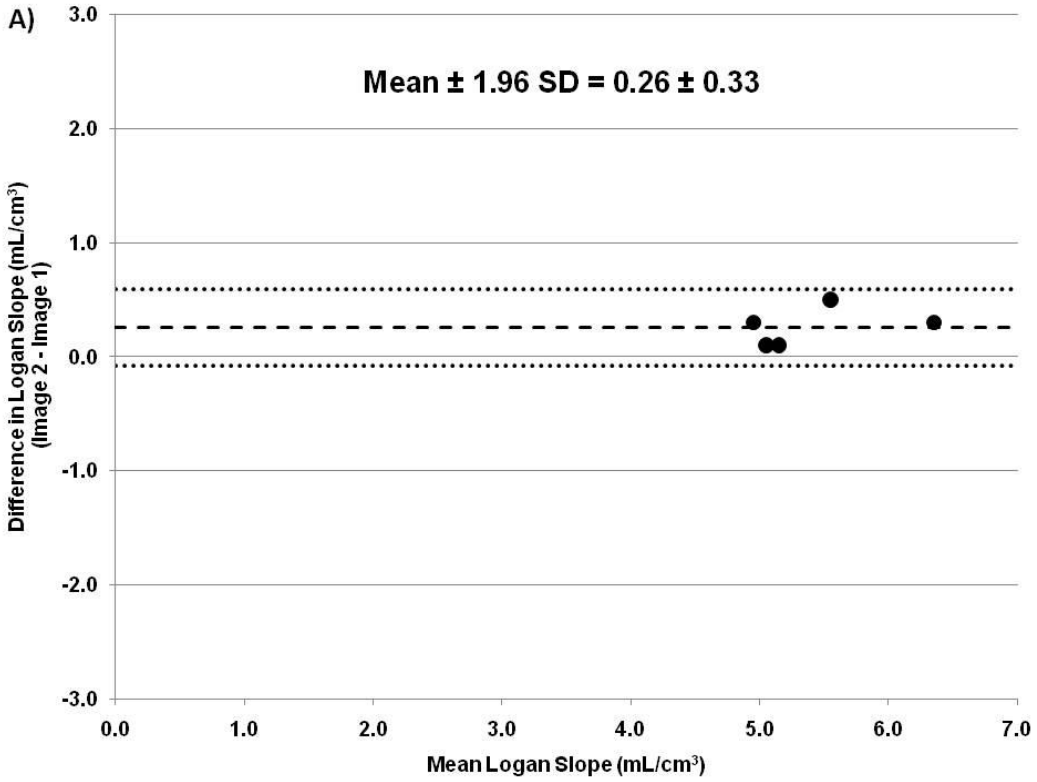


B)

| Change to Observe (%) | Estimated Sample Size (n) |
|---|---|
| 5 | 109 |
| 10 | 26 |
| 15 | 12 |
| 20 | 8 |
| 25 | 7 |
| 30 | <6 |
| 35 | <6 |
| 40 | <6 |
| 45 | <6 |
| 50 | <6 |

**FIGURE 4.6. A)** Bland-Altman plot comparing test-retest Logan slope values for (*R*)-[$^{11}$C]rolipram in rat LV. Mean difference between Logan slope repeated measures (n=5, image 2 – image 1) was 0.26, representing a small but significant bias of 5% ($p < 0.05$). The repeatability coefficient was 0.33 mL/cm$^3$, or 6% of the mean. **B)** Results of a sample size estimation for a given percent change in PDE4 binding.

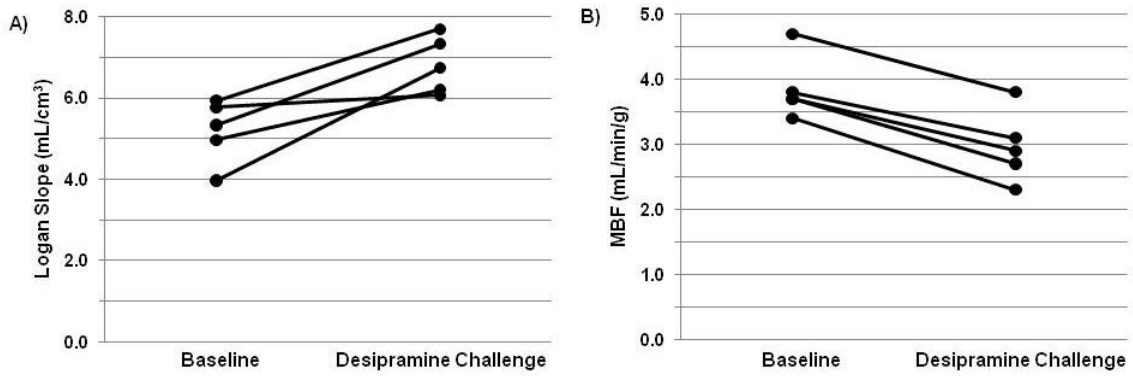


**FIGURE 4.7.** Baseline vs. desipramine challenge (20 mg/kg, 3hr pre-tracer, i.p.) studies in rat LV. **A)** Increased Logan slope values following desipramine challenge ($p < 0.01$) and **B)** decreased MBF following desipramine challenge ($p < 0.001$).

The dual tracer investigation of the effect of desipramine on MBF in these rats revealed a significant, 23% reduction in MBF with desipramine challenge in treated vs. untreated rats ($p < 0.001$, figure 4.7). In absolute terms, this resulted in mean MBF values of 3.9 mL/min/g in untreated rats, dropping to 3.0 mL/min/g 3 hours following desipramine administration.

## *4.2 Investigation of PDE4 Alterations in STZ/HFD-Induced Hyperglycemia*

### 4.2.1 Animals

The experimental animal population was composed of: 22 vehicle-treated controls, 26 STZ-treated hyperglycemic and 17 STZ-treated euglycemic rats. STZ-hyperglycemic animals at 8-weeks post-treatment had depressed weight gain (figure 4.8), overt hyperglycemia (figure 4.9) and increased food consumption (figure 4.10) compared to vehicle-treated controls and STZ-treated euglycemics. Fed-state plasma TGs were significantly elevated in STZ-treated hyperglycemics compared to controls at 8 weeks post-treatment ($p < 0.05$), while FFA and circulating insulin levels were reduced ($p < 0.05$; table 2).

### 4.2.2 (*R*)-[$^{11}$C]Rolipram Imaging

Cardiac images of (*R*)-[$^{11}$C]rolipram display uniform uptake and good contrast to background (figure 4.11) in all treatment groups. Quantitative analysis revealed no significant difference in Logan slope value for cardiac (*R*)-[$^{11}$C]rolipram uptake and retention between treatment groups at 8 weeks post-treatment ($p > 0.05$; figure 4.12).

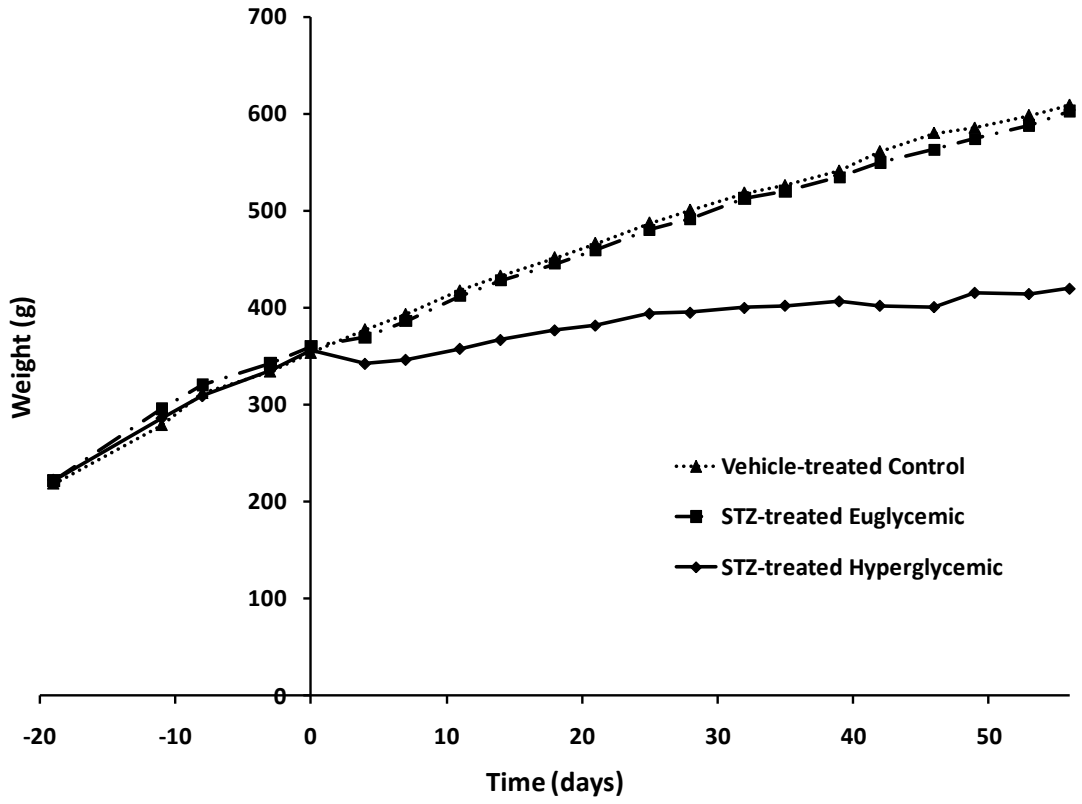


**FIGURE 4.8.** Weight gain in vehicle-treated control, STZ-treated euglycemic and STZ-treated hyperglycemic rats. Depressed weight gain in STZ-treated hyperglycemic rats is observed following STZ treatment (t = 0).

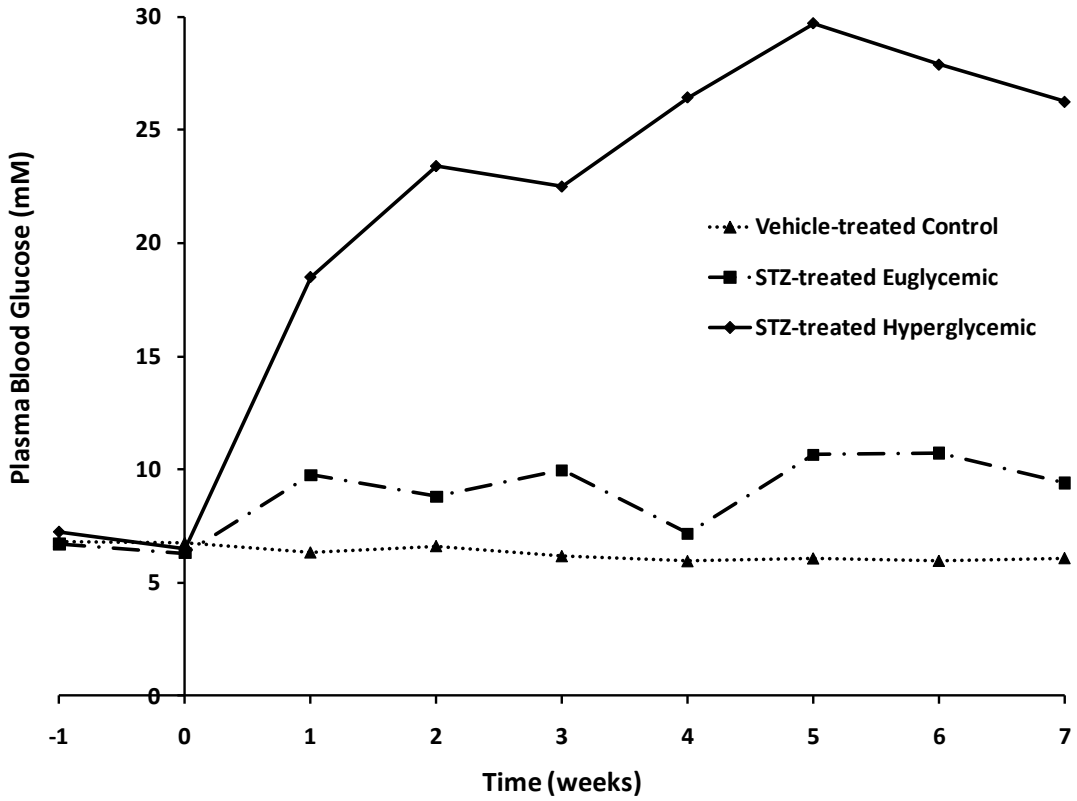


**FIGURE 4.9.** Fed-state blood glucose levels in vehicle-treated control, STZ-treated euglycemic and STZ-treated hyperglycemic rats. Elevated blood glucose is observed in STZ-treated hyperglycemic rats following STZ treatment (t = 0).

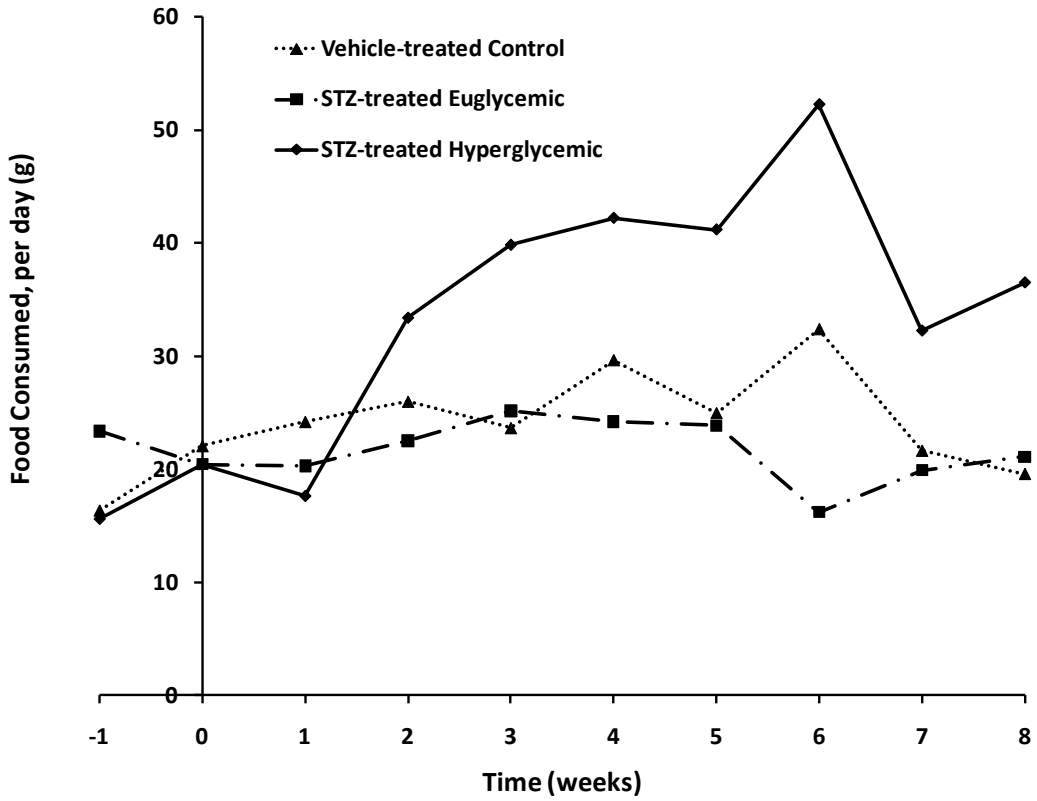


**FIGURE 4.10.** Food consumption for vehicle-treated control, STZ-treated euglycemic and STZ-treated hyperglycemic rats. Increased food consumption was observed in STZ-treated hyperglycemic rats following STZ treatment (t = 0).

**TABLE 2.** Effect of STZ/HFD induced hyperglycemia on body weight and blood markers in rats at 8 weeks post-treatment.

| | Units | Control (n=22) | Euglycemic (n=17) | Hyperglycemic (n=26) |
|---|---|---|---|---|
| Body Weight | g | 609 | 603 | 420*† |
| Plasma Glucose | mmol | 6.3 | 9.1 | 25.4*† |

| | Units | Control (n=3) | Euglyceic (n=3) | Hyperglycemic (n=4) |
|---|---|---|---|---|
| Insulin | ng/mL | 2.57 | 1.17 | 0.093*† |
| TG | mM | 136.4 | 157.5* | 182.5* |
| FFA | mM | 10.1 | 11.5 | 4.35*† |

* $p < 0.05$ vs. Vehicle-treated controls

† $p < 0.05$ vs. STZ-treated euglycemics

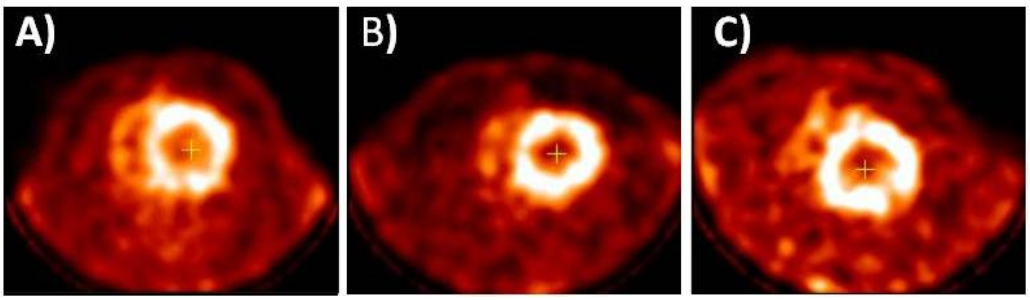


**FIGURE 4.11.** Representative reconstructed transaxial (*R*)-[$^{11}$C]rolipram images showing tracer uptake in the rat LV for **A)** vehicle-treated control (44.4 MBq, 0.00018 mg/kg injected dose), **B)** STZ-treated euglycemic (30.7 MBq, 0.00017 mg/kg) and **C)** STZ-treated hyperglycemic (37 MBq, 0.00017 mg/kg injected dose) groups at 8 weeks post-STZ treatment.

Similarly, desipramine challenge at 10 weeks post-treatment treatment did not reveal a significant difference in (*R*)-[$^{11}$C]rolipram uptake ($p > 0.05$; figure 4.12) in the left ventricle for any group. However, comparison of Logan slope values at 8 weeks and at 10 weeks with desipramine challenge revealed significant increases of 20% 24% 20% in vehicle-treated controls, STZ-treated euglycemics, and STZ-treated hyperglycemics, respectively.

### 4.2.3 [$^{13}$N]Ammonia Imaging

There was no difference between groups in quantitative MBF at either 8 weeks or 10 weeks of diabetes with desipramine challenge (figure 4.13). However, there was a significant decrease in MBF following desipramine challenge at 10 weeks compared to 8 weeks in STZ-treated euglycemics ($p < 0.05$), while a similar trend was observed with the vehicle-treated controls and STZ-treated hyperglycemics in the absence of statistical significance (figure 4.13).

### 4.2.4 *Ex vivo* Biodistribution

Cardiac retention of (*R*)-[$^{11}$C]rolipram at 45 minutes was consistent between vehicle-treated controls, STZ-treated euglycemic, and STZ-treated hyperglycemic groups (figure 4.14). Cardiac binding was effectively blocked by coadministration of cold rolipram by 28-42% in vehicle-treated controls, 32-45% in STZ-treated euglycemics and 29-37% in STZ-treated hyperglycemics. These reductions were not significant between groups ($p > 0.05$). Pre-treatment with desipramine resulted in a marked increase in cardiac binding by 37-38% in vehicle-treated controls, 19-21% in STZ-treated

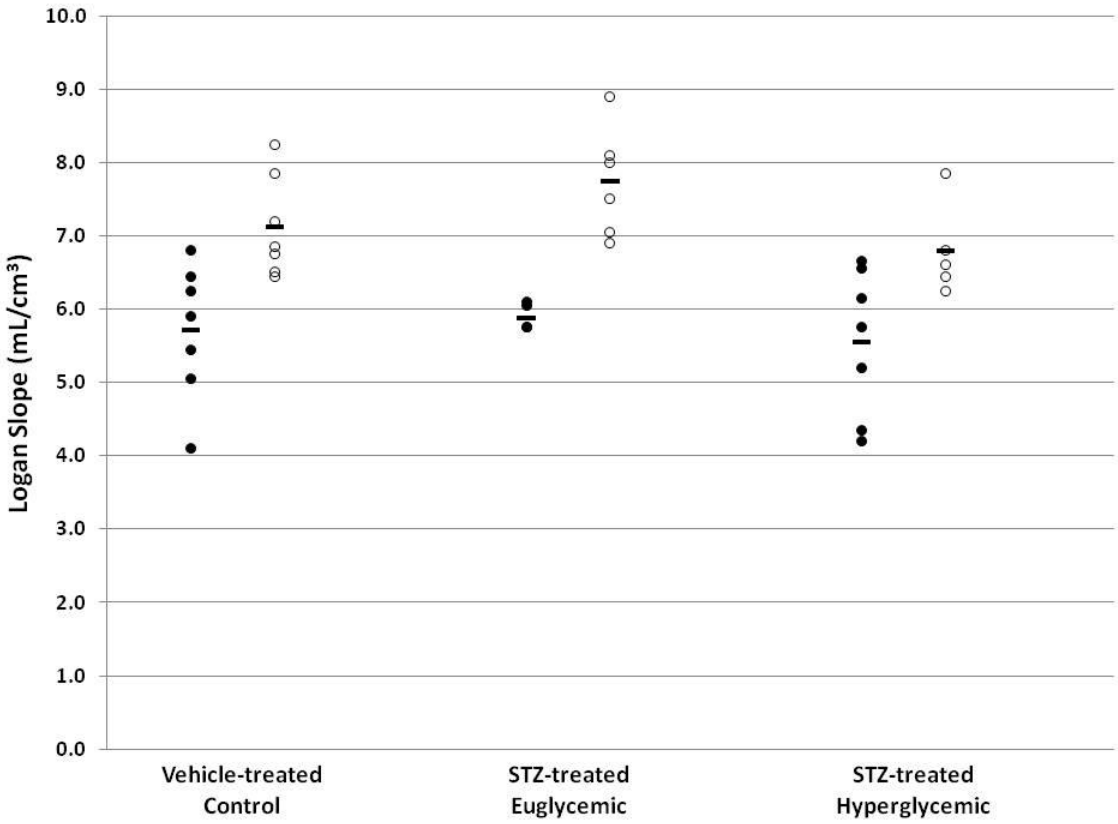


**FIGURE 4.12.** Quantitative cardiac (*R*)-[$^{11}$C]rolipram PET for vehicle-treated control, STZ-treated euglycemic and STZ-treated hyperglycemic groups expressed as Logan slope (mL/cm$^3$); closed circles represent 8 week data (n=7 control; n=5 euglycemic; n=7 hyperglycemic), open circles represent 10 week with desipramine data (20 mg/kg, ip; n=7 control; n=6 euglycemic; n=5 hyperglycemic). Horizontal bars represent mean Logan slopes, within group. No significant differences between groups ($p > 0.05$). * = significant difference ($p < 0.05$) from 8 week mean without desipramine, within group.

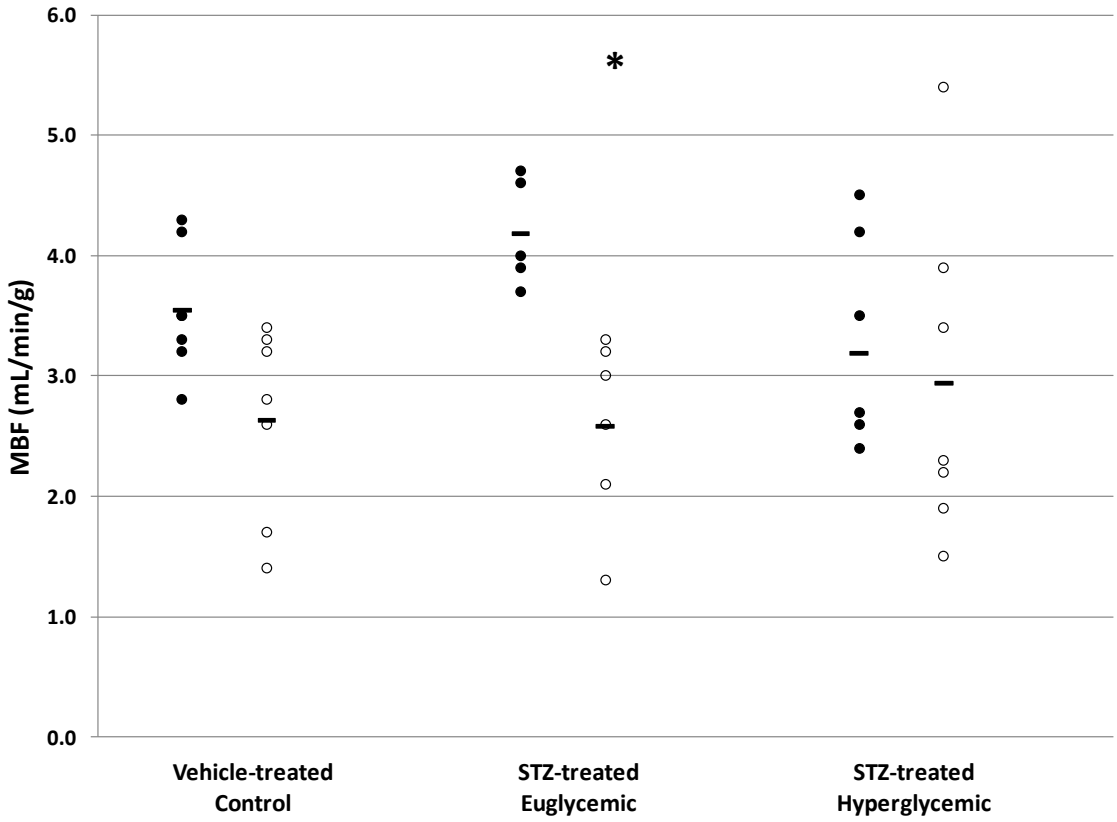


**FIGURE 4.13.** Quantitative evaluation of [$^{13}$N]ammonia MBF (mL/min/g) for vehicle-treated control, STZ-treated euglycemic and STZ-treated hyperglycemic groups; closed circles represent 8 week data (n=7 control; n=5 euglycemic; n=7 hyperglycemic), open circles represent 10 week with desipramine data (20 mg/kg, ip; n=7 control; n=7 euglycemic; n=7 hyperglycemic). Horizontal bars represent mean MBF, within group. * = significant difference ($p < 0.05$) from 8 week mean without desipramine, within group.

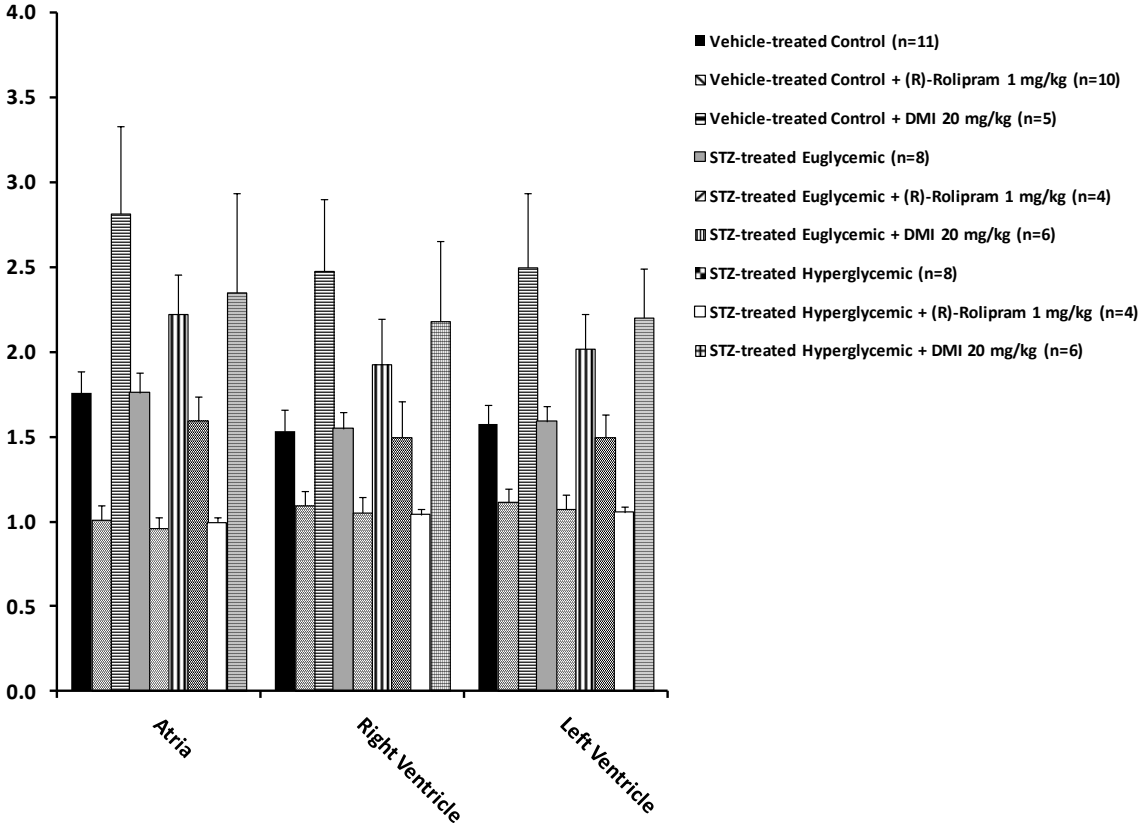


**FIGURE 4.14.** (*R*)-[$^{11}$C]Rolipram biodistribution results at 45 minutes post-tracer injection in the rat atrium, right and left ventricle for vehicle-treated control, STZ-treated euglycemic and STZ-treated hyperglycemic groups at 8 weeks post-STZ treatment. Data are presented as percent injected dose per gram of tissue standardized to body weight, compared as a ratio of tissue-to-blood.

euglycemics and 29-37% in STZ-treated hyperglycemics, with significance seen only with STZ-treated euglycemics compared to vehicle-treated controls ($p < 0.05$).

### 4.2.5 In Vitro Studies

#### *4.2.5.1 PDE4 Expression*

PDE4A, PDE4B and PDE4D LV expression was unchanged between groups at both 8 weeks and 10 weeks post-treatment with desipramine ($p > 0.05$, figure 4.15). No difference in expression was observed within groups between 8 week and desipramine-treated, 10 week states ($p > 0.05$).

#### *4.2.5.2 PDE4 Enzyme Activity*

Total LV PDE and PDE4-specific catalytic activity for the cAMP substrate was unchanged between groups at either 8 weeks post-treatment or 10 weeks post-treatment with desipramine ($p > 0.05$, figure 4.16). No significant changes in total or PDE4-specific activity were seen within groups between 8 week and desipramine-treated, 10 week states ($p > 0.05$).

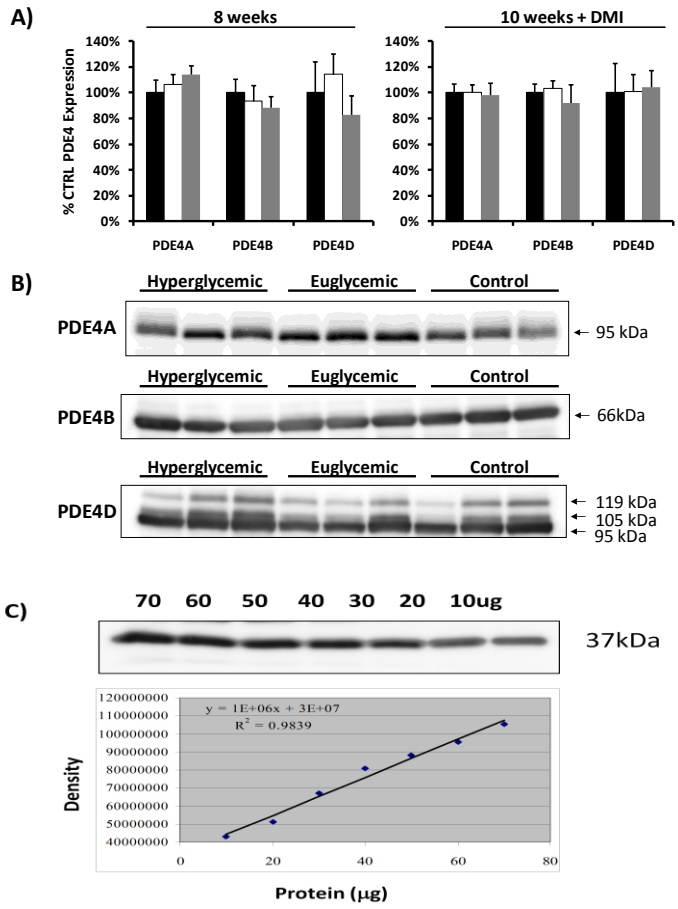


**FIGURE 4.15.** Expression of PDE4A, PDE4B and PDE4D protein expression in rat hearts of vehicle-treated control, STZ-treated euglycemic and STZ-treated hyperglycemic groups. **A)** Protein expression of PDE4 isoforms normalized to vehicle-treated control value for 8 and 10 weeks with desipramine (20 mg/kg, ip). Black bars = vehicle-treated. **C** control, white bars = STZ-treated euglycemic, grey bars STZ-treated hyperglycemic. **B)** Representative image of 8 week post-treatment PDE4 isoform bands on PVDF membrane as visualized with chemiluminescence. **C)** Image of GAPDH bands on PVDF membrane as visualized with chemiluminescence used for loading control calibration; graph demonstrating acceptable linearity from 10-70 µg of loaded protein ($r^2 = 0.9839$).

**A)**

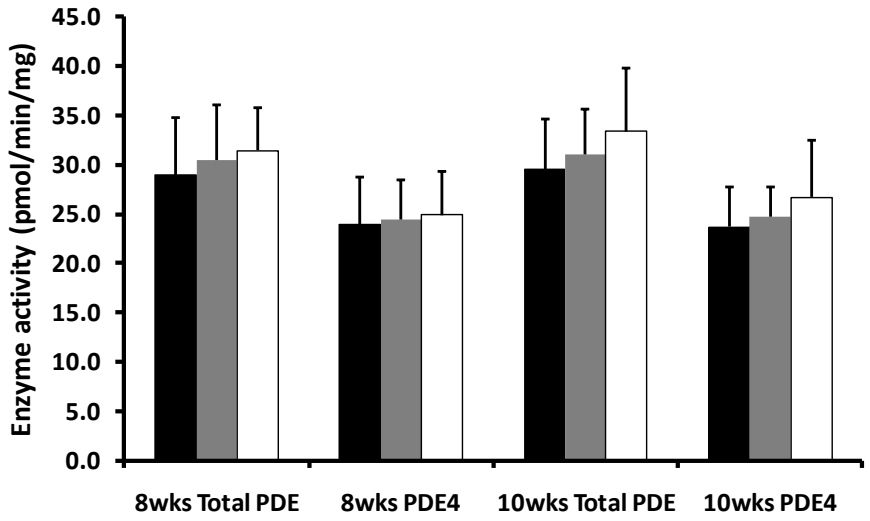


**B)**

| Group | Total PDE | Std. Dev | PDE4 | Std. Dev. |
|---|---|---|---|---|
| 8wks CTRL (n=4) | 28.9 | 5.8 | 23.9 | 4.9 |
| 8wks STZ EGLY (n=3) | 30.4 | 5.6 | 24.4 | 4.1 |
| 8wks STZ HYP (n=4) | 31.4 | 4.4 | 24.9 | 4.5 |
| 10wks CTRL (n=4) | 29.5 | 5.1 | 23.7 | 4.1 |
| 10wks STZ EGLY (n=3) | 31.0 | 4.6 | 24.7 | 3.1 |
| 10wks STZ HYP (n=4) | 33.4 | 6.4 | 26.7 | 5.7 |

**FIGURE 4.16. A)** PDE and PDE4 enzyme activity of rat heart at 8 and 10 weeks in vehicle-treated control, STZ-treated euglycemic and STZ-treated hyperglycemic groups. Black bars = vehicle-treated control, white bars = STZ-treated euglycemic, grey bars STZ-treated hyperglycemic. **B)** Summary table indicates calculated values and standard deviations. No significant differences between groups at 8 weeks and 10 weeks post-treatment with desipramine pretreatment ($p > 0.05$).

# 5. Discussion

Cardiac function is mediated through SNS dependent cell signalling by the agonist NE and the β-ARs. Activation of this receptor population stimulates production of the intracellular secondary messenger cAMP, leading to activation of PKA and the subsequent phosphorylation of target proteins involved in cardiac contraction and pacing.[1] PDE enzymes, through their ability to hydrolyze cyclic nucleotides, play a critical role in limiting and attenuating cell signalling. In the heart, cAMP-specific PDE4 is of particular functional importance as it hydrolyzes the majority of cAMP produced in response to SNS stimulation.[78-80] Further, cAMP levels act to regulate PDE4 expression and activity through negative feedback mechanisms.[69,203] Given this relationship between PDE4 and cAMP, PDE4-specific (*R*)-[$^{11}$C]rolipram distribution volume is reflective of the cardiac β-AR signalling environment and using this radioligand with small animal PET can provide an *in vivo* window to this intracellular signalling cascade.

## *5.1 In Vivo Tracer Characterization*

### 5.1.1 Arterial Input Function

The work relating to the arterial input function corrections revealed rapid tracer metabolism in rat plasma. As quickly as 5 minutes after tracer administration, the parent compound was reduced to ~50%, while at 15 minutes unchanged compound was reduced to < 30% of the radioactive signal. Rapid (*R*)-[$^{11}$C]rolipram plasma metabolism was also noted by Fujita et al.,[119] where similar metabolism rates were seen. In metabolism/clearance studies of rolipram, Krause and Kuhne reported rolipram plasma

clearance occurring with a rapid half-life ($t_{1/2}$ < 15 mins) following i.v. administration, along with a significant metabolic first-pass effect noted in rats.[204] Rapid metabolism of the parent tracer results in a reduced quantity available for tissue and specific binding to PDE4, but can be accounted for in the quantitative evaluation by using the fitted correction function (section 4.1.1.2) applied over the duration of the scan.

Accurate determination of the arterial input is further complicated by the changes in the ratio between radioactivity in whole blood and plasma over time. Our own previous observations support this effect, as red blood cells in the whole-blood fraction have high retention of (*R*)-[$^{11}$C]rolipram.[201] However, as time proceeds, the fraction of radioactivity in plasma increases as the ratio of activity in plasma to whole-blood nears and surpasses unity at approximately 35 minutes. The shift in radioactivity from whole blood to plasma could be due to the appearance of labeled metabolites at later time points. A secondary contributor may be the release of parent (*R*)-[$^{11}$C]rolipram over time by competitive displacement by unlabeled compound.

### 5.1.2 (*R*)-[$^{11}$C]Rolipram Imaging - General

PET imaging with (*R*)-[$^{11}$C]rolipram consistently shows the highest retention in the heart, brain and liver. High liver activity is typical of radiotracers that undergo hepatic metabolism, and further, it has been demonstrated that liver activity associated with (*R*)-[$^{11}$C]rolipram does not represent specific binding.[128,201] Conversely, the tracer accumulation in cardiac and brain tissues confirms previous *in vivo* biodistribution studies[128,129,201,205] and imaging experiments,[119,133-135] reflecting the high PDE4 levels reported in these tissues.[83-85]

### 5.1.3 PDE4 Enzyme Saturations Studies

Enzyme saturation studies over a range of injected masses (0.00016-1.09 mg/kg) revealed an inverse relationship between increasing injected mass and decreasing Logan slope, consistent with greater PDE4 enzyme saturation by unlabeled compound. Graphically, this effect follows the shape of a sigmoid curve, indicating > 90% saturation of the available enzyme with injected masses > 0.02 mg/kg. Based on these studies, the *in vivo* cardiac $ED_{50}$ for (*R*)-rolipram is ~ 0.002 mg/kg. Two values of interest have been reported previously: an $ED_{50}$ of 0.03 mg/kg in rat hearts presented by Kenk et al. 2007[128] and a second estimate of 0.002 mg/kg is given by Parker et al.,[137] after evaluating *(R)*-[$^{11}$C]rolipram in pig brains. Our estimated *in* vivo $ED_{50}$ is approximately an order of magnitude smaller than the value reported by Kenk et al., but is virtually identical to the more conservative value reported by Parker et al.

Based on the $ED_{50}$ established here, we estimate the *in vivo* receptor occupancy of PDE4 by unlabeled rolipram using the equation presented by Hume[116] (section 3.2.4)to be less than 5% at injected mass doses of < 0.0001 mg/kg, and less than 10% at injected doses < 0.0002 mg/kg in the rat heart. Unfortunately radiochemistry limitations in achievable specific-activities prevented the investigation of < 5% occupancy. Thus, due to practical limitations, a value of < 0.0002 mg/kg, corresponding to < 10% occupancy, was targeted for imaging in the low-occupancy condition. Despite our baseline studies being in the range of 10% occupancy, contrary to receptor ligand studies typically occurring below 5% occupancy,[116,117] the final results and conclusions appear to be only modestly affected as the observed results are in good agreement with prior characterization studies.[128-130]

In the complete PDE4 enzyme saturation studies, pre-administration of (*R*)-rolipram (> 1 mg/kg) was sufficient to decrease (*R*)-[$^{11}$C]rolipram accumulation to non-specific levels, with a mean Logan slope of ~3.3 mL/cm$^3$ and substantial blocking occurring with doses as low as 0.02 mg/kg. Qualitatively this results in a dramatically reduced MBR of the PET image, while quantitatively the reduction in Logan slope compared to baseline suggests ~40% specific binding of (*R*)-[$^{11}$C]rolipram assuming that the bias from labeled metabolites is relatively small and constant across all images. The reduction seen here closely parallels the *ex vivo* findings in Kenk et al.,[130] where PDE4 cardiac-specific binding at 45 minutes post-tracer was determined to be 41% in rats.

### 5.1.4 (*R*)-[$^{11}$C]Rolipram Reproducibility Studies

With a partial enzyme saturation effect observed with increasing injected masses, we sought to determine quantitative reproducibility at the baseline condition (< 10% occupancy). The low-occupancy, baseline condition of (*R*)-[$^{11}$C]rolipram imaging revealed a mean Logan slope value of ~5.5 mL/cm$^3$, which is confirmed through test-retest studies within the same animal and in measurements of independent animals. Indeed, the reproducibility of tracer DV was highly robust, as test-retest studies within the same animal resulted in differences of < 5%. As expected, variability between inter-animal studies is higher than that seen in intra-animal studies.

The greater variability seen with inter-rat studies may be owed to the use of a population-wide metabolite and plasma-to-whole blood activity corrections. Variability in the arterial input corrections was evident, which could lead to greater variability among independent animals,[200] whereas the impact of the correction variability would be limited in a test-retest protocol. Indeed this observation of low intra-animal variability

speaks to the power of small animal PET imaging, which affords the opportunity for repeated measures on the same animal allowing the detection of *in vivo* differences more readily with smaller samples.[110]

Based on the variability determined from these reproducibility studies, a power study was conducted to determine the size of animal populations for future studies (figure 4.7, panel B); to quantify a 20-30% change in myocardial PDE4 binding, a sample size of 6-8 animals is needed.

### 5.1.5 Response to Acute NE Elevation

Desipramine challenge studies at low-occupancy, baseline conditions resulted in a significant 24-30% increase in Logan slope compared to baseline. This mirrors the increase reported using *ex vivo* biodistribution where a 21% increase in (*R*)-[$^{11}$C]rolipram specific binding in the heart was attributed to desipramine treatment[129] and similarly a 17-24% increase in (*R*)-[$^{11}$C]rolipram left ventricle accumulation of 2-week, diet resistant rats after desipramine challenge.[139] Interestingly, a 23% reduction in MBF was observed in these studies using [$^{13}$N]-ammonia imaging, theoretically reducing the delivery of (*R*)-[$^{11}$C]rolipram to the heart. Our baseline and enzyme saturation studies reveal normal MBF,[196] suggesting this reduction is a direct response to desipramine challenge. This reduced hemodynamic effect is noted at high dosages of imipramine,[202] the active metabolite of desipramine. Thus the reduction of myocardial flow opposite to the increase in (*R*)-[$^{11}$C]rolipram uptake provides additional evidence of the tracer's specific and directed uptake related to PDE4 levels.

## 5.2 Investigation of PDE4 Alterations in STZ/HFD-Induced Hyperglycemia

T2DM has a marked and troublesome association with increased cardiovascular disease mortality.[151,206] A distinct and negative relationship exists between the heart and diabetes, whereby diabetes confers a 2-4 fold increase in coronary heart disease (CHD)[148] and mortality in heart failure is increased 1.5-2 times that of nondiabetics.[149] This phenomenon may stem in part from chronic activation of the SNS. T2DM typically presents with a collection of factors, such as hyperglycemia,[176] hyperinsulinemia,[173,207,208] and metabolic inflexibility[209,210] that each lead to an SNS pressor response. Over active SNS signalling is known to alter intracellular signalling in the heart and is best exemplified by changes seen in HF and diabetic cardiomyopathy. Specifically, it is believed that the persistently over active SNS in T2DM will result in the downregulation of left ventricle total β-ARs,[22,23,156-158,211] namely $\beta_1$-AR,[154] leading to reduced cAMP cell signalling. Taken further, as cAMP levels are regulated through negative feedback by PDE4 via PKA,[68,69] it is predicted that the reduction in cAMP accumulation will correspond to a reduction in PDE4 activity and expression.

In this study, the aim was to measure PDE4 binding in a STZ/HFD rat model of hyperglycemia and insulin resistance with *in vivo* PDE4-specific (*R*)-[$^{11}$C]rolipram small animal PET to better understand the role of T2DM-dependent cardiac intracellular signalling changes. This was extended further to examine if the heart was still responsive to NE elevations by desipramine challenge. Lastly, *in vivo* measures were validated against *in vitro* protein expression and activity of PDE4.

### 5.2.1 Animal Model

The STZ/HFD induced rat model of T2DM used herein offers a platform to investigate the late stages of T2DM where hyperglycemia prevails, progressive hypoinsulemia is observed,[154] HbA1c is significantly elevated and cardiovascular deficiencies are magnified.[191] Insulin resistance, conversely, is induced through the HFD component of the treatment.[184-186]

The STZ-induced hyperglycemic success rate reported here of ~60% following a single, moderate-dose STZ injection is comparable to success rates in our lab (unpublished data) and indicates the pharmacologic treatment was well performed. The total population size utilized in each experimental group was based off the sample size calculation derived from characterization studies (section 5.1.4); groups of 6-8 animals were expected to discriminate changes of 20-30% in PDE4 presence.

Our STZ-treated hyperglycaemic animals displayed depressed weight gain and overt hyperglycemia consistent with successful induction of the animal model.[189-191] Further, the STZ-treated hyperglycemics, but not the STZ-treated euglycemics or vehicle-treated controls, suffered from diuresis and polydipsia consistent with uncontrolled diabetes,[212] indicating the STZ/HFD rat model was well represented in our studies compared to other reports.

#### *5.2.1.1 Critique of the STZ/HFD Animal Model*

##### 5.2.1.1.1 Blood Glucose Levels

The STZ-treated hyperglycemic animals used in this study exhibit overt hyperglycemia (25.4 mM) which is in good agreement with previous description of the

model, both in our lab[154] and elsewhere.[189,213] Although lower dose STZ (30-35 mg/kg) models result in a more clinically relevant blood glucose level of 7-8.5 mM,[213] the success rate of hyperglycemia induction is dramatically reduced (10-35% absolute success[213]), requiring a much larger animal population to achieve the necessary numbers in each group. In addition, it is likely that any changes in cardiac PDE4 due to hyperglycemia would take far longer to develop; considering we saw no change at the 8 week time point with frank hyperglycemia, the prospect of observing differences with modest hyperglycemia of 7-8 mM in this same timeframe seems unlikely.

#### 5.2.1.1.2 Lack of Increased Weight Gain in STZ-treated Hyperglycemics

It is well documented that the STZ-treated hyperglycaemic animals do not display increased weight relative to controls[189-191,212] as might be typical of the Type-2 diabetic, thus limiting the pressor effect on the SNS by excess mass.[168,175] Despite this, marked changes in cardiac $\beta_1$-AR[154] expression and calcium handling are apparent in numerous studies (section 1.3.2.1), thus confirming the occurrence of the SNS pressor effect we sought to study.

#### 5.2.1.1.3 TGs and FFAs

The reduced FFAs measured here is a cause for concern, as multiple groups report elevated levels of this circulating marker.[189,190] In contrast, no significant differences were seen in the fed state of either circulating TG/FFAs or myocardial TG/FFA in chow-fed 55 mg/kg STZ rats.[214]

Curiously, however, we did observe an increase in circulating TGs, which would be expected to lead to an increase in FFAs, but was not the case in our animal population.

This is consistent with Menard et al., who report decreased fasting FFAs, despite increased fasting TGs.[215] Though they observe a reduction in FFA levels, they report significantly reduced stroke volume and ejection fraction, while demonstrating myocardial preference for FFA substrate oxidation over glucose,[215] suggesting that cardiac deficiencies are still present and not dependent on FFA levels in the STZ model. The mismatch of increased TGs/decreased FFAs is somewhat supported by a HFD (45% fat), without diabetes, resulting in a 100% increase in cardiac FFA levels compared to controls as early 1 week and maintained until 24 weeks, while no increases in cardiac TG levels was observed.[216] Though this is the opposite situation as seen in these studies, it does demonstrate that the relationship between TG and FFA is not necessarily linear or direct.

#### 5.2.1.1.4 Hypoinsulemia in the model

Reduced circulating insulin levels were seen in the STZ-treated hyperglycemics and is consistent with our previous reports on STZ/HFD animals.[154] This is in agreement with the 75% reduction in fasting circulating insulin in a 45 mg/kg STZ model with HFD (22% fat) at 8 weeks.[213] This had a functional impact in glucose clearance rate during an intraperotoneal glucose tolerance test, where blood glucose levels were 70% higher than the basal value at 2 hours, while the control animals had returned to basal values.[213] Indeed, this model described by Zhang et al. is highly similar to the one used here indicating that hypoinsulemia may be common with this animal model design. In a 35 mg/kg model, STZ and HFD (58% fat) reduced insulin by over 50%,[190] supporting the findings here between the STZ-treated hyperglycemics and vehicle-treated controls. Though Reed et al. show an increase in plasma insulin with the combination of STZ and

HFD compared to chow-fed STZ animals, the elevation is blunted compared to the effect of chow vs. HFD in the absence of STZ treatment.[189] This suggests that addition of STZ to HFD causes a decrease in plasma insulin, again lending support to our finding. This notion is endorsed by a 55 mg/kg, chow-fed STZ rat model that resulted in a 70% reduction circulating insulin levels in the fed-state,[214] implicating STZ as the cause of hypoinsulemia, consistent with its mechanism of action. The hypoinsulinemic state observed in these animals indicates that the model used here is most representative of late-stage T2DM where β-cell mass is reduced and apoptosis is widespread.[147]

#### *5.2.1.2 Duration of Study*

It is possible that the 8 week study duration may have been too brief to allow for detectable hyperglycemia-induced changes in PDE4 presence to occur, however several reports suggest otherwise. Alloxan diabetes altered PDE4 activity within 24-48 hours in the heart, liver, adipose tissue and uterus.[179] Reduced calcium handling was observed at 4-6 weeks of 45 mg/kg[162] and 50 mg/kg[35,163] STZ rats. Altered inotropic responses to AR stimulation were reduced at 6 weeks in 55 mg/kg animals.[217] Six week STZ diabetes led to reduced activities at the SERCA2a and RyR, contributing to an increased intracellular end-diastolic [$Ca^{2+}$], leading to deficiencies in LV developed pressure.[218]

Further, significant elevations in NE of STZ (65 mg/kg) rats were observed at 8 weeks[172] indicating that the chronic SNS effect we sought should have been present. Dampened responses to ISO and NE were also seen at this 8 week timepoint,[211] and are supported by reduced β-AR expression at 8 weeks in 45,[154] 50,[153] and 65 mg/kg

animals.[157] Indeed, the cumulative evidence supports the notion that cell signalling alterations had substantially long enough to develop using an 8-week protocol.

Finally, the research design was limited to an 8 week time course as this was arguably the furthest we could have ethically taken these animals while respecting Animal Care guidelines in preventing undue and excessive pain/discomfort in animal studies.[219] At the time of animal sacrifice at 8 weeks (or 10 weeks in a subset of animals), the rampant, uncontrolled elevation of blood glucose in the STZ-treated hyperglycemics had visibly worn on the health of the animals.

### 5.2.2 PET Imaging

*In vivo* PET imaging with (*R*)-[$^{11}$C]rolipram did not demonstrate significant differences in tracer uptake and retention at 8 weeks post-treatment or 10 weeks post-treatment with desipramine challenge between either of the STZ-treatment groups compared to vehicle-treated controls. Desipramine challenge significantly increased (*R*)-[$^{11}$C]rolipram accumulation within each group relative to their 8 week measures. This mean increase of 21% for all groups indicates that the cardiomyocytes maintain PDE4 responsiveness to acute NE elevations in a hyperglycemic state, consistent with the increased response to desipramine in healthy rats, observed with small animal PET,[220] and with *ex vivo* biodistribution.[128,129] The maintenance of increased PDE4 binding after desipramine treatment in diabetes is in stark contrast to other disease models that exhibit a reduced/impaired PDE4 response to acute norepinephrine stimulation, including adriamycin-induced cardiotoxicity,[140] and diet-induced obesity.[139] This finding with the PDE4-specific (*R*)-[$^{11}$C]rolipram radioligand would support the notion that PDE4 is not

altered in the presence chronic hyperglycemia, despite a reduction in postsynaptic $\beta_1$-ARs.[154]

### 5.2.3 *Ex Vivo* Biodistribution

In agreement with the (*R*)-[$^{11}$C]rolipram small animal PET finding, *ex vivo* biodistribution results reveal no significant difference between (*R*)-[$^{11}$C]rolipram accumulation in heart regions of the three groups. In further support, these same *ex vivo* biodistribution results showed that cardiac (*R*)-[$^{11}$C]rolipram retention increased in response to desipramine challenge at 8 weeks, similar to the PET findings at 10 weeks with desipramine.

### 5.2.4 In Vitro Assays

The *in vitro* assay findings confirm the above radioligand measures, as there were no significant differences in PDE4A, PDE4B and PDE4D expression or PDE4 activity in STZ-treated hyperglycemics compared to the STZ-treated euglycemic and vehicle-treated control groups. Interestingly, however, significant increases in PDE4 expression or activity were not observed between the 8 and 10 week desipramine challenge studies to parallel the findings with (*R*)-[$^{11}$C]rolipram seen in the *in vivo* PET imaging.

From a methodological perspective, one explanation for the mismatch reported here between the (*R*)-[$^{11}$C]rolipram measures and *in vitro* results in response to desipramine stimulation at 10 weeks would be that (*R*)-[$^{11}$C]rolipram is a pan-PDE4 measure for both enzyme expression and activity, while the Western blotting techniques made use of isoform specific antibodies (PDE4A, B and D) and enzyme activity is assessed as its own independent measure. It is conceivable that small, nonsignificant changes observed with

isoform specific detection using Western blotting and/or enzyme activity could combine to create a significant change at the overall PDE4 level, which would be reflected by (*R*)-[$^{11}$C]rolipram imaging.

From a physiological perspective, evidence for increased PDE4 activity/expression due to desipramine treatment can be seen in the rat brain. Two hour electroconvulsive seizure therapy elevated PDE4A and PDE4B mRNA levels in brain, but did not increase PDE activity.[221] Chronic 14-day propanol treatment, reducing NE stimulation, altered PDE4A variants by 15-50% decreases, despite a 33% increase in β-AR $B_{max}$.[222] Alternately, enhanced NE stimulation by 14-day chronic desipramine treatment increased PDE4A by ~80%, despite an ~50% reduction in β-AR population.[223] These findings were confirmed again using desipramine as well as other antidepressants, including monoamine oxidase inhibitor (phenelzine) and serotonin reuptake inhibitor (fluoxetine).[120] Fourteen day chronic desipramine treatment elevated PDE4A and PDE4B, but not PDE4D, mRNA expression in rat frontal cortex.[224] Consistent with this, PDE4A and PDE4B protein expression also elevated significantly (140 and 133%, respectively) in the frontal cortex, but not with PDE4D. These studies indicate that measurable changes in PDE4 activity and expression are evidenced following 14-day chronic desipramine treatment in the brain, and may be seen as soon as 2 hours following treatment. The latter timeline is quite analogous to the 3 hour pre-treatment utilized in the present studies, however no change in activity was observed and protein expression changes were not measured with the 2 hour acute treatment.[221]

This observation of no change in PDE4 activity, despite increased mRNA expression highlights the challenge of accurately quantifying cAMP hydrolysis. Indeed, cAMP

levels are extremely transient in nature,[26] demanding finely tuned PDE responses for cAMP regulation. Thus, small perturbations in homeostasis could potentially have dramatic effects at the cAMP/PDE level. To this end, manipulation of animals in the collection of tissue may be substantial enough to evoke stress responses in the animals, leading to enhanced SNS activity and directly altering cAMP/PDE response. As any experienced animal handler will recognize, not all animals react equally to such stresses[219] and a differing, non-quantifiable effect may be confounding the results of such measures. A solution to this issue would require use of living animals for such assays, however, these are not presently available.

### 5.2.5 Implication of Unaltered PDE4 in STZ/HFD Induced Hyperglycemia

According to literature searches, this is one of the first investigations of cardiac PDE4 in a diabetic animal model. Das and Chain[178] report a 25-35% reduction of cAMP dependent phosphodiesterase in the perfused rat heart in response to STZ-induced diabetes. Similarly, Perez de Gracia et al.[179] described a 33% reduction cardiac cAMP hydrolysis in rat hearts in an Alloxan model of diabetes, as well as activity reductions in liver, adipose tissue and uterus activity.

Mixed results regarding PDE4 changes are observed in various other tissues. No change in PDE4 activity was seen in the T2DM rat kidney.[225] Several studies investigate PDE4 T2DM-dependent alterations in metabolic tissues such as the liver,[181] white and brown adipose tissue[180,226] revealing decreases in response to T2DM. Regarding the PDE3 isoform, overexpression in pancreatic β-cells resulted in the rapid development of glucose intolerance and insulin resistance,[227] while Cilostazol, a PDE3 inhibitor, showed

positive results in the reduction of carotid atherosclerosis in T2DM in humans,[228] inferring an upregulated or over active PDE3 contribution.

#### *5.2.5.1 Increased NE, Reduced $\beta_1$-AR, Unaltered PDE4 Levels?*

A potential explanation for the lack of change in cardiac PDE4 in our study may arise from the interplay between increased cardiac NE and the reduction in $\beta_1$-AR receptor. Duman et al. highlight this possible interaction quite elegantly.[229] Describing the mechanism of antidepressant treatment, which is based on increasing cAMP levels, they postulate that untreated depression results in a certain basal level of cAMP. Following depression treatment, with a reuptake inhibitor such as imipramine, synaptic levels of NE would be markedly raised and cause a temporary elevation in cAMP production until the reflex in β-ARs downregulation occurs.[229] Despite this downregulation, they propose that the NE increases caused by the antidepressant would still enhance cAMP levels to near or above those seen in the basal, untreated state. A mechanism of this nature would account for the maintained level of cAMP, and subsequently PDE4. This situation is analogous to the chronic NE activation of β-ARs seen in diabetes. The end result of this hypothesized scenario is that there is essentially no change in the cAMP production; the reduction in β-ARs is cancelled out by the excess synaptic NE. Indeed, the fundamental purpose of this mechanism would be to protect against chronic overstimulation while maintaining normal cell function, as we have evidenced in our findings with maintained response to elevated NE levels following desipramine challenge.

### *5.2.5.2 Compensatory Role of $\beta_2$-AR*

A second possible explanation may be attributed to the compensatory activity of the $\beta_2$-AR population for the deficiencies experienced by cardiac $\beta_1$-AR reduction. $\beta_1$-AR dominates the healthy myocardium with an approximate 3:1 ratio relative to $\beta_2$-AR in human left ventricle[21] and isolated cardiomyocyte homogenates from canines.[19] Though the majority of the functional outcome of SNS cardiac regulation in the healthy state occurs through $\beta_1$-AR due to its enhanced affinity for NE relative to $\beta_2$-ARs,[230,231] $\beta_2$-ARs are also capable of producing maximum contraction in response to catecholamines in human ventricle preparations.[232,233] Increased functional capacity of $\beta_2$-ARs is also demonstrated in patients receiving $\beta_1$-AR blockade.[234] The ability of $\beta_2$-ARs to achieve this may owe to the fact that the $\beta_2$-AR/$G_{\alpha s}$ efficiency for cAMP production is greater than that of the $\beta_1$-AR/$G_{\alpha s}$ efficiency. If the receptor ratio is altered as expected, the $\beta_2$-AR's ability to generate maximal contraction with fewer receptors present would imply that sufficient cAMP is generated by the remaining total β-AR population and that functional heart deficiencies stem from complications outside of cAMP synthesis.

### *5.2.5.3 Increased Role of $G_{\alpha i}$*

A final explanation may be that the $\beta_2$-ARs, who couple to the inhibitory $G_{\alpha i}$ would suppress cAMP levels by reducing AC activity at the level of cAMP formation. This hypothesis is supported by Gøtzsche,[34] who reports a 50% reduction in ventricular cAMP production in response to acute ISO, with no differences at basal production levels, indicating lack of cardiomyocytes response to acute β-AR stimulation in STZ-

induced diabetes. Surprisingly, this was the case without a reduction in β−AR population. Given that the β−AR population was unaffected in this study, it may suggest the receptors are uncoupled from $G_{\alpha s}$, or sensitized to inhibitory $G_{\alpha i}$ by preference for $\beta_2$-AR signalling in response to ISO. Additional evidence is inferred from calcium measures, where basal and peak calcium levels were unchanged compared to controls in STZ rat myocytes, but β−AR stimulation resulted in a depressed calcium transient current.[35] Also, caffeine stimulated sodium-calcium exchange current was reduced compared to controls.[235]

Against this hypothesis, Gando et al.[161] report reduced cardiac inotropic activities, alongside a 50% drop in β-AR protein and a 65% reduction in $G_{\alpha i}$ protein expression, with a differential effect on $G_{\alpha s}$ isoforms. The concomitant reduction in cardiac function and $G_{\alpha i}$ protein expression would suggest a mechanism independent of $G_{\alpha i}$, potentially occurring beyond the level of AC action.

# 6. Conclusion

## *6.1 Summary of Scientific Findings*

(*R*)-[$^{11}$C]Rolipram small animal PET imaging demonstrates PDE4-specific binding in rat heart that is sensitive to increases in NE levels and is saturable by unlabeled (*R*)-rolipram. Quantification of the tracer distribution volume by Logan graphical analysis is reproducible. PDE4 cardiac expression and enzyme activity are not altered by hyperglycemia in the moderate dose STZ/HFD rat model as measured by PDE4-specific (*R*)-[$^{11}$C]rolipram small animal PET, *ex vivo* biodistribution or *in vitro* measures. Increased (*R*)-[$^{11}$C]rolipram uptake was observed in 8 weeks compared to 10 weeks post-treatment with desipramine using small animal PET, indicating that the cardiomyocytes of the left ventricle exhibit normal cell signalling that remains responsive to elevated NE stimulation despite reductions in $\beta_1$−AR.

## 6.2 Future Directions

The *in vivo* small animal PET characterization studies provide encouraging evidence that this radioligand is measuring PDE4 presence accurately, with the reproducibility results being quite optimistic. The lack of significant differences in (*R*)-[$^{11}$C]rolipram retention in hyperglycemics compared to euglycemics and controls was a surprising result, however, it was encouraging to learn that this finding was supported by *in vitro* techniques of protein expression and activity. Thus, the role of (*R*)-[$^{11}$C]rolipram may have limited applicability in diabetes, but certainly maintains its investigative potential for other pathologies, such as heart failure or obesity, that present challenges related to altered cardiac cell signalling.

# 7. References

1. Dzimiri N. Regulation of beta-adrenoceptor signaling in cardiac function and disease. *Pharmacol Rev.* 1999;51(3):465-501.
2. Salazar NC, Chen J, Rockman HA. Cardiac GPCRs: GPCR signaling in healthy and failing hearts. *Biochim Biophys Acta.* 2007;1768(4):1006-1018.
3. Lebeche D, Davidoff AJ, Hajjar RJ. Interplay between impaired calcium regulation and insulin signaling abnormalities in diabetic cardiomyopathy. *Nat Clin Pract Cardiovasc Med.* 2008;5(11):715-724.
4. Esler M, Rumantir M, Wiesner G, Kaye D, Hastings J, Lambert G. Sympathetic nervous system and insulin resistance: from obesity to diabetes. *Am J Hypertens.* 2001;14(11 Pt 2):304S-309S.
5. Triposkiadis F, Karayannis G, Giamouzis G, Skoularigis J, Louridas G, Butler J. The sympathetic nervous system in heart failure physiology, pathophysiology, and clinical implications. *J Am Coll Cardiol.* 2009;54(19):1747-1762.
6. Kaumann AJ, Molenaar P. Modulation of human cardiac function through 4 beta-adrenoceptor populations. *Naunyn Schmiedebergs Arch Pharmacol.* 1997;355(6):667-681.
7. Piascik MT, Perez DM. Alpha1-adrenergic receptors: new insights and directions. *J Pharmacol Exp Ther.* 2001;298(2):403-410.
8. Rozec B, Gauthier C. beta3-adrenoceptors in the cardiovascular system: putative roles in human pathologies. *Pharmacol Ther.* 2006;111(3):652-673.
9. Molenaar P, Chen L, Semmler AB, Parsonage WA, Kaumann AJ. Human heart beta-adrenoceptors: beta1-adrenoceptor diversification through 'affinity states' and polymorphism. *Clin Exp Pharmacol Physiol.* 2007;34(10):1020-1028.
10. Gyires K, Zadori ZS, Torok T, Matyus P. alpha(2)-Adrenoceptor subtypes-mediated physiological, pharmacological actions. *Neurochem Int.* 2009;55(7):447-453.
11. Kohout TA, Takaoka H, McDonald PH, Perry SJ, Mao L, Lefkowitz RJ, Rockman HA. Augmentation of cardiac contractility mediated by the human beta(3)-adrenergic receptor overexpressed in the hearts of transgenic mice. *Circulation.* 2001;104(20):2485-2491.
12. Gauthier C, Tavernier G, Charpentier F, Langin D, Le Marec H. Functional beta3-adrenoceptor in the human heart. *J Clin Invest.* 1996;98(2):556-562.
13. Devic E, Xiang Y, Gould D, Kobilka B. Beta-adrenergic receptor subtype-specific signaling in cardiac myocytes from beta(1) and beta(2) adrenoceptor knockout mice. *Mol Pharmacol.* 2001;60(3):577-583.
14. Emorine LJ, Marullo S, Briend-Sutren MM, Patey G, Tate K, Delavier-Klutchko C, Strosberg AD. Molecular characterization of the human beta 3-adrenergic receptor. *Science.* 1989;245(4922):1118-1121.

15. Heitz A, Schwartz J, Velly J. Beta-adrenoceptors of the human myocardium: determination of beta 1 and beta 2 subtypes by radioligand binding. *Br J Pharmacol.* 1983;80(4):711-717.
16. Michel MC, Pingsmann A, Beckeringh JJ, Zerkowski HR, Doetsch N, Brodde OE. Selective regulation of beta 1- and beta 2-adrenoceptors in the human heart by chronic beta-adrenoceptor antagonist treatment. *Br J Pharmacol.* 1988;94(3):685-692.
17. Brodde OE, Karad K, Zerkowski HR, Rohm N, Reidemeister JC. Coexistence of beta 1- and beta 2-adrenoceptors in human right atrium. Direct identification by (+/-)-[125I]iodocyanopindolol binding. *Circ Res.* 1983;53(6):752-758.
18. Stiles GL, Taylor S, Lefkowitz RJ. Human cardiac beta-adrenergic receptors: subtype heterogeneity delineated by direct radioligand binding. *Life Sci.* 1983;33(5):467-473.
19. Laurent CE, Cardinal R, Rousseau G, Vermeulen M, Bouchard C, Wilkinson M, Armour JA, Bouvier M. Functional desensitization to isoproterenol without reducing cAMP production in canine failing cardiocytes. *Am J Physiol Regul Integr Comp Physiol.* 2001;280(2):R355-364.
20. Kaumann AJ, Lemoine H. Beta 2-adrenoceptor-mediated positive inotropic effect of adrenaline in human ventricular myocardium. Quantitative discrepancies with binding and adenylate cyclase stimulation. *Naunyn Schmiedebergs Arch Pharmacol.* 1987;335(4):403-411.
21. Bristow MR, Minobe W, Rasmussen R, Larrabee P, Skerl L, Klein JW, Anderson FL, Murray J, Mestroni L, Karwande SV, et al. Beta-adrenergic neuroeffector abnormalities in the failing human heart are produced by local rather than systemic mechanisms. *J Clin Invest.* 1992;89(3):803-815.
22. Kashiwagi A, Nishio Y, Saeki Y, Kida Y, Kodama M, Shigeta Y. Plasma membrane-specific deficiency in cardiac beta-adrenergic receptor in streptozocin-diabetic rats. *Am J Physiol.* 1989;257(2 Pt 1):E127-132.
23. Sellers DJ, Chess-Williams R. The effect of streptozotocin-induced diabetes on cardiac beta-adrenoceptor subtypes in the rat. *J Auton Pharmacol.* 2001;21(1):15-21.
24. Brodde OE, O'Hara N, Zerkowski HR, Rohm N. Human cardiac beta-adrenoceptors: both beta 1- and beta 2-adrenoceptors are functionally coupled to the adenylate cyclase in right atrium. *J Cardiovasc Pharmacol.* 1984;6(6):1184-1191.
25. Surya A, Stadel JM, Knox BE. Evidence for multiple, biochemically distinguishable states in the G protein-coupled receptor, rhodopsin. *Trends Pharmacol Sci.* 1998;19(7):243-247.
26. Leroy J, Abi-Gerges A, Nikolaev VO, Richter W, Lechene P, Mazet JL, Conti M, Fischmeister R, Vandecasteele G. Spatiotemporal dynamics of beta-adrenergic cAMP signals and L-type Ca2+ channel regulation in adult rat ventricular myocytes: role of phosphodiesterases. *Circ Res.* 2008;102(9):1091-1100.

27. Brooker G. Oscillation of cyclic adenosine monophosphate concentration during the myocardial contraction cycle. *Science.* 1973;182(115):933-934.
28. Tang T, Gao MH, Lai NC, Firth AL, Takahashi T, Guo T, Yuan JX, Roth DM, Hammond HK. Adenylyl cyclase type 6 deletion decreases left ventricular function via impaired calcium handling. *Circulation.* 2008;117(1):61-69.
29. Xiao RP, Cheng H, Zhou YY, Kuschel M, Lakatta EG. Recent advances in cardiac beta(2)-adrenergic signal transduction. *Circ Res.* 1999;85(11):1092-1100.
30. Kaumann AJ, Sanders L, Lynham JA, Bartel S, Kuschel M, Karczewski P, Krause EG. Beta 2-adrenoceptor activation by zinterol causes protein phosphorylation, contractile effects and relaxant effects through a cAMP pathway in human atrium. *Mol Cell Biochem.* 1996;163-164:113-123.
31. Engelhardt S, Hein L, Wiesmann F, Lohse MJ. Progressive hypertrophy and heart failure in beta1-adrenergic receptor transgenic mice. *Proc Natl Acad Sci U S A.* 1999;96(12):7059-7064.
32. Chruscinski AJ, Rohrer DK, Schauble E, Desai KH, Bernstein D, Kobilka BK. Targeted disruption of the beta2 adrenergic receptor gene. *J Biol Chem.* 1999;274(24):16694-16700.
33. Hulme JT, Westenbroek RE, Scheuer T, Catterall WA. Phosphorylation of serine 1928 in the distal C-terminal domain of cardiac CaV1.2 channels during beta1-adrenergic regulation. *Proc Natl Acad Sci U S A.* 2006;103(44):16574-16579.
34. Gotzsche O. The adrenergic beta-receptor adenylate cyclase system in heart and lymphocytes from streptozotocin-diabetic rats. In vivo and in vitro evidence for a desensitized myocardial beta-receptor. *Diabetes.* 1983;32(12):1110-1116.
35. Ha T, Kotsanas G, Wendt I. Intracellular Ca2+ and adrenergic responsiveness of cardiac myocytes in streptozotocin-induced diabetes. *Clin Exp Pharmacol Physiol.* 1999;26(4):347-353.
36. Kuschel M, Zhou YY, Cheng H, Zhang SJ, Chen Y, Lakatta EG, Xiao RP. G(i) protein-mediated functional compartmentalization of cardiac beta(2)-adrenergic signaling. *J Biol Chem.* 1999;274(31):22048-22052.
37. Daaka Y, Luttrell LM, Lefkowitz RJ. Switching of the coupling of the beta2-adrenergic receptor to different G proteins by protein kinase A. *Nature.* 1997;390(6655):88-91.
38. Xiao RP, Ji X, Lakatta EG. Functional coupling of the beta 2-adrenoceptor to a pertussis toxin-sensitive G protein in cardiac myocytes. *Mol Pharmacol.* 1995;47(2):322-329.
39. Zheng M, Zhang SJ, Zhu WZ, Ziman B, Kobilka BK, Xiao RP. beta 2-adrenergic receptor-induced p38 MAPK activation is mediated by protein kinase A rather than by Gi or gbeta gamma in adult mouse cardiomyocytes. *J Biol Chem.* 2000;275(51):40635-40640.

40. Bers DM. Sarcoplasmic reticulum Ca release in intact ventricular myocytes. *Front Biosci.* 2002;7:d1697-1711.
41. Morimoto S, J OU, Kawai M, Hoshina T, Kusakari Y, Komukai K, Sasaki H, Hongo K, Kurihara S. Protein kinase A-dependent phosphorylation of ryanodine receptors increases Ca2+ leak in mouse heart. *Biochem Biophys Res Commun.* 2009;390(1):87-92.
42. Sarma S, Li N, van Oort RJ, Reynolds C, Skapura DG, Wehrens XH. Genetic inhibition of PKA phosphorylation of RyR2 prevents dystrophic cardiomyopathy. *Proc Natl Acad Sci U S A.* 2010;107(29):13165-13170.
43. Kohr MJ, Traynham CJ, Roof SR, Davis JP, Ziolo MT. cAMP-independent activation of protein kinase A by the peroxynitrite generator SIN-1 elicits positive inotropic effects in cardiomyocytes. *J Mol Cell Cardiol.* 2010;48(4):645-648.
44. Patel HH, Hamuro LL, Chun BJ, Kawaraguchi Y, Quick A, Rebolledo B, Pennypacker J, Thurston J, Rodriguez-Pinto N, Self C, Olson G, Insel PA, Giles WR, Taylor SS, Roth DM. Disruption of protein kinase A localization using a trans-activator of transcription (TAT)-conjugated A-kinase-anchoring peptide reduces cardiac function. *J Biol Chem.* 2010;285(36):27632-27640.
45. Kaumann A, Bartel S, Molenaar P, Sanders L, Burrell K, Vetter D, Hempel P, Karczewski P, Krause EG. Activation of beta2-adrenergic receptors hastens relaxation and mediates phosphorylation of phospholamban, troponin I, and C-protein in ventricular myocardium from patients with terminal heart failure. *Circulation.* 1999;99(1):65-72.
46. Molenaar P, Bartel S, Cochrane A, Vetter D, Jalali H, Pohlner P, Burrell K, Karczewski P, Krause EG, Kaumann A. Both beta(2)- and beta(1)-adrenergic receptors mediate hastened relaxation and phosphorylation of phospholamban and troponin I in ventricular myocardium of Fallot infants, consistent with selective coupling of beta(2)-adrenergic receptors to G(s)-protein. *Circulation.* 2000;102(15):1814-1821.
47. Colson BA, Bekyarova T, Locher MR, Fitzsimons DP, Irving TC, Moss RL. Protein kinase A-mediated phosphorylation of cMyBP-C increases proximity of myosin heads to actin in resting myocardium. *Circ Res.* 2008;103(3):244-251.
48. Tong CW, Stelzer JE, Greaser ML, Powers PA, Moss RL. Acceleration of crossbridge kinetics by protein kinase A phosphorylation of cardiac myosin binding protein C modulates cardiac function. *Circ Res.* 2008;103(9):974-982.
49. Hanft LM, McDonald KS. Sarcomere length dependence of power output is increased after PKA treatment in rat cardiac myocytes. *Am J Physiol Heart Circ Physiol.* 2009;296(5):H1524-1531.
50. Ferguson SS. Evolving concepts in G protein-coupled receptor endocytosis: the role in receptor desensitization and signaling. *Pharmacol Rev.* 2001;53(1):1-24.
51. Ferguson SS, Caron MG. G protein-coupled receptor adaptation mechanisms. *Semin Cell Dev Biol.* 1998;9(2):119-127.

52. Muntz KH, Zhao M, Miller JC. Downregulation of myocardial beta-adrenergic receptors. Receptor subtype selectivity. *Circ Res.* 1994;74(3):369-375.
53. Kudej RK, Iwase M, Uechi M, Vatner DE, Oka N, Ishikawa Y, Shannon RP, Bishop SP, Vatner SF. Effects of chronic beta-adrenergic receptor stimulation in mice. *J Mol Cell Cardiol.* 1997;29(10):2735-2746.
54. Pitcher JA, Freedman NJ, Lefkowitz RJ. G protein-coupled receptor kinases. *Annu Rev Biochem.* 1998;67:653-692.
55. Lohse MJ, Benovic JL, Caron MG, Lefkowitz RJ. Multiple pathways of rapid beta 2-adrenergic receptor desensitization. Delineation with specific inhibitors. *J Biol Chem.* 1990;265(6):3202-3211.
56. Gurevich VV, Gurevich EV. The structural basis of arrestin-mediated regulation of G-protein-coupled receptors. *Pharmacol Ther.* 2006;110(3):465-502.
57. Luttrell LM, Lefkowitz RJ. The role of beta-arrestins in the termination and transduction of G-protein-coupled receptor signals. *J Cell Sci.* 2002;115(Pt 3):455-465.
58. Oakley RH, Laporte SA, Holt JA, Barak LS, Caron MG. Association of beta-arrestin with G protein-coupled receptors during clathrin-mediated endocytosis dictates the profile of receptor resensitization. *J Biol Chem.* 1999;274(45):32248-32257.
59. Krueger KM, Daaka Y, Pitcher JA, Lefkowitz RJ. The role of sequestration in G protein-coupled receptor resensitization. Regulation of beta2-adrenergic receptor dephosphorylation by vesicular acidification. *J Biol Chem.* 1997;272(1):5-8.
60. Trejo J, Coughlin SR. The cytoplasmic tails of protease-activated receptor-1 and substance P receptor specify sorting to lysosomes versus recycling. *J Biol Chem.* 1999;274(4):2216-2224.
61. Anderson FL, Port JD, Reid BB, Larrabee P, Hanson G, Bristow MR. Myocardial catecholamine and neuropeptide Y depletion in failing ventricles of patients with idiopathic dilated cardiomyopathy. Correlation with beta-adrenergic receptor downregulation. *Circulation.* 1992;85(1):46-53.
62. McMartin L, Summers RJ. Functional analysis of desensitization of the beta-adrenoceptor signalling pathway in rat cardiac tissues following chronic isoprenaline infusion. *Br J Pharmacol.* 1999;127(4):1012-1020.
63. Mardon K, Montagne O, Elbaz N, Malek Z, Syrota A, Dubois-Rande JL, Meignan M, Merlet P. Uptake-1 carrier downregulates in parallel with the beta-adrenergic receptor desensitization in rat hearts chronically exposed to high levels of circulating norepinephrine: implications for cardiac neuroimaging in human cardiomyopathies. *J Nucl Med.* 2003;44(9):1459-1466.
64. Kawai H, Mohan A, Hagen J, Dong E, Armstrong J, Stevens SY, Liang CS. Alterations in cardiac adrenergic terminal function and beta-adrenoceptor density in pacing-induced heart failure. *Am J Physiol Heart Circ Physiol.* 2000;278(5):H1708-1716.

65. Kaye DM, Lefkovits J, Jennings GL, Bergin P, Broughton A, Esler MD. Adverse consequences of high sympathetic nervous activity in the failing human heart. *J Am Coll Cardiol.* 1995;26(5):1257-1263.
66. Bristow MR, Hershberger RE, Port JD, Minobe W, Rasmussen R. Beta 1- and beta 2-adrenergic receptor-mediated adenylate cyclase stimulation in nonfailing and failing human ventricular myocardium. *Mol Pharmacol.* 1989;35(3):295-303.
67. Steinfath M, Lavicky J, Schmitz W, Scholz H, Doring V, Kalmar P. Regional distribution of beta 1- and beta 2-adrenoceptors in the failing and nonfailing human heart. *Eur J Clin Pharmacol.* 1992;42(6):607-611.
68. Conti M, Beavo J. Biochemistry and physiology of cyclic nucleotide phosphodiesterases: essential components in cyclic nucleotide signaling. *Annu Rev Biochem.* 2007;76:481-511.
69. Maurice DH, Palmer D, Tilley DG, Dunkerley HA, Netherton SJ, Raymond DR, Elbatarny HS, Jimmo SL. Cyclic nucleotide phosphodiesterase activity, expression, and targeting in cells of the cardiovascular system. *Mol Pharmacol.* 2003;64(3):533-546.
70. Houslay MD, Baillie GS, Maurice DH. cAMP-Specific phosphodiesterase-4 enzymes in the cardiovascular system: a molecular toolbox for generating compartmentalized cAMP signaling. *Circ Res.* 2007;100(7):950-966.
71. Baillie GS. Compartmentalized signalling: spatial regulation of cAMP by the action of compartmentalized phosphodiesterases. *FEBS J.* 2009;276(7):1790-1799.
72. Jurevicius J, Skeberdis VA, Fischmeister R. Role of cyclic nucleotide phosphodiesterase isoforms in cAMP compartmentation following beta2-adrenergic stimulation of ICa,L in frog ventricular myocytes. *J Physiol.* 2003;551(Pt 1):239-252.
73. Mongillo M, McSorley T, Evellin S, Sood A, Lissandron V, Terrin A, Huston E, Hannawacker A, Lohse MJ, Pozzan T, Houslay MD, Zaccolo M. Fluorescence resonance energy transfer-based analysis of cAMP dynamics in live neonatal rat cardiac myocytes reveals distinct functions of compartmentalized phosphodiesterases. *Circ Res.* 2004;95(1):67-75.
74. Zaccolo M, Pozzan T. Discrete microdomains with high concentration of cAMP in stimulated rat neonatal cardiac myocytes. *Science.* 2002;295(5560):1711-1715.
75. Tasken KA, Collas P, Kemmner WA, Witczak O, Conti M, Tasken K. Phosphodiesterase 4D and protein kinase a type II constitute a signaling unit in the centrosomal area. *J Biol Chem.* 2001;276(25):21999-22002.
76. Yang J, Drazba JA, Ferguson DG, Bond M. A-kinase anchoring protein 100 (AKAP100) is localized in multiple subcellular compartments in the adult rat heart. *J Cell Biol.* 1998;142(2):511-522.
77. Dodge KL, Khouangsathiene S, Kapiloff MS, Mouton R, Hill EV, Houslay MD, Langeberg LK, Scott JD. mAKAP assembles a protein kinase A/PDE4 phosphodiesterase cAMP signaling module. *EMBO J.* 2001;20(8):1921-1930.

78. Lugnier C, Keravis T, Le Bec A, Pauvert O, Proteau S, Rousseau E. Characterization of cyclic nucleotide phosphodiesterase isoforms associated to isolated cardiac nuclei. *Biochim Biophys Acta.* 1999;1472(3):431-446.
79. Nikolaev VO, Bunemann M, Schmitteckert E, Lohse MJ, Engelhardt S. Cyclic AMP imaging in adult cardiac myocytes reveals far-reaching beta1-adrenergic but locally confined beta2-adrenergic receptor-mediated signaling. *Circ Res.* 2006;99(10):1084-1091.
80. Rochais F, Abi-Gerges A, Horner K, Lefebvre F, Cooper DM, Conti M, Fischmeister R, Vandecasteele G. A specific pattern of phosphodiesterases controls the cAMP signals generated by different Gs-coupled receptors in adult rat ventricular myocytes. *Circ Res.* 2006;98(8):1081-1088.
81. Christ T, Galindo-Tovar A, Thoms M, Ravens U, Kaumann AJ. Inotropy and L-type Ca2+ current, activated by beta1- and beta2-adrenoceptors, are differently controlled by phosphodiesterases 3 and 4 in rat heart. *Br J Pharmacol.* 2009;156(1):62-83.
82. Xu RX, Hassell AM, Vanderwall D, Lambert MH, Holmes WD, Luther MA, Rocque WJ, Milburn MV, Zhao Y, Ke H, Nolte RT. Atomic structure of PDE4: insights into phosphodiesterase mechanism and specificity. *Science.* 2000;288(5472):1822-1825.
83. Bertin R, Portet R. 3':5'-Cyclic-AMP phosphodiesterase activities in white and brown adipose tissues of cold-acclimated rats. *Can J Biochem.* 1975;53(12):1301-1308.
84. Conti M, Jin SL. The molecular biology of cyclic nucleotide phosphodiesterases. *Prog Nucleic Acid Res Mol Biol.* 1999;63:1-38.
85. Houslay MD, Adams DR. PDE4 cAMP phosphodiesterases: modular enzymes that orchestrate signalling cross-talk, desensitization and compartmentalization. *Biochem J.* 2003;370(Pt 1):1-18.
86. Pyne NJ, Furman BL. Cyclic nucleotide phosphodiesterases in pancreatic islets. *Diabetologia.* 2003;46(9):1179-1189.
87. Liu S, Laliberte F, Bobechko B, Bartlett A, Lario P, Gorseth E, Van Hamme J, Gresser MJ, Huang Z. Dissecting the cofactor-dependent and independent bindings of PDE4 inhibitors. *Biochemistry.* 2001;40(34):10179-10186.
88. Percival MD, Yeh B, Falgueyret JP. Zinc dependent activation of cAMP-specific phosphodiesterase (PDE4A). *Biochem Biophys Res Commun.* 1997;241(1):175-180.
89. Laliberte F, Liu S, Gorseth E, Bobechko B, Bartlett A, Lario P, Gresser MJ, Huang Z. In vitro PKA phosphorylation-mediated human PDE4A4 activation. *FEBS Lett.* 2002;512(1-3):205-208.
90. Laliberte F, Han Y, Govindarajan A, Giroux A, Liu S, Bobechko B, Lario P, Bartlett A, Gorseth E, Gresser M, Huang Z. Conformational difference between PDE4 apoenzyme and holoenzyme. *Biochemistry.* 2000;39(21):6449-6458.
91. Oki N, Takahashi SI, Hidaka H, Conti M. Short term feedback regulation of cAMP in FRTL-5 thyroid cells. Role of PDE4D3 phosphodiesterase activation. *J Biol Chem.* 2000;275(15):10831-10837.

92. Liu H, Maurice DH. Phosphorylation-mediated activation and translocation of the cyclic AMP-specific phosphodiesterase PDE4D3 by cyclic AMP-dependent protein kinase and mitogen-activated protein kinases. A potential mechanism allowing for the coordinated regulation of PDE4D activity and targeting. *J Biol Chem.* 1999;274(15):10557-10565.

93. Alvarez R, Sette C, Yang D, Eglen RM, Wilhelm R, Shelton ER, Conti M. Activation and selective inhibition of a cyclic AMP-specific phosphodiesterase, PDE-4D3. *Mol Pharmacol.* 1995;48(4):616-622.

94. Corbin JD, Beebe SJ, Blackmore PF. cAMP-dependent protein kinase activation lowers hepatocyte cAMP. *J Biol Chem.* 1985;260(15):8731-8735.

95. Gettys TW, Vine AJ, Simonds MF, Corbin JD. Activation of the particulate low Km phosphodiesterase of adipocytes by addition of cAMP-dependent protein kinase. *J Biol Chem.* 1988;263(21):10359-10363.

96. Hoffmann R, Wilkinson IR, McCallum JF, Engels P, Houslay MD. cAMP-specific phosphodiesterase HSPDE4D3 mutants which mimic activation and changes in rolipram inhibition triggered by protein kinase A phosphorylation of Ser-54: generation of a molecular model. *Biochem J.* 1998;333 ( Pt 1):139-149.

97. Sette C, Conti M. Phosphorylation and activation of a cAMP-specific phosphodiesterase by the cAMP-dependent protein kinase. Involvement of serine 54 in the enzyme activation. *J Biol Chem.* 1996;271(28):16526-16534.

98. Hoffmann R, Baillie GS, MacKenzie SJ, Yarwood SJ, Houslay MD. The MAP kinase ERK2 inhibits the cyclic AMP-specific phosphodiesterase HSPDE4D3 by phosphorylating it at Ser579. *EMBO J.* 1999;18(4):893-903.

99. Baillie GS, MacKenzie SJ, McPhee I, Houslay MD. Sub-family selective actions in the ability of Erk2 MAP kinase to phosphorylate and regulate the activity of PDE4 cyclic AMP-specific phosphodiesterases. *Br J Pharmacol.* 2000;131(4):811-819.

100. MacKenzie SJ, Baillie GS, McPhee I, Bolger GB, Houslay MD. ERK2 mitogen-activated protein kinase binding, phosphorylation, and regulation of the PDE4D cAMP-specific phosphodiesterases. The involvement of COOH-terminal docking sites and NH2-terminal UCR regions. *J Biol Chem.* 2000;275(22):16609-16617.

101. Beard MB, Olsen AE, Jones RE, Erdogan S, Houslay MD, Bolger GB. UCR1 and UCR2 domains unique to the cAMP-specific phosphodiesterase family form a discrete module via electrostatic interactions. *J Biol Chem.* 2000;275(14):10349-10358.

102. Mayr B, Montminy M. Transcriptional regulation by the phosphorylation-dependent factor CREB. *Nat Rev Mol Cell Biol.* 2001;2(8):599-609.

103. Gonzalez GA, Montminy MR. Cyclic AMP stimulates somatostatin gene transcription by phosphorylation of CREB at serine 133. *Cell.* 1989;59(4):675-680.

104. Chrivia JC, Kwok RP, Lamb N, Hagiwara M, Montminy MR, Goodman RH. Phosphorylated CREB binds specifically to the nuclear protein CBP. *Nature.* 1993;365(6449):855-859.

105. Le Jeune IR, Shepherd M, Van Heeke G, Houslay MD, Hall IP. Cyclic AMP-dependent transcriptional up-regulation of phosphodiesterase 4D5 in human airway smooth muscle cells. Identification and characterization of a novel PDE4D5 promoter. *J Biol Chem.* 2002;277(39):35980-35989.
106. Tilley DG, Maurice DH. Vascular smooth muscle cell phosphodiesterase (PDE) 3 and PDE4 activities and levels are regulated by cyclic AMP in vivo. *Mol Pharmacol.* 2002;62(3):497-506.
107. Liu H, Palmer D, Jimmo SL, Tilley DG, Dunkerley HA, Pang SC, Maurice DH. Expression of phosphodiesterase 4D (PDE4D) is regulated by both the cyclic AMP-dependent protein kinase and mitogen-activated protein kinase signaling pathways. A potential mechanism allowing for the coordinated regulation of PDE4D activity and expression in cells. *J Biol Chem.* 2000;275(34):26615-26624.
108. Wu JC, Bengel FM, Gambhir SS. Cardiovascular molecular imaging. *Radiology.* 2007;244(2):337-355.
109. Ametamey SM, Honer M, Schubiger PA. Molecular imaging with PET. *Chem Rev.* 2008;108(5):1501-1516.
110. Hume SP, Jones T. Positron Emission Tomography (PET) Methodology for Small Animal and its Application in Radiopharmaceutical Preclinical Investigation. *Nuclear Medicine and Biology.* 1998;25:729-732.
111. Hume SP, Myers R. Dedicated Small Animal Scanners: A New Tool for Drug Development? *Current Pharmaceutical Design.* 2002;8:1497-1511.
112. Wahl RL. *Principles and Practice of Positron Emission Tomography*. Philadelphia, PA, USA: Lippincott Williams & Wilkins; 2002.
113. Lammertsma AA. Radioligand studies: imaging and quantitative analysis. *Eur Neuropsychopharmacol.* 2002;12(6):513-516.
114. Gunn RN, Gunn SR, Cunningham VJ. Positron emission tomography compartmental models. *J Cereb Blood Flow Metab.* 2001;21(6):635-652.
115. Kung MP, Kung HF. Mass effect of injected dose in small rodent imaging by SPECT and PET. *Nucl Med Biol.* 2005;32(7):673-678.
116. Hume SP, Gunn RN, Jones T. Pharmacological constraints associated with positron emission tomographic scanning of small laboratory animals. *European Journal of Nuclear Medicine.* 1998;25:173-176.
117. Jagoda EM, Vaquero JJ, Seidel J, Green MV, Eckelman WC. Experiment assessment of mass effects in the rat: implications for small animal PET imaging. *Nucl Med Biol.* 2004;31(6):771-779.
118. Alexoff DL, Vaska P, Marsteller D, Gerasimov T, Li J, Logan J, Fowler JS, Taintor NB, Thanos PK, Volkow ND. Reproducibility of 11C-raclopride binding in the rat brain measured with the microPET R4: effects of scatter correction and tracer specific activity. *J Nucl Med.* 2003;44(5):815-822.

119. Fujita M, Zoghbi SS, Crescenzo MS, Hong J, Musachio JL, Lu JQ, Liow JS, Seneca N, Tipre DN, Cropley VL, Imaizumi M, Gee AD, Seidel J, Green MV, Pike VW, Innis RB. Quantification of brain phosphodiesterase 4 in rat with (R)-[11C]Rolipram-PET. *Neuroimage.* 2005;26(4):1201-1210.

120. Ye Y, Jackson K, O'Donnell JM. Effects of repeated antidepressant treatment of type 4A phosphodiesterase (PDE4A) in rat brain. *J Neurochem.* 2000;74(3):1257-1262.

121. DaSilva JN, Lourenco CM, Wilson AA, Houle S. Syntheses of the phosphodiesterase-4 inhibitors [11C]Ro 20-1724, R-,R/S and S-[11C]rolipram. *Journal of Labeled Compounds in Radiopharmacology.* 2001;44:373-384.

122. Hebenstreit GF, Fellerer K, Fichte K, Fischer G, Geyer N, Meya U, Sastre-y-Hernandez M, Schony W, Schratzer M, Soukop W, et al. Rolipram in major depressive disorder: results of a double-blind comparative study with imipramine. *Pharmacopsychiatry.* 1989;22(4):156-160.

123. Hirose R, Manabe H, Nonaka H, Yanagawa K, Akuta K, Sato S, Ohshima E, Ichimura M. Correlation between emetic effect of phosphodiesterase 4 inhibitors and their occupation of the high-affinity rolipram binding site in Suncus murinus brain. *Eur J Pharmacol.* 2007;573(1-3):93-99.

124. Robichaud A, Savoie C, Stamatiou PB, Tattersall FD, Chan CC. PDE4 inhibitors induce emesis in ferrets via a noradrenergic pathway. *Neuropharmacology.* 2001;40(2):262-269.

125. Schneider HH, Schmiechen R, Brezinski M, Seidler J. Stereospecific binding of the antidepressant rolipram to brain protein structures. *Eur J Pharmacol.* 1986;127(1-2):105-115.

126. Houslay MD, Sullivan M, Bolger GB. The multienzyme PDE4 cyclic adenosine monophosphate-specific phosphodiesterase family: intracellular targeting, regulation, and selective inhibition by compounds exerting anti-inflammatory and antidepressant actions. *Adv Pharmacol.* 1998;44:225-342.

127. Wang P, Myers JG, Wu P, Cheewatrakoolpong B, Egan RW, Billah MM. Expression, purification, and characterization of human cAMP-specific phosphodiesterase (PDE4) subtypes A, B, C, and D. *Biochem Biophys Res Commun.* 1997;234(2):320-324.

128. Kenk M, Greene M, Thackeray J, deKemp RA, Lortie M, Thorn S, Beanlands RS, DaSilva JN. In vivo selective binding of (R)-[11C]rolipram to phosphodiesterase-4 provides the basis for studying intracellular cAMP signaling in the myocardium and other peripheral tissues. *Nucl Med Biol.* 2007;34(1):71-77.

129. Lourenco CM, Kenk M, Beanlands RS, DaSilva JN. Increasing synaptic noradrenaline, serotonin and histamine enhances in vivo binding of phosphodiesterase-4 inhibitor (R)-[11C]rolipram in rat brain, lung and heart. *Life Sci.* 2006;79(4):356-364.

130. Kenk M, Greene M, Lortie M, Dekemp RA, Beanlands RS, Dasilva JN. Use of a column-switching high-performance liquid chromatography method to assess the

presence of specific binding of (R)- and (S)-[(11)C]rolipram and their labeled metabolites to the phosphodiesterase-4 enzyme in rat plasma and tissues. *Nucl Med Biol.* 2008;35(4):515-521.

131. Tsukada H, Harada N, Ohba H, Nishiyama S, Kakiuchi T. Facilitation of dopaminergic neural transmission does not affect [(11)C]SCH23390 binding to the striatal D(1) dopamine receptors, but the facilitation enhances phosphodiesterase type-IV activity through D(1) receptors: PET studies in the conscious monkey brain. *Synapse.* 2001;42(4):258-265.

132. DaSilva JN, Lourenco CM, Meyer JH, Hussey D, Potter WZ, Houle S. Imaging cAMP-specific phosphodiesterase-4 in human brain with R-[11C]rolipram and positron emission tomography. *Eur J Nucl Med Mol Imaging.* 2002;29(12):1680-1683.

133. Fujita M, Imaizumi M, D'Sa C, Zoghbi SS, Crescenzo MS, Hong J, Musachio JL, Gee AD, Seidel J, Green MV, Pike VW, Duman RS, Innis RB. In vivo and in vitro measurement of brain phosphodiesterase 4 in rats after antidepressant administration. *Synapse.* 2007;61(2):78-86.

134. Itoh T, Abe K, Zoghbi SS, Inoue O, Hong J, Imaizumi M, Pike VW, Innis RB, Fujita M. PET measurement of the in vivo affinity of 11C-(R)-rolipram and the density of its target, phosphodiesterase-4, in the brains of conscious and anesthetized rats. *J Nucl Med.* 2009;50(5):749-756.

135. Itoh T, Abe K, Hong J, Inoue O, Pike VW, Innis RB, Fujita M. Effects of cAMP-dependent protein kinase activator and inhibitor on in vivo rolipram binding to phosphodiesterase 4 in conscious rats. *Synapse.* 2010;64(2):172-176.

136. Zhao Y, Zhang HT, O'Donnell JM. Antidepressant-induced increase in high-affinity rolipram binding sites in rat brain: dependence on noradrenergic and serotonergic function. *J Pharmacol Exp Ther.* 2003;307(1):246-253.

137. Parker CA, Matthews JC, Gunn RN, Martarello L, Cunningham VJ, Dommett D, Knibb ST, Bender D, Jakobsen S, Brown J, Gee AD. Behaviour of [11C]R(-)- and [11C]S(+)-rolipram in vitro and in vivo, and their use as PET radiotracers for the quantificative assay of PDE4. *Synapse.* 2005;55(4):270-279.

138. Lortie M, DaSilva JN, Kenk M, Thorn S, Beanlands R, DeKemp RA. Kinetics of (R)-[11C]rolipram and (S)-[11C]rolipram in the Dog Heart: Investigation of four compartment models. *IEEE Medical Imaging Conference. San Diego, California*; 2006.

139. Greene M, Thackeray JT, Kenk M, Thorn SL, Bevilacqua L, Harper ME, Beanlands RS, Dasilva JN. Reduced in vivo phosphodiesterase-4 response to acute noradrenaline challenge in diet-induced obese rats. *Can J Physiol Pharmacol.* 2009;87(3):196-202.

140. Kenk M, Thackeray JT, Thorn SL, Dhami K, Chow BJ, Ascah KJ, DaSilva JN, Beanlands RS. Alterations of pre- and postsynaptic noradrenergic signaling in a rat model of adriamycin-induced cardiotoxicity. *J Nucl Cardiol.* 2010;17(2):254-263.

141. Calera MR, Martinez C, Liu H, Jack AK, Birnbaum MJ, Pilch PF. Insulin increases the association of Akt-2 with Glut4-containing vesicles. *J Biol Chem.* 1998;273(13):7201-7204.
142. Taegtmeyer H, McNulty P, Young ME. Adaptation and maladaptation of the heart in diabetes: Part I: general concepts. *Circulation.* 2002;105(14):1727-1733.
143. Czech MP, Corvera S. Signaling mechanisms that regulate glucose transport. *J Biol Chem.* 1999;274(4):1865-1868.
144. Saad MF, Pettitt D, Mott DM, Knowler WC, Nelson RG, Bennett PH. Sequential Changes in Serum Insulin Concentration During Development of Non-Insulin-Dependent Diabetes. *Lancet.* 1989:1356-1359.
145. Kahn BB. Lilly lecture 1995. Glucose transport: pivotal step in insulin action. *Diabetes.* 1996;45(11):1644-1654.
146. Krentz AJ. Insulin resistance. *BMJ.* 1996;313(7069):1385-1389.
147. Butler AE, Janson J, Bonner-Weir S, Ritzel R, Rizza RA, Butler PC. Beta-cell deficit and increased beta-cell apoptosis in humans with type 2 diabetes. *Diabetes.* 2003;52(1):102-110.
148. Beller GA. Coronary heart disease in the first 30 years of the 21st century: challenges and opportunities: The 33rd Annual James B. Herrick Lecture of the Council on Clinical Cardiology of the American Heart Association. *Circulation.* 2001;103(20):2428-2435.
149. Choy CK, Rodgers JE, Nappi JM, Haines ST. Type 2 diabetes mellitus and heart failure. *Pharmacotherapy.* 2008;28(2):170-192.
150. Dawson A, Morris AD, Struthers AD. The epidemiology of left ventricular hypertrophy in type 2 diabetes mellitus. *Diabetologia.* 2005;48(10):1971-1979.
151. Mazzone T, Chait A, Plutzky J. Cardiovascular disease risk in type 2 diabetes mellitus: insights from mechanistic studies. *Lancet.* 2008;371(9626):1800-1809.
152. Saunders J, Mathewkutty S, Drazner MH, McGuire DK. Cardiomyopathy in type 2 diabetes: update on pathophysiological mechanisms. *Herz.* 2008;33(3):184-190.
153. Williams RS, Schaible TF, Scheuer J, Kennedy R. Effects of experimental diabetes on adrenergic and cholinergic receptors of rat myocardium. *Diabetes.* 1983;32(10):881-886.
154. Thackeray JT, Parsa-Nezhad M, Kenk M, Thorn SL, Kolajova M, Beanlands RS, Dasilva JN. Reduced cardiac beta-adrenoreceptor density in hyperglycemic high fat diet-fed streptozotocin-induced diabetic rats. *Life Sciences.* 2010.
155. Dincer UD, Bidasee KR, Guner S, Tay A, Ozcelikay AT, Altan VM. The effect of diabetes on expression of beta1-, beta2-, and beta3-adrenoreceptors in rat hearts. *Diabetes.* 2001;50(2):455-461.
156. Savarese JJ, Berkowitz BA. beta-Adrenergic receptor decrease in diabetic rat hearts. *Life Sci.* 1979;25(24-25):2075-2078.

157. Heyliger CE, Pierce GN, Singal PK, Beamish RE, Dhalla NS. Cardiac alpha- and beta-adrenergic receptor alterations in diabetic cardiomyopathy. *Basic Res Cardiol.* 1982;77(6):610-618.
158. Nishio Y, Kashiwagi A, Kida Y, Kodama M, Abe N, Saeki Y, Shigeta Y. Deficiency of cardiac beta-adrenergic receptor in streptozocin-induced diabetic rats. *Diabetes.* 1988;37(9):1181-1187.
159. Ingebretsen CG, Hawelu-Johnson C, Ingebretsen WR, Jr. Alloxan-induced diabetes reduces beta-adrenergic receptor number without affecting adenylate cyclase in rat ventricular membranes. *J Cardiovasc Pharmacol.* 1983;5(3):454-461.
160. Atkins FL, Dowell RT, Love S. beta-Adrenergic receptors, adenylate cyclase activity, and cardiac dysfunction in the diabetic rat. *J Cardiovasc Pharmacol.* 1985;7(1):66-70.
161. Gando S, Hattori Y, Akaishi Y, Nishihira J, Kanno M. Impaired contractile response to beta adrenoceptor stimulation in diabetic rat hearts: alterations in beta adrenoceptors-G protein-adenylate cyclase system and phospholamban phosphorylation. *J Pharmacol Exp Ther.* 1997;282(1):475-484.
162. Tamada A, Hattori Y, Houzen H, Yamada Y, Sakuma I, Kitabatake A, Kanno M. Effects of beta-adrenoceptor stimulation on contractility, [Ca2+]i, and Ca2+ current in diabetic rat cardiomyocytes. *Am J Physiol.* 1998;274(6 Pt 2):H1849-1857.
163. Yaras N, Ugur M, Ozdemir S, Gurdal H, Purali N, Lacampagne A, Vassort G, Turan B. Effects of diabetes on ryanodine receptor Ca release channel (RyR2) and Ca2+ homeostasis in rat heart. *Diabetes.* 2005;54(11):3082-3088.
164. Zhong Y, Ahmed S, Grupp IL, Matlib MA. Altered SR protein expression associated with contractile dysfunction in diabetic rat hearts. *Am J Physiol Heart Circ Physiol.* 2001;281(3):H1137-1147.
165. Lu Z, Jiang YP, Xu XH, Ballou LM, Cohen IS, Lin RZ. Decreased L-type Ca2+ current in cardiac myocytes of type 1 diabetic Akita mice due to reduced phosphatidylinositol 3-kinase signaling. *Diabetes.* 2007;56(11):2780-2789.
166. Peterson LR, Herrero P, Schechtman KB, Racette SB, Waggoner AD, Kisrieva-Ware Z, Dence C, Klein S, Marsala J, Meyer T, Gropler RJ. Effect of obesity and insulin resistance on myocardial substrate metabolism and efficiency in young women. *Circulation.* 2004;109(18):2191-2196.
167. Lillioja S, Mott DM, Spraul M, Ferraro R, Foley JE, Ravussin E, Knowler WC, Bennett PH, Bogardus C. Insulin resistance and insulin secretory dysfunction as precursors of non-insulin-dependent diabetes mellitus. Prospective studies of Pima Indians. *N Engl J Med.* 1993;329(27):1988-1992.
168. Troisi RJ, Weiss ST, Parker DR, Sparrow D, Young JB, Landsberg L. Relation of obesity and diet to sympathetic nervous system activity. *Hypertension.* 1991;17(5):669-677.

169. Christensen NJ, Brandsborg O. The relationship between plasma catecholamine concentration and pulse rate during exercise and standing. *Eur J Clin Invest.* 1973;3(4):299-306.
170. Fushimi H, Inoue T, Namikawa H, Kishino B, Nishikawa M, Tochino Y, Funakawa S. Increased norepinephrine content in diabetic rat heart. *J Biochem.* 1982;91(5):1805-1807.
171. Paulson DJ, Light KE. Elevation of serum and ventricular norepinephrine content in the diabetic rat. *Res Commun Chem Pathol Pharmacol.* 1981;33(3):559-562.
172. Akiyama N, Okumura K, Watanabe Y, Hashimoto H, Ito T, Ogawa K, Satake T. Altered acetylcholine and norepinephrine concentrations in diabetic rat hearts. Role of parasympathetic nervous system in diabetic cardiomyopathy. *Diabetes.* 1989;38(2):231-236.
173. Anderson EA, Hoffman RP, Balon TW, Sinkey CA, Mark AL. Hyperinsulinemia produces both sympathetic neural activation and vasodilation in normal humans. *J Clin Invest.* 1991;87(6):2246-2252.
174. Hausberg M, Mark AL, Hoffman RP, Sinkey CA, Anderson EA. Dissociation of sympathoexcitatory and vasodilator actions of modestly elevated plasma insulin levels. *J Hypertens.* 1995;13(9):1015-1021.
175. Masuo K, Kawaguchi H, Mikami H, Ogihara T, Tuck ML. Serum uric acid and plasma norepinephrine concentrations predict subsequent weight gain and blood pressure elevation. *Hypertension.* 2003;42(4):474-480.
176. Levin BE, Sullivan AC. Glucose-induced sympathetic activation in obesity-prone and resistant rats. *Int J Obes.* 1989;13(2):235-246.
177. O'Dea K, Esler M, Leonard P, Stockigt J, Nestel P. Noradrenaline turnover during under- and over-eating in normal weight subjects. *Metabolism.* 1982;31:896-899.
178. Das I, Chain EB. An effect of insulin on the adenosine 3':5'-cyclic monophosphate phosphodiesterase and guanosine 3':5'-cyclic monophosphate phosphodiesterase activities in the perfused Langendorff and working hearts of normal and diabetic rats. *Biochem J.* 1972;128(3):95P-96P.
179. Perez de Gracia B, Rhoads AR, West WL. The response of cyclic 3',5'-AMP and cyclic 3',5'-GMP phosphodiesterases to experimental diabetes. *Experientia.* 1980;36(7):824-825.
180. Engfeldt P, Arner P, Bolinder J, Ostman J. Phosphodiesterase activity in human subcutaneous adipose tissue in insulin- and noninsulin-dependent diabetes mellitus. *J Clin Endocrinol Metab.* 1982;55(5):983-988.
181. Solomon SS, Deaton J, Shankar TP, Palazzolo M. Cyclic AMP phosphodiesterase in diabetes. Effect of glyburide. *Diabetes.* 1986;35(11):1233-1236.
182. Ofulue AF, Nijjar MS. Effects of streptozotocin-induced diabetes on calmodulin and cyclic AMP phosphodiesterase activity in rat lungs. *Lung.* 1982;160(6):303-310.

183. Lenzen S. The mechanisms of alloxan- and streptozotocin-induced diabetes. *Diabetologia.* 2008;51(2):216-226.

184. Tanaka S, Hayashi T, Toyoda T, Hamada T, Shimizu Y, Hirata M, Ebihara K, Masuzaki H, Hosoda K, Fushiki T, Nakao K. High-fat diet impairs the effects of a single bout of endurance exercise on glucose transport and insulin sensitivity in rat skeletal muscle. *Metabolism.* 2007;56(12):1719-1728.

185. Zhao S, Chu Y, Zhang C, Lin Y, Xu K, Yang P, Fan J, Liu E. Diet-induced central obesity and insulin resistance in rabbits. *J Anim Physiol Anim Nutr (Berl).* 2008;92(1):105-111.

186. Flanagan AM, Brown JL, Santiago CA, Aad PY, Spicer LJ, Spicer MT. High-fat diets promote insulin resistance through cytokine gene expression in growing female rats. *J Nutr Biochem.* 2008;19(8):505-513.

187. Randle PJ, Garland PB, Hales CN, Newsholme EA. The glucose fatty-acid cycle. Its role in insulin sensitivity and the metabolic disturbances of diabetes mellitus. *Lancet.* 1963;1(7285):785-789.

188. Samuel VT, Petersen KF, Shulman GI. Lipid-induced insulin resistance: unravelling the mechanism. *Lancet.*375(9733):2267-2277.

189. Reed MJ, Meszaros K, Entes LJ, Claypool MD, Pinkett JG, Gadbois TM, Reaven GM. A new rat model of type 2 diabetes: the fat-fed, streptozotocin-treated rat. *Metabolism.* 2000;49(11):1390-1394.

190. Srinivasan K, Viswanad B, Asrat L, Kaul CL, Ramarao P. Combination of high-fat diet-fed and low-dose streptozotocin-treated rat: a model for type 2 diabetes and pharmacological screening. *Pharmacol Res.* 2005;52(4):313-320.

191. Marsh SA, Dell'italia LJ, Chatham JC. Interaction of diet and diabetes on cardiovascular function in rats. *Am J Physiol Heart Circ Physiol.* 2009;296(2):H282-292.

192. Valdivia AC, Mason S, Collins J, Buckley KR, Coletta P, Beanlands RS, Dasilva JN. Radiosynthesis of N-[(11)C]-methyl-hydroxyfasudil as a new potential PET radiotracer for rho-kinases (ROCKs). *Appl Radiat Isot.* 2010;68(2):325-328.

193. Parks NJ, Krohn KA. The Synthesis of 13N Labeled Ammonia, Dinitrogen, Nitrite, and Nitrate using a Single Cyclotron Target System. *The International journal of applied radiation and isotopes.* 1978;29:754-756.

194. Wieland B, Bida G, Padgett H, Hendry G, Zippi E, Kabalka G, Morelle JL, Verbruggen R, Ghyoot M. In-target production of [13N]ammonia via proton irradiation of dilute aqueous ethanol and acetic acid mixtures. *Int J Rad Appl Instrum A.* 1991;42(11):1095-1098.

195. Kaufmann PA, Camici PG. Myocardial blood flow measurement by PET: technical aspects and clinical applications. *J Nucl Med.* 2005;46(1):75-88.

196. Lamoureux M, Thorn SL, Dumouchel T, Klein R, Renaud JM, Mason S, Lortie M, DaSilva JN, Beanlands RS, de Kemp RA. Uniformity and reproducibility of normal

resting myocardial blood floq in rats with [13N]ammonia and small animal PET. *J Nucl Med.* 2010.

197. Logan J, Fowler JS, Volkow ND, Wang GJ, Ding YS, Alexoff DL. Distribution volume ratios without blood sampling from graphical analysis of PET data. *J Cereb Blood Flow Metab.* 1996;16(5):834-840.

198. Logan J, Fowler JS, Volkow ND, Wolf AP, Dewey SL, Schlyer DJ, MacGregor RR, Hitzemann R, Bendriem B, Gatley SJ, et al. Graphical analysis of reversible radioligand binding from time-activity measurements applied to [N-11C-methyl]-(-)-cocaine PET studies in human subjects. *J Cereb Blood Flow Metab.* 1990;10(5):740-747.

199. DeGrado TR, Hanson MW, Turkington TG, Delong DM, Brezinski DA, Vallee JP, Hedlund LW, Zhang J, Cobb F, Sullivan MJ, Coleman RE. Estimation of myocardial blood flow for longitudinal studies with 13N-labeled ammonia and positron emission tomography. *J Nucl Cardiol.* 1996;3(6 Pt 1):494-507.

200. Laruelle M, Slifstein M, Huang Y. Positron emission tomography: imaging and quantification of neurotransporter availability. *Methods.* 2002;27(3):287-299.

201. Lourenco CM, Houle S, Wilson AA, DaSilva JN. Characterization of r-(11)C]rolipram for PET imaging of phosphodieterase-4: in vito binding, metabolism, and dosimetry studies in rats. *Nucl Med Biol.* 2001;28(4):347-358.

202. Langslet A, Johansen WG, Ryg M, Skomedal T, Oye I. Effects of dibenzepine and imipramine on the isolated rat heart. *Eur J Pharmacol.* 1971;14(4):333-339.

203. Sands WA, Palmer TM. Regulating gene transcription in response to cyclic AMP elevation. *Cell Signal.* 2008;20(3):460-466.

204. Krause W, Kuhne G. Pharmacokinetics of rolipram in the rhesus and cynomolgus monkeys, the rat and the rabbit. Studies on species differences. *Xenobiotica.* 1988;18(5):561-571.

205. Lourenco CM, DaSilva JN, Warsh JJ, Wilson AA, Houle S. Imaging of cAMP-specific phosphodiesterase-IV: comparison of [11C]rolipram and [11C]Ro 20-1724 in rats. *Synapse.* 1999;31(1):41-50.

206. Fox CS, Coady S, Sorlie PD, D'Agostino RB, Sr., Pencina MJ, Vasan RS, Meigs JB, Levy D, Savage PJ. Increasing cardiovascular disease burden due to diabetes mellitus: the Framingham Heart Study. *Circulation.* 2007;115(12):1544-1550.

207. Moan A, Hoieggen A, Nordby G, Birkeland K, Eide I, Kjeldsen SE. The glucose clamp procedure activates the sympathetic nervous system even in the absence of hyperinsulinemia. *J Clin Endocrinol Metab.* 1995;80(11):3151-3154.

208. Kern W, Peters A, Born J, Fehm HL, Schultes B. Changes in blood pressure and plasma catecholamine levels during prolonged hyperinsulinemia. *Metabolism.* 2005;54(3):391-396.

209. Hafstad AD, Solevag GH, Severson DL, Larsen TS, Aasum E. Perfused hearts from Type 2 diabetic (db/db) mice show metabolic responsiveness to insulin. *Am J Physiol Heart Circ Physiol.* 2006;290(5):H1763-1769.

210. Oakes ND, Thalen P, Aasum E, Edgley A, Larsen T, Furler SM, Ljung B, Severson D. Cardiac metabolism in mice: tracer method developments and in vivo application revealing profound metabolic inflexibility in diabetes. *Am J Physiol Endocrinol Metab.* 2006;290(5):E870-881.
211. Dincer UD, Onay A, Ari N, Ozcelikay AT, Altan VM. The effects of diabetes on beta-adrenoceptor mediated responsiveness of human and rat atria. *Diabetes Res Clin Pract.* 1998;40(2):113-122.
212. Katovich MJ, Meldrum MJ, Vasselli JR. Beneficial effects of dietary acarbose in the streptozotocin-induced diabetic rat. *Metabolism.* 1991;40(12):1275-1282.
213. Zhang M, Lv XY, Li J, Xu ZG, Chen L. The characterization of high-fat diet and multiple low-dose streptozotocin induced type 2 diabetes rat model. *Exp Diabetes Res.* 2008;2008:704045.
214. Ghosh S, Qi D, An D, Pulinilkunnil T, Abrahani A, Kuo KH, Wambolt RB, Allard M, Innis SM, Rodrigues B. Brief episode of STZ-induced hyperglycemia produces cardiac abnormalities in rats fed a diet rich in n-6 PUFA. *Am J Physiol Heart Circ Physiol.* 2004;287(6):H2518-2527.
215. Menard SL, Croteau E, Sarrhini O, Gelinas R, Brassard P, Ouellet R, Bentourkia M, van Lier JE, Des Rosiers C, Lecomte R, Carpentier AC. Abnormal in vivo myocardial energy substrate uptake in diet-induced type 2 diabetic cardiomyopathy in rats. *Am J Physiol Endocrinol Metab.* 2010;298(5):E1049-1057.
216. Wilson CR, Tran MK, Salazar KL, Young ME, Taegtmeyer H. Western diet, but not high fat diet, causes derangements of fatty acid metabolism and contractile dysfunction in the heart of Wistar rats. *Biochem J.* 2007;406(3):457-467.
217. Yu Z, McNeill JH. Altered inotropic responses in diabetic cardiomyopathy and hypertensive-diabetic cardiomyopathy. *J Pharmacol Exp Ther.* 1991;257(1):64-71.
218. Ligeti L, Szenczi O, Prestia CM, Szabo C, Horvath K, Marcsek ZL, van Stiphout RG, van Riel NA, Op den Buijs J, Van der Vusse GJ, Ivanics T. Altered calcium handling is an early sign of streptozotocin-induced diabetic cardiomyopathy. *Int J Mol Med.* 2006;17(6):1035-1043.
219. Canadian Council of Animal Care. Ethics and Animal Experimentation. *http://www.ccac.ca/en/CCAC_Programs/Guidelines_Policies/GUIDES/ENGLISH/toc_v1.htm.* 2010.
220. Thomas AJ, Dasilva JN, Lortie M, Renaud JM, Kenk M, Beanlands RS, de Kemp RA. PET of (R)-11C-Rolipram Binding to Phosphodiesterase-4 Is Reproducible and Sensitive to Increased Norepinephrine in the Rat Heart. *J Nucl Med.* 2011.
221. Suda S, Nibuya M, Ishiguro T, Suda H. Transcriptional and translational regulation of phosphodiesterase type IV isozymes in rat brain by electroconvulsive seizure and antidepressant drug treatment. *J Neurochem.* 1998;71(4):1554-1563.
222. Ye Y, Conti M, Houslay MD, Farooqui SM, Chen M, O'Donnell JM. Noradrenergic activity differentially regulates the expression of rolipram-sensitive, high-

affinity cyclic AMP phosphodiesterase (PDE4) in rat brain. *J Neurochem.* 1997;69(6):2397-2404.

223. Alcazar L, Alfaro R, Tamarit M, Gomez-Angulo JC, Ortega JM, Aragones P, Jerez P, Salazar F, del Pozo JM. Delayed intracerebral hemorrhage after ventriculoperitoneal shunt insertion. Case report and literature review. *Neurocirugia (Astur).* 2007;18(2):128-133.

224. Takahashi M, Terwilliger R, Lane C, Mezes PS, Conti M, Duman RS. Chronic antidepressant administration increases the expression of cAMP-specific phosphodiesterase 4A and 4B isoforms. *J Neurosci.* 1999;19(2):610-618.

225. Hoskins B, Luong HB. Cyclic nucleotides and cyclic nucleotide phosphodiesterases in kidneys from rats with experimental diabetes. *Res Commun Chem Pathol Pharmacol.* 1981;33(2):381-384.

226. Suzuki T, Makino H, Kanatsuka A, Kuribayashi S, Hashimoto N, Yoshida S. Insulin-sensitive phosphodiesterase and insulin receptor binding in fat cells from spontaneously obese rats. *Diabetologia.* 1985;28(5):286-290.

227. Walz HA, Harndahl L, Wierup N, Zmuda-Trzebiatowska E, Svennelid F, Manganiello VC, Ploug T, Sundler F, Degerman E, Ahren B, Holst LS. Early and rapid development of insulin resistance, islet dysfunction and glucose intolerance after high-fat feeding in mice overexpressing phosphodiesterase 3B. *J Endocrinol.* 2006;189(3):629-641.

228. Katakami N, Kim YS, Kawamori R, Yamasaki Y. The phosphodiesterase inhibitor cilostazol induces regression of carotid atherosclerosis in subjects with type 2 diabetes mellitus: principal results of the Diabetic Atherosclerosis Prevention by Cilostazol (DAPC) study: a randomized trial. *Circulation.*121(23):2584-2591.

229. Duman RS, Heninger GR, Nestler EJ. A molecular and cellular theory of depression. *Arch Gen Psychiatry.* 1997;54(7):597-606.

230. Lemoine H, Schonell H, Kaumann AJ. Contribution of beta 1- and beta 2-adrenoceptors of human atrium and ventricle to the effects of noradrenaline and adrenaline as assessed with (-)-atenolol. *Br J Pharmacol.* 1988;95(1):55-66.

231. Kaumann AJ, Lemoine H, Schwederski-Menke U, Ehle B. Relations between beta-adrenoceptor occupancy and increases of contractile force and adenylate cyclase activity induced by catecholamines in human ventricular myocardium. Acute desensitization and comparison with feline ventricle. *Naunyn Schmiedebergs Arch Pharmacol.* 1989;339(1-2):99-112.

232. Gille E, Lemoine H, Ehle B, Kaumann AJ. The affinity of (-)-propranolol for beta 1- and beta 2-adrenoceptors of human heart. Differential antagonism of the positive inotropic effects and adenylate cyclase stimulation by (-)-noradrenaline and (-)-adrenaline. *Naunyn Schmiedebergs Arch Pharmacol.* 1985;331(1):60-70.

233. Kaumann AJ, Hall JA, Murray KJ, Wells FC, Brown MJ. A comparison of the effects of adrenaline and noradrenaline on human heart: the role of beta 1- and beta 2-

adrenoceptors in the stimulation of adenylate cyclase and contractile force. *Eur Heart J.* 1989;10 Suppl B:29-37.

234. Hall JA, Kaumann AJ, Brown MJ. Selective beta 1-adrenoceptor blockade enhances positive inotropic responses to endogenous catecholamines mediated through beta 2-adrenoceptors in human atrial myocardium. *Circ Res.* 1990;66(6):1610-1623.

235. Chattou S, Diacono J, Feuvray D. Decrease in sodium-calcium exchange and calcium currents in diabetic rat ventricular myocytes. *Acta Physiol Scand.* 1999;166(2):137-144.